Hybrid Silica-Microbial Materials for Bioremediation Applications

A DISSERTATION
SUBMITTED TO THE FACULTY OF
UNIVERSITY OF MINNESOTA
BY

Sujin Yeom

IN PARTIAL FULFILLMENT OF THE REQUIREMENTS
FOR THE DEGREE OF
DOCTOR OF PHILOSOPHY

Adviser: Lawrence P. Wackett

June 2017

Acknowledgements

I would like to express my deep appreciation to my adviser, Professor Larry Wackett. It's been such a great opportunity to learn not only science but also what a true scholar is under your supervision. You always inspired me with your enthusiasm for science and I'm grateful for all the support you have given me over the years. Thank you for letting me join your group and continue research after my transfer.

I would also like to thank all the present and past lab members that I was able to work with during my Ph.D. study: Dr. Kelly Aukema, Dr. Asim Bera, Dr. Stephan Cameron, Mason Chan, Dr. Seunghee Cho, Dr. James Christenson, Dr. Tony Dodge, Ana Kim, Dr. Neissa Pinzon, Dr. Adi Radian, Dr. Jack Richman, Serina Robinson , Dr. Jennifer Serffernick, Michael Turnbull, Dr. Baris Mutlu, Jonathan Sakkos , Joey Benson , Diego Escalante, Lisa Kasinkas, Dr. Boris Tong, Ryan Han. Thank you especially Baris. Thank you for supporting me during my ups and downs. It was a great pleasure to work with an intelligent scholar like you. Tony, Kelly, and Jack, thanks for helping me all the time. I wouldn't be able to figure things out without your help. Jonathan, I was able to get through my last part of my research because of your help. Thanks for working and having fun with me.

I am grateful to my doctoral committee, Professor Alptekin Aksan, Professor Fumiaki Katagiri, Professor Burckhard Seelig, and Professor Jeongsik Yong. Dr. Aksan, I

appreciate your discussion and advice on my research. My experience of working with you and your group allowed me to build up ability to collaborate with people outside of my field. I am grateful to have that privilege which not every students can have. Dr. Yong, I thank you for all your advice on my career and life. I've been lucky to have you as my chair and mentor. Dr. Katagiri, thanks for your feedback and advice on my research and exams.

Finally, I would like to thank my family and friends. Mom, you are the one that I respect the most. Every time I encounter a difficulty, I was able to overcome because of you being there for me. You always remained calm even though I faced huge challenges. It made me look at the situation rationally. I can't put how much I thank you in words. I couldn't have done this without you. My brother, you are my best friend. Thank you for taking care of me over the years to keep my sanity. My husband, I never imagined I would be able to meet my soul mate in my life. I was able to get through my final step to earn my Ph.D. because of your support. You complete me. My friends, Nari, Hyunju, Minhae, and Bomi. Thanks you all for cheering me up and I am so lucky to have all of you.

Dedication

This dissertation is dedicated to my mother, my brother, and my husband. I would not be here today without your love, sacrifice, and support.

Abstract

The research presented here is focused on developing an advanced bioremediation technique to remove environmental pollutants by integrating microbial biodegradation and material science. The research is based on microbial enzymes used in combination with a silica support material to metabolize *s*-trazine ring compounds and aromatic hydrocarbons for applications in environmental cleanup and biotechnology. A genetically-engineered bacterium expressing atrazine chlorohydrolase was encapsulated into novel silica gel compositions. The biodegradation ability of the developed hybrid material was tested in a continuous-flow bioreactor filtration system for atrazine removal in wastewater. The materials-biocatalyst hybrid was further applied to a different enzyme system and a different chemical to expand the scope of applications. Cyanuric acid was chosen because there is no current remediation method available although there is a need for such method. Three different bacterial cyanuric acid hydrolases were compared with respect to stability and effectiveness in the silica matrix. Cyanuric acid hydrolase from a thermophilic bacterium was further investigated in a simulated bioactive filter system using a solution prepared in the laboratory as well as actual water samples. The results from both experiments showed the efficacy of the process. The materials-biocatalyst also was investigated to create a synthetic ecosystem consisting of two distinct bacterial species to degrade aromatic hydrocarbons. In this system, heterotrophic bacteria performed aerobic biodegradation requiring a high oxygen level, while phototrophic bacteria produced oxygen via photosynthesis. Experimental results showed the system

was more effective for oxygenation than external supplementation. The materials-biocatalyst was further modified to be applied for bioremediation of atrazine spills. In order to treat high concentration of waste chemicals, hydrophobic silica materials were used to allow rapid adsorption of the chemical prior to biodegradation. The hydrophobic materials-biocatalyst was characterized in terms of mechanical properties and biodegradation ability. The study showed that the hydrophobic silica with cells adsorb chemicals selectively, releasing biodegradation products, which makes the material self-regenerating.

Table of Contents

List of Tables

List of Figures

List of Abbreviations

TMOS	Tetramethoxysilane
TEOS	Tetraethoxysilane
PTES	Phenyltriethoxysilane
SNP	Silica nanoparticles
CAH	Cyanuric acid hydrolase
PBS	Phosphate buffered saline
MSB	Minimal salts buffer

CHAPTER 1 Introduction

1.1 *s*-Triazines

s-Triazine, also known as 1,3,5-triazine is a six-membered heterocyclic aromatic ring with the formula $(HCN)_3$ (Fig 1.1). Its derivatives are manufactured on a large scale for a variety of purposes such as herbicides, resin intermediates, disinfectants, and reactive dyes. It was first synthesized in 1859 and industrial production of *s*-triazines begun in the 1950s[1].

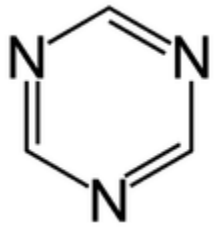

Figure 1. 1 *s*-Triazine (1,3,5-triazine) structure[2]

The industrial *s*-triazine derivatives include atrazine, trichloroisocyanuric acid, and melamine (Fig 1.2). Atrazine is an herbicide used to control weeds in crops and will be discussed later in detail. Melamine is added to produce a resin that has flame-retardant properties. Trichloroisocyanuric acid is commonly used as disinfectants and bleaching agents. The microbial biodegradation pathways for the *s*-trazine derivatives funnel into the common intermediate, cyanuric acid (Fig 1.2).

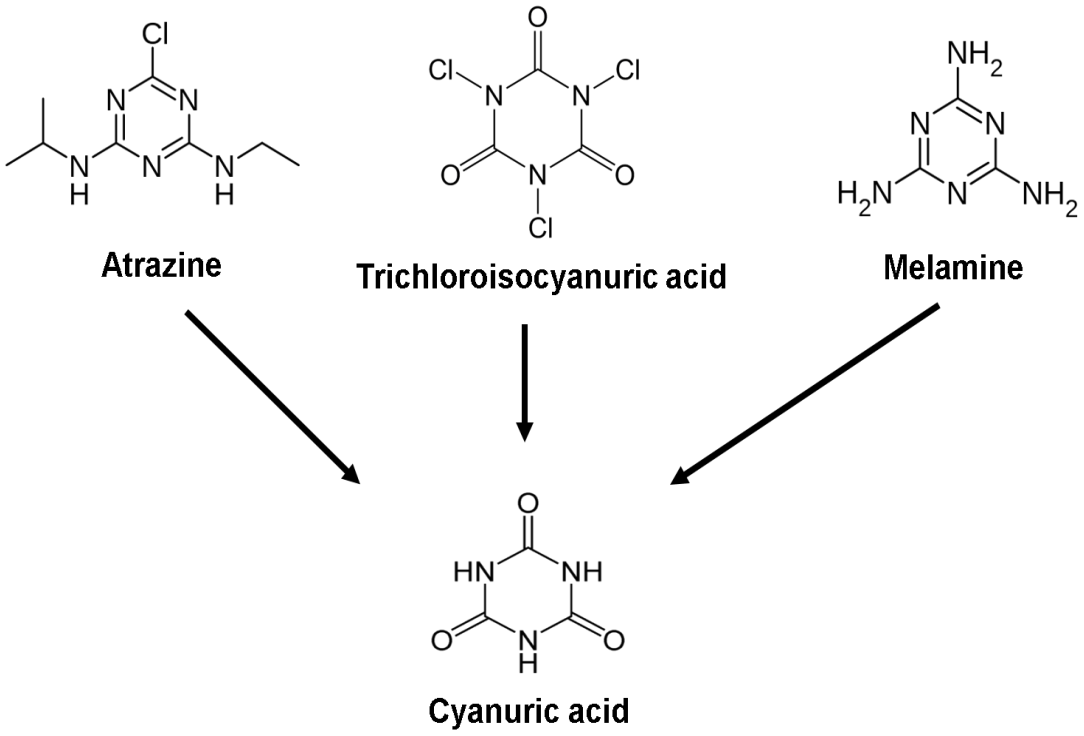

Figure 1. 2 Cyanuric acid is the common intermediate of microbial biodegradation pathways of *s*-trizines

1.2 Atrazine

Atrazine is one of the *s*-triazine derivatives and was introduced in the 1950s as an herbicide. Atrazine is the most heavily used herbicides in the world and applied annually up to 36,000 tons[3]. Atrazine is mobile in the environment due to its low adsorption in the soil resulting in sporadic detection in ground water [4, 5].

In Europe atrazine was banned in 2004 however, atrazine still is the most abundant pesticide in ground water samples from Germany[6]. Its toxicity on mammals and humans is unclear because there has been not much data accumulated. However, the results with

putative estrogen receptor GPR30 appear to reveal that atrazine might be involved in a signaling mechanism carrying the potential for estrogenic compounds[7]. The feminization of frogs was reported, but the work has not been replicated by other groups[8]. Maximum concentrations for atrazine in public drinking water established by the United States Environmental Protection Agency is 3ppb (µg/L)[9].

Atrazine undergoes slow abiotic hydrolysis only at or below pH 4 [10, 11], although biodegradation is the principal process controlling its fate. Microbial degradation of atrazine has been studied extensively and is illustrated in Fig 1.3 [12, 13]. Atrazine conversion to cyanuric acid is achieved via three distinct pathways. Further mineralization of cyanuric acid will be discussed later in detail. One of the three pathways only occurs by a hydrolytic reaction. The hydrolytic pathway has been extensively characterized in *Pseudomonas* sp. ADP achieved by three gene products of *atzA*, *atzB*, and *atzC*. The gene *atzA* encodes atrazine chlorohydrolase catalyzing dechlorinaton of atrazine, yielding hydroxyatrazine. AtzB and AtzC hydrolyze *N*-alkyl substituents from the *s*-trizine ring, yielding cyanuric acid.

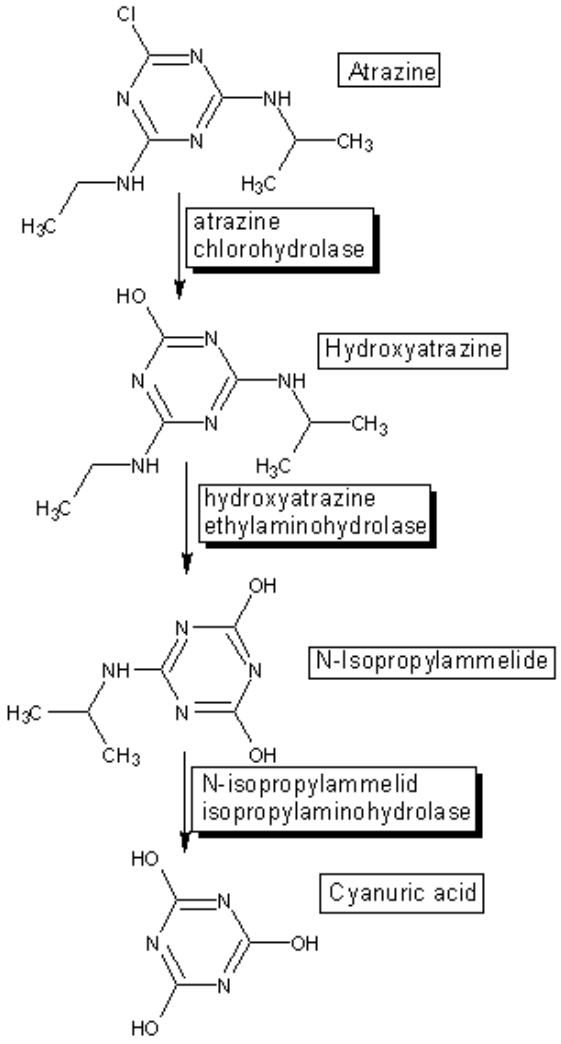

Figure 1. 3 Hydrolytic atrazine catabolic pathway. Pathways derived from the EAWAG-BBD[14]

Two of the other pathways involve mixed oxidative and hydrolytic reactions (Fig 1.4)[12, 13]. The oxidative *N*-dealkylation of atrazine to deisopropylatrazine or deethylatrazine is initiated by atrazine monooxygenase. Deisopropylatrazine is further dealkylated to deisopropyldeethylatrazine and deaminated to yield cyanuric acid. Deethylatrazine is subjected to hydrolytic dechlorination and dealkylation to yield cyanuric acid.

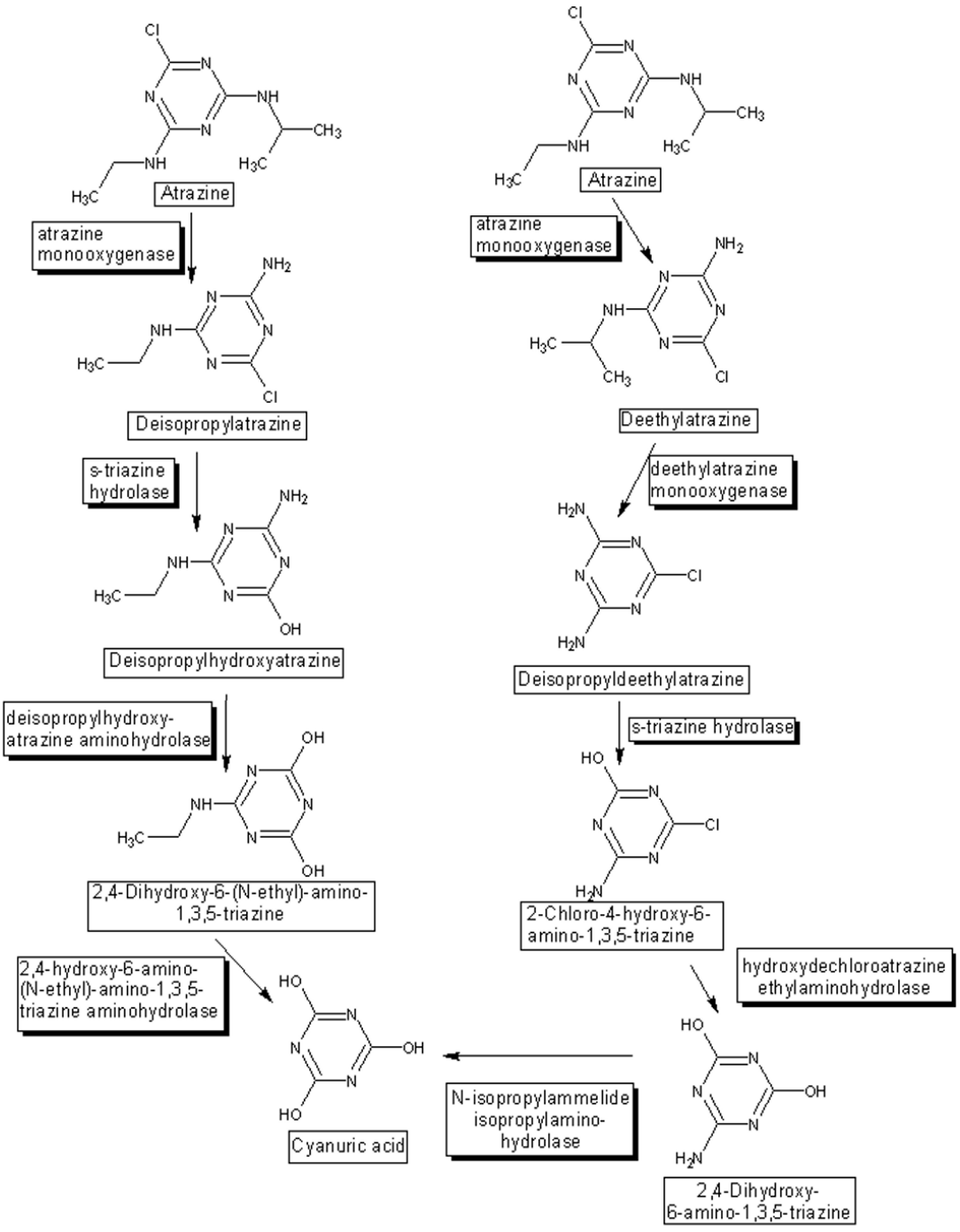

Figure 1. 4 Oxidative/hydrolytic atrazine catabolic pathway. Pathways derived from the EAWAG-BBD[15]

1.3 Cyanuric Acid

Cyanuric acid is also an important derivative of *s*-triazine and is widely used as a precursor to chlorinated cyanurates to disinfect water. Cyanuric acid is a metabolic intermediate in the degradation of many *s*-triazine compounds and has come under increased scrutiny because of its potential involvement in comediating toxicity resulting from the ingestion of melamine. Cyanuric acid is formed during the degradation of melamine in the human body resulting in the formation of melamine-cyanuric acid (CA.M) crystals: this leads to the precipitation of CA.M within the kidneys, which causes renal failure (Fig 1.5). Dietary exposure to melamine has been reported as an effect of the use of cyromazine (pesticide). Melamine is sometimes illegally used to manufacture food products to increase the apparent protein content [16].

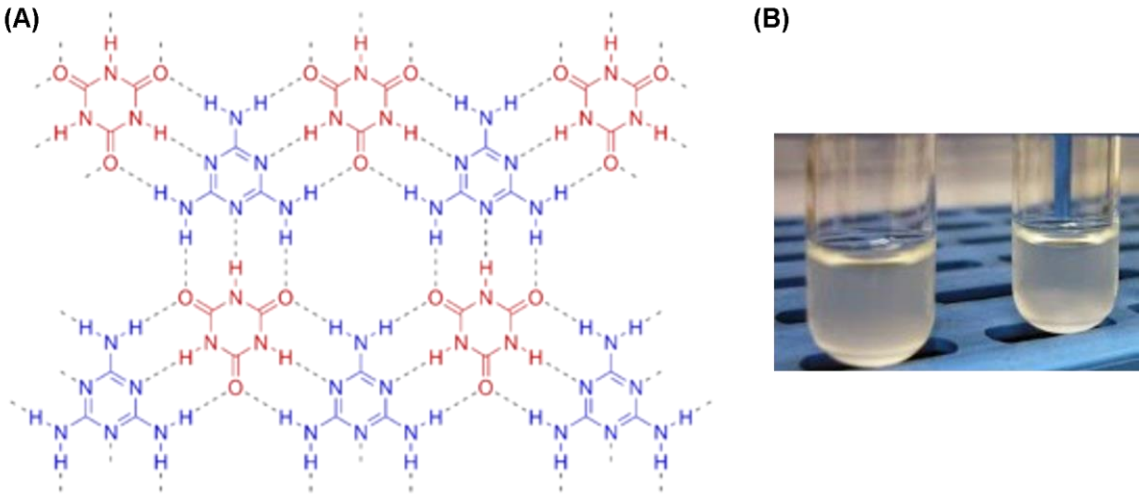

Figure 1. 5 Melamine-cyanuric acid (CA.M) crystals. (A) Cyanuric acid (red) hydrogen bonds with melamine (blue)[17]; (B) Precipitation of CA.M crystals.

Chlorinated cyanuric acid compounds (di-, trichloroisocyanuric acid) are a disinfectant used mainly in outdoor pools and spas and also used as a bleaching agent. They release chlorine slowly in water and building up cyanuric acid (Fig 1.6)[12, 13]. Cyanuric acid stabilizes the chlorine in the pool and prevents the chlorine from being quickly consumed by sunlight. An ideal level of cyanuric acid is 30 to 50 ppm (mg/L) to prevent rapid chlorine loss. High levels of cyanuric acid reduce disinfection efficacy, such that disinfection is not achieved. Currently swimming pools are drained and refilled with fresh water to lower the cyanuric acid level.

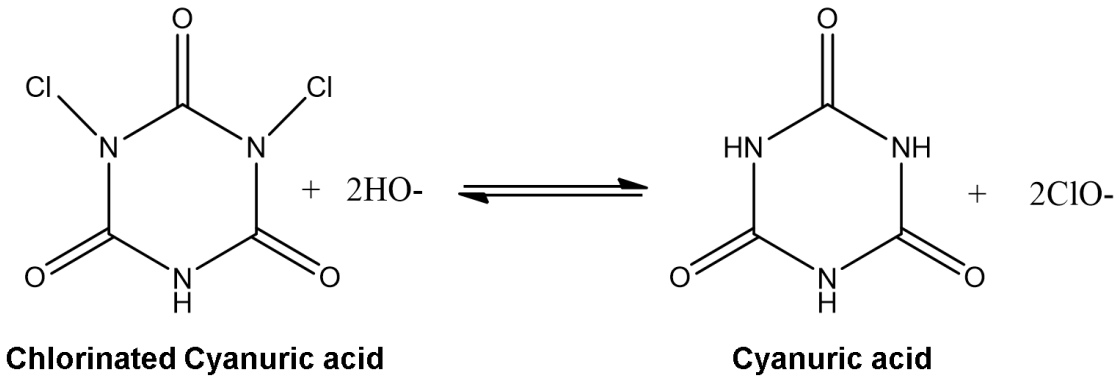

Figure 1. 6 The disinfection reaction of chlorinated cyanuric acids

The degradation of cyanuric acid in microbes is occurred via hydrolytic cleavage of the *s*-triazine ring. Cyanuric acid hydrolase catalyzes hydrolysis reaction of cyanuric acid, yielding biuret. The consecutive enzymatic hydrolysis of biuret and allophanate takes place to produce ammonium and carbon dioxide (Fig 1.7)[12, 13]. The enzymes involved in cyanuric acid degradation have been well characterized in *Pseudomonas* sp. ADP which are encoded by the *atzDEF* operon. Expression of *atzDRF* operon is positively regulated

by *atzR*, a LysR-type transcriptional regulator, in response to cyanuric acid and nitrogen limitation[18, 19].

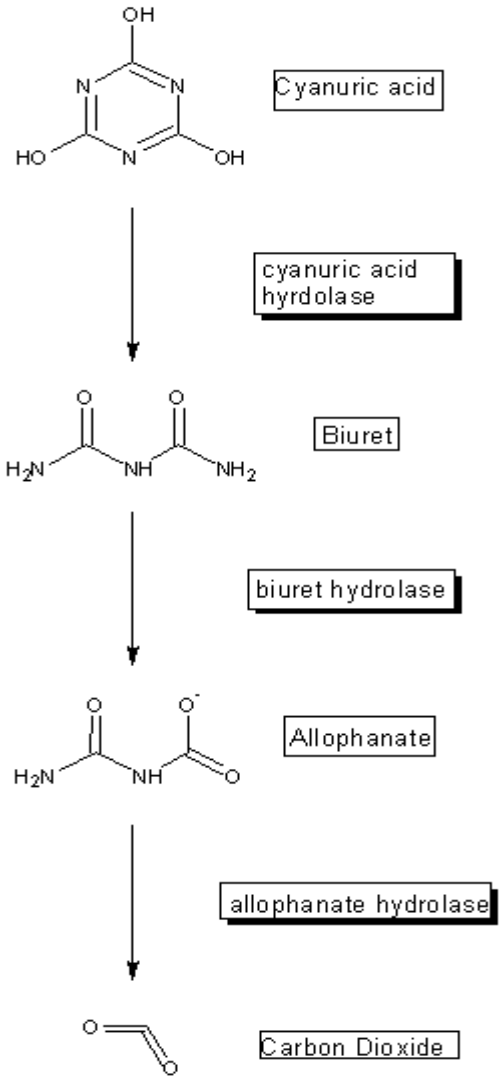

Figure 1. 7 Cyanuric acid catabolic pathway. Pathways derived from the EAWAG-BBD[20]

1.4 *s*-Trizine Remediation Techniques

The current technique for removing *s*-trizine herbicides from water is using active carbon as an adsorbent[21]. Activated carbon can adsorb contaminants non-specifically and eventually needs to be landfilled or incinerated. The mechanical method requires high cost and energy. On the other hand, bioremediation, if that is applied *in situ*, would be the most economical and environmentally friendly approach to remove herbicide from groundwater by transforming it to non-hazardous chemicals. Bioremediation technologies are classified broadly into two categories: *ex situ* and *in situ*[22]. *Ex situ* technologies involve the physical removal of the contaminated material for treatment process which has basically the same disadvantages with the mechanical method. In contrast, *in situ* techniques involve the treatment of the contaminated material in place.

The most significant challenge in bioremediation is introducing laboratory bacteria strains, because a contaminated environment is not favorable for laboratory strains to sustain good degradation activity without a support structure. The cell encapsulation method can offer a physical barrier for encapsulated bacteria, protecting them from the harsh environment and thus introducing the potential for a long-term solution for contaminated water remediation.

1.5 Encapsulation

The encapsulation of biological components, including active proteins and viable cells, within a matrix has a broad application, such as drug delivery, biosensing, bioreactors, and catalysis[23]. The classification of encapsulated cell systems can be based on the physical mechanism of cell localization and on the nature of the support material. Silica gel encapsulation proposed in this research is categorized as entrapment within porous matrices.

A wide variety of natural (polysaccharides and proteins) and synthetic polymers has been gelled into matrices to allow cell entrapment [23]. A significant amount of work in the bioencapsulation field has been done with organic polymers such as alginate, agar, carrageenan, etc. Natural polymers are biocompatible, but high purification cost is required. Alginate gel has limitations because uncontrollable and unpredictable dissolution has been observed. Agar cannot ensure mechanical strength, which makes it impossible to be applied to large-scale treatment[24]. On the other hand, silica is chemically inert, and porous structure and mechanical strength can be adjustable by changing encapsulation components. Silica encapsulation can also sustain long-term enzyme activities due to its robustness and porous structure. It was reported that, for the first time in our research group, silica-encapsulated bacteria held activity after four months' storage[25].

1.6 Encapsulation process

Silica gels are produced by the hydrolysis and condensation of silicon alkoxide precursors such as tetramethoxysilane (TMOS), tetraethoxysilane (TEOS) or phenyltriethoxysilane (PTES) referred to as the sol-gel process (Fig 1.8)[26]. The precursor is partially hydrolysed with acid to produce a prehydrolysed liquid.

$Si(OR)_4 + H_2O \rightarrow HO\text{-}Si(OR)_3 + ROH$ *hydrolysis*

The liquid is then mixed with a suspension of the bacterial cells (green circle) and silica nanoparticles (blue circles, SNP), initiating gelation as a result of the pH value, which is higher than 7 (Fig 1.9).

$(OR)_3Si\text{-}OH + HO\text{-}Si(OR)_3 \rightarrow (OR)_3Si\text{-}O\text{-}Si(OR)_3 + H_2O$ *condensation*

After the gelation step, condensation reactions keep occurring during what is called the aging step, thus increasing the strength of the gel[27].

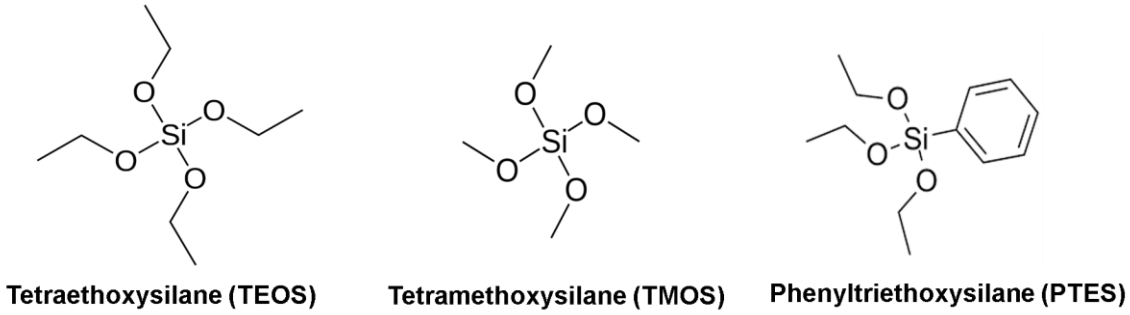

Figure 1. 8 Silica precursors used in the study

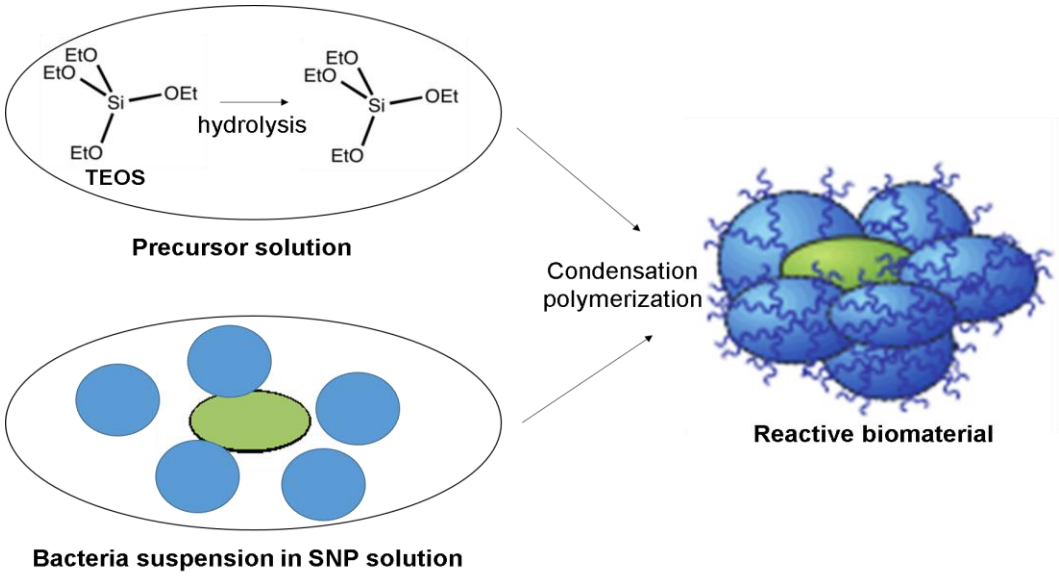

Figure 1. 9 The process of silica encapsulation. Green: Bacteria, Blue: Silica nanoparticles

1.7 Overview of dissertation

The main objective of the dissertation research is to develop an advanced bioremediation technique by combining microbial biodegradation and material science to improve current existing remediation technology. In order to achieve this objective, the research was partitioned into three specific aims:

SPECIFIC AIM 1: Develop a method for hybrid materials made of silica gel.
The goal of Aim 1 was to develop a hybrid material that can be applied to waste water treatment. A method to make hybrid silica materials was established and this aim is addressed in Chapter 2.

SPECIFIC AIM 2: Expand the scope of applications for the materials-biocatalyst hybrids.
The method and material developed in Aim 1 was applied to multiple bacterial strains to bioremediate different chemicals to test its versatility and robustness. This aim is addressed in Chapter 3 and 4.

SPECIFIC AIM 3: Investigate silca-biocatalyst hybrids to make materials that adsorb and degrade chemicals.
The hydrophobic silca-biocatalyst was developed to remove high concentrations of hydrophobic chemical spills. A new bioremediation technology can treat herbicide spills on site as addressed in Chapter 5.

CHAPTER 2 Silicon Alkoxide Cross-Linked Silica Nanoparticle Gels for Encapsulation of Bacterial Biocatalysts

2.1 Summary

A method is developed for encapsulation of bacterial biocatalysts in silica gels formed by silica nanoparticles (SNP) and a silicon alkoxide crosslinker. Formulation of the gel was optimized by changing the SNP size, SNP to crosslinker ratio and crosslinker functionality. Hydrolysis and condensation reactions of silicon alkoxide were controlled by water to alkoxide ratio (*r*) and pH of the solution. FTIR analysis verified that a reactive and temporally stable silicon alkoxide crosslinker was obtained. As a case study, recombinant *Escherichia coli (E.coli)* cells expressing atrazine dechlorinating enzyme AtzA were encapsulated. Synthesized catalytic biomaterials (silica gel encapsulated bacterial biocatalysts) were evaluated based on their gelation time, biocatalytic activity and mechanical strength. Diffusivity assays and SEM were used for characterization of the gel structure. We found that SNP to crosslinker ratio affected all the evaluation features, whereas crosslinker functionality primarily affected gelation time and SNP size affected the mechanical strength and diffusivity. Based on systematic evaluation, we selected three gel formulations and subjected them to long-term activity assay in a continuous-flow bioreactor for removing trace levels of atrazine. The effluent atrazine

concentration was sustained below 30% of the influent concentration, < 3ppb, for 2 months.

2.2 Introduction

Silica gels have been extensively studied for encapsulation of whole cells for different applications in biotechnology and biomedical engineering. In most of these applications, ensuring biocompatibility (*i.e*. encapsulated cell viability) during the encapsulation process and in the resulting gel has been a major challenge. Many studies were conducted to increase the biocompatibility of the encapsulation processes[28] by removing the alcohol produced by the gelation process[29] or by incorporating additives (such as polyethylene glycol (PEG), glycerol) into the gel [30, 31]. However, recent studies reported that biocompatibility is not essential for biocatalysis applications where a thermodynamically favorable reaction is catalyzed by intracellular enzymes. For example, Fennouh *et al.* reported catalytic activity in silica gels that contained encapsulated *E. coli* cells with compromised cell membranes (observed by electron microscopy) [32], Nassif and Livage suggested that encapsulated bacteria can function as a "bag of enzymes" and suggested that the cells can still be enzymatically active even if they had compromised membrane integrity [33]. In two different studies [34, 35], it was shown that activity of the intracellular enzyme β-galactosidase increased significantly when encapsulated *E.coli* were treated with organic solvents to enhance the permeability of the cell membrane (and by potentially compromising it). These results showed that for biocatalysis applications that

do not require cell viability, steps to increase biocompatibility (such as alcohol removal during encapsulation or incorporation of costly organic polymer additives to protect the cells) can be eliminated. In the present study, our aim was to sustain and potentially enhance biocatalytic activity while preventing leakage of intracellular enzymes from the biomaterial. Moreover, we sought to keep the cost of the process and the biomaterials low by bypassing the need to preserve cell viability.

Gel microstructure directly affects diffusivity of the chemicals through, and mechanical strength of, the porous silica material. Therefore, it is desirable to develop encapsulation methods that maintain catalytic activity of the encapsulated organisms, while simultaneously optimizing chemical and physical properties of the gels. The conventional silica gel encapsulation method is the sol-gel transition of a silicon alkoxide [36]. In a typical process, a silicon alkoxide such as tetraethyl orthosilicate (TEOS) is hydrolyzed in the presence of water and an acidic catalyst. Depending on the pH and temperature of the solution, the reactive silanol (Si-OH) groups of the hydrolyzed silicon alkoxide go through condensation reactions to form siloxane (Si-O-Si) bonds, developing a 3D porous gel structure. The cells are added to the solution after the hydrolysis reaction is completed and they get entrapped within the gel during the condensation process (polymerization). One limitation of this method is realized when the cells are exposed to acid, which can hamper the activity of the intracellular enzymes or inactivate them irreversibly. To eliminate this problem, the common practice is to adjust the pH of the solution before adding cells. While neutralization of the pH can preserve enzyme activity, it may

sacrifice gel microstructure control, resulting in gels of inadequate diffusion or inferior mechanical properties.

Silica nanoparticles (SNPs) are also appealing as precursors for silica encapsulation of bacteria due to their commercial availability at high volumes and low cost. SNPs are available in various sizes ranging from nanometers to micrometers, enabling the microstructure of a silica gel to be fine-tuned by using SNPs of different diameters. SNPs are commonly stabilized in highly alkaline solutions and by lowering the pH of the solution it is possible to obtain a gel. Finnie *et al.* have shown that sulfate-reducing bacteria can be encapsulated in such a gel obtained by lowering the pH of Ludox SM-30 SNP sol [37]. However, cell encapsulation by using SNPs exclusively enables limited control on the process and the properties of the formed gel. Therefore, SNPs are more commonly used in combination with other precursors such as sodium silicate [35]. However, it was reported that mechanical stability, as determined by Young's modulus of the gel, of sodium silicate + SNP gels decreases when the SNP concentration is increased [38]. Therefore, in this study, we opted to use a silicon alkoxide precursor (TEOS or MTES) to act as a crosslinker for the SNPs. After the pH of the SNP sol was neutralized, the bacteria were mixed with the aqueous sol and hydrolyzed silicon alkoxide was added to induce cross-linking and foster polymerization. Using this approach, it was possible to fine-tune the microstructure, and therefore the diffusivity of the gel, by altering the SNP size. A range of SNP to silicon alkoxide ratios were investigated to ensure formation of

an SNP-governed microstructure and silicon alkoxide functionality was investigated for its potential effects on the process and gel structure.

We applied the methods described above to an important practical problem, using recombinant *E. coli* cells expressing the atrazine dechlorinating enzyme AtzA to transform atrazine to hydroxyatrazine. Atrazine (2-chloro-4-ethylamine-6-isopropylamino-*s*-triazine) is one of the most commonly used agricultural herbicides in the U.S. and its concentration in drinking water is regulated by Environmental Protection Agency (EPA). The World Health Organization (WHO) determined an acceptable daily intake limit of 0.1 mg/L (~100 ppb) for atrazine in drinking water [39]; whereas EPA determined an upper limit of 3 ppb as an annual average [40]. Currently, atrazine is removed from drinking water by filtration methods that rely on adsorption, most commonly activated carbon, that has to subsequently be disposed of or incinerated with some loss of the material. In this regard, a biocatalytic material that degrades atrazine is desirable for environmental sustainability provided that it is cost competitive. The overall challenges for a silica-based bioremediation system are that it needs to: (1) function well with trace levels of atrazine found in drinking water (< 10 ppb), (2) sustain function for weeks or months in a continuous, flow-through process, (3) be mechanically strong and stable under continuous flow conditions.

Successful applications of atrazine bioremediation at high concentrations (samples from farm run-off waters or buffer solutions fortified with atrazine), from 10 to 30 ppm, have

been reported [41-44] but most laboratory studies have used much higher atrazine concentrations that do not mimic actual environmental situations. Galindez-Najera *et al.* reported complete removal (*i.e*. effluent concentration below detection limit of assay) of atrazine using a two-stage biofilm reactor with a binary culture of *Stenotrophomonas maltophilia* and *Arthrobacter* sp., at over 30,000 ppb influent atrazine concentration [42]. Liu *et al.* reported above 90% removal efficiency of atrazine from wastewater using a membrane bioreactor containing *Pseudomonas* sp. ADP, at ~15,000 ppb influent atrazine concentration [43]. While these approaches are suitable for removal of atrazine at high concentrations, effluent concentrations are still significantly higher than 3 ppb, despite the high removal efficiency. In a recent study, Buttigleri *et al.* utilized a membrane bioreactor (MBR) with a denitrifying mixed culture atrazine treatment at low concentrations. [45] With a 10 ppb influent concentration, an average removal of 15% was obtained over a 3-month period. In addition to the low performance of the reactor at low atrazine concentrations, it is also not desirable to have living bacteria in a reactor for drinking water treatment. This requires further downstream processing to ensure that any bacteria that leach from the system are removed from water, increasing the overall cost of the system.

Our research group recently encapsulated recombinant *E. coli* cells expressing atrazine dechlorinating enzyme AtzA into silica gels and the cells were killed by a post-encapsulation heat treatment process. Batch activity tests were run with an ~30,000 ppb atrazine solution and biocatalytic activity of non-viable encapsulated cells (0.44-0.66

μmol/g cells-min) was comparable to free cell activity (0.61 μmol/g-min) but sustained for a much longer time,4 months, compared to free cells [25]. However, at low concentrations of atrazine (10 ppb), the biocatalytic activity of the cells was several orders of magnitude lower and the atrazine degradation of the encapsulated cells in a packed bed reactor gradually decreased to an immeasurable rate within 2 weeks. Mechanical integrity of the gels was also shown to degrade significantly during that time (data not shown).

To overcome the limitations of the previous studies, while also developing an economically feasible product, the present study sought to develop catalytic silica biomaterials that maintained high atrazine removal for long durations at a low influent concentration. Utilizing three of the developed formulations in a flow-through packed bed reactor system, effluent atrazine concentration was maintained at a level below 30% of the 10 ppb influent for 2 months. Additionally, as compared to our previous study [25], mechanical strength of the material was improved from a yield load of 0.2 N to a maximum of 3 N and cost of the product is significantly reduced by eliminating high cost silica precursors and organic polymer additives from the formulation. The design was conducted through a step-by-step evaluation/elimination process, based on biomaterial characteristics such as gelation time, transient catalytic activity at high concentration and mechanical strength (Fig 2.1). Additional characterization studies (diffusivity and cell viability assays, SEM) were also performed for better interpretation of the results. Our results suggest that the developed catalytic biomaterial(s) can be used

for continuous treatment of water to remove environmentally-relevant concentrations of atrazine from drinking water. On a broader note, the proposed method can also be used to encapsulate different biocatalysts, aimed to treat other low concentration contaminants (pharmaceuticals, personal care products, endocrine disruptors, etc.) from drinking water supplies.

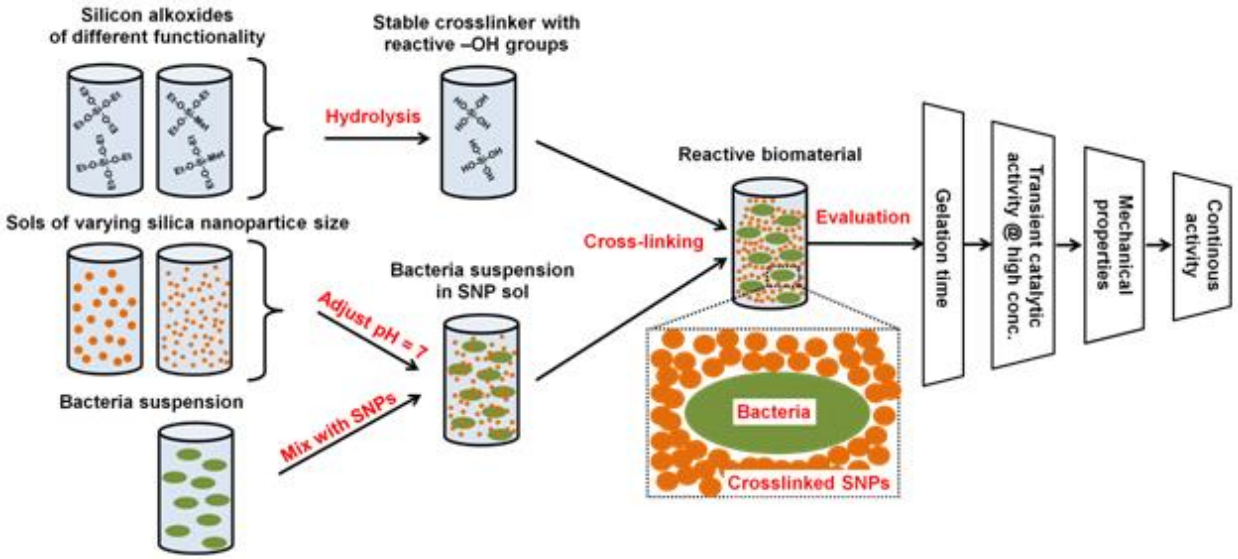

Figure 2. 1 Schematic of encapsulation and evaluation method

2.3 Materials and Methods

2.3.1 Materials

Tetraethoxysilane (TEOS: $Si(OC_2H_5)_4$) and triethoxymethylsilane (MTES: $CH_3Si(OC_2H_5)_3$) of reagent and technical grades, respectively were purchased from Sigma-Aldrich (Sigma-Aldrich Corp. St. Louis, MO, USA). Ludox HS40 and Ludox TM40 SNP sols were purchased from Sigma-Aldrich and NexSil 85-40 and NexSil 125-40 SNP sols were generously provided by Nyacol (Nyacol Nano Technologies Inc., Ashland, MA, USA). All the SNP sols had 40% SiO_2 content by mass and were stabilized by sodium ions. The only difference between different SNPs is the nanoparticle size and their initial pH, as shown in Table 2.1. Technical grade atrazine was provided by Syngenta (Syngenta Crop Protection, NC, USA). All the chemicals were used as received. Ultrapure water (UPW) was used in all the experiments. UPW was prepared by filtering deionized water through a Milli-Q water purification system (Millipore, Billerica, MA, USA) to a final electrical resistance of > 18.2 MΩ/cm.

Table 2. 1 Properties of the SNP sols used in this study

Commercial Name	Abbreviation	Average particle diameter [nm]	Density [g/mL]	Initial pH
Ludox HS40	HS40	12	1.3	9.7
Ludox TM40	TM40	22	1.3	9.0
Nexsil 85-40	NS85	50	1.2	9.5
Nexsil 125-40	NS125	85	1.2	9.5

2.3.2 Bacterial strains and growth conditions

The growth conditions were identical to those described previously, except for some minor modifications. [25] *E. coli* DH5 α (pMD4) [46] was grown at 37 °C in superbroth medium with vigorous aeration, supplemented with 30 μg/ml chloramphenicol. Intermediate cultures were grown by inoculation with 1% (v/v) starter culture and diluted 100-fold in production flasks containing the same medium. Cells were harvested by centrifugation at 6,000 x g for 20 min at 4 °C.

2.3.3 Catalytic biomaterial synthesis and encapsulation

Hydrolysis and condensation reactions of silicon alkoxides were controlled by adjusting water to silicon alkoxide molar ratio (*r*) and pH of the solution. 1:5.3:0.0013 molar ratio of silicon alkoxide:water:HCl was used to obtain $r = 5.3$ and a pH of 4, which resulted in a fully-hydrolyzed silicon alkoxide solution with a slow condensation rate. The values for *r* and pH were selected based on previous literature reports. Brinker reported that, during hydrolysis with sub-stoichiometric amounts of water ($r < 4$), condensation starts before complete hydrolysis and alcohol-producing condensation reactions are favored. [47] However, increasing *r* excessively can promote depolymerization of the gel by siloxane bond cleavage reactions. Therefore, an *r* value that is slightly over 4 was selected. In the pH 3-8 range, hydrolysis rate of alkoxysilanes increases when acidity or alkalinity of the solution increases and condensation rate increases with increased alkalinity. [48] Therefore, the pH of the solution was adjusted to 4 to obtain fast hydrolysis and slow condensation

reactions. This ensured that the silicon alkoxide did not polymerize by itself but cross-linked the SNPs. The hydrolyzed silicon alkoxides were kept in an ice bath until they were used to further slowdown condensation reactions.

For verification of the desired (fully hydrolyzed, slow condensation) state of the silicon alkoxide, progress of the hydrolysis and condensation reactions were observed by IR spectroscopy. After the initial phase separation of the silicon alkoxide-water-HCl solution disappeared, 0.15 μL samples were extracted from the solution in 15 minute time intervals. Samples were placed between two BaF_2 windows. The windows were sealed with vacuum grease to prevent evaporation. The sealed sample was transferred to an infrared microscope attached to an FTIR spectrometer (Thermo-Nicolet Continuum equipped with a Mercury Cadmium Telluride detector, Thermo Electron, Waltham, MA, USA). The FTIR sampling resolution was 4 cm^{-1}, and 128 IR scans were averaged per spectrum in the 4000-740 cm^{-1} wavenumber range. The IR spectra were analyzed using OMNIC (Thermo-Nicolet) software. This experiment was run in duplicate. The state of hydrolysis and condensation reaction rates was determined by measuring the intensity of δ-OH bending peak of water at 1650 cm^{-1} and the CH_3 bending peak of silicon alkoxide (TEOS, MTES) and produced ethanol at 1384 cm^{-1}.

The pH of the SNP sol was adjusted to neutral pH by adding 1M hydrochloric acid to avoid inactivation of the enzyme and to eliminate initial pH variations between different SNP sols. After pH adjustment, bacteria were momentarily suspended in a 1 g/mL

aqueous suspension and added to the SNP sol. The added amount was adjusted such that the final concentration of encapsulated bacteria in the gel was 0.125 grams/mL of silica precursor (SNPs and silicon alkoxide combined).

Silicon alkoxide was added to the bacteria + SNP solution by pipetting a few times to obtain a homogeneous sample. SNP sol to silicon alkoxide ratios were selected as 7:1, 3:1 and 1:1 (v/v). Mass contribution of silica precursors to the gel microstructure can be estimated using two assumptions: (1) Silicon alkoxide is fully hydrolyzed (2) All SNPs are cross-linked by silicon alkoxide. With these assumptions, Table 2.2 shows the estimated silica content contribution from different precursors of the gels.

Table 2. 2 Total silica contribution ratio of SNP sol/crosslinker by mass based on volumetric ratio

Crosslinker	**TEOS**			**MTES**	
SNP sol/crosslinker (v/v)	**7:1**	**3:1**	**1:1**	**7:1**	**3:1**
Ludox HS40	8.45	3.62	1.20	7.54	3.23
Ludox TM40	8.45	3.62	1.20	7.54	3.23
Nexsil 85-40	7.80	3.34	1.11	6.96	2.98
Nexsil 125-40	7.80	3.34	1.11	6.96	2.98

The final product was either placed in molds or vials for gelation, depending upon the specifics of the experiment to be conducted. The gelation occurred within seconds to hours depending on the formula used. For molding of fast gelation time formulations, precursors were cooled by immersion in an ice bath to slow gelation. During gelation and storage, the vials were kept closed and molds were sealed with a PVDC film to prevent drying.

2.3.4 Characterization

2.3.4.1 Gelation time

Biomaterials were synthesized in glass scintillation vials and gently shaken intermittently to determine the degree of crosslinking of the gel. The time intervals between observations were increased with increasing duration of the experiment. Gelation time was determined as the time when solution in the container no longer exhibited observable flow when agitated.

2.3.4.2 Biocatalytic activity assays

Catalytic activity of the biomaterial is determined by transient and steady-flow activity assays. In transient activity assays, biomaterials were synthesized in glass scintillation vials as 2 mL cylindrical blocks (3.5 mm thickness and ~570 mm^2 surface area), in triplicate. Three mL of 150 μM (32.4 ppm) atrazine solution in 0.1 M potassium phosphate buffer (at pH 7.0) was added on top of each gel and vials were placed on a

rotary shaker. Samples were collected after 60 min of incubation and immediately immersed in a 90°C water bath to stop their catalytic activity by denaturing the enzyme. After inactivation of the enzyme, samples were filtered through a 0.2-µm pore size PTFE syringe filter to remove any particulates that may be released from the material. The concentrations of atrazine and its metabolite, hydroxyatrazine, were measured by using high performance liquid chromatography (HPLC) as described by de Souza *et al.* [46] Transient activity assays were performed right after encapsulation (day 0) and after 4 days of storage within scintillation vials at room temperature. The vials were kept tightly closed to prevent samples from drying.

For steady-flow activity measurements, biomaterials were synthesized in stainless steel molds as hemispherical beads of 1.5 mm diameter. 6.6 grams of beads were transferred into 15 mL glass bioreactors (Buchner funnels, coarse grade) that were connected to a peristaltic pump drive (Masterflex L/S variable speed modular drive, Cole-Parmer, Vernon Hills, IL, USA). Ten ppb atrazine solution in 0.1 M potassium phosphate buffer (at pH 7.0) was used as influent solution to the bioreactors and was replenished whenever required during experimentation. A slow flow rate of 0.05 mL/min was chosen to maximize residence time (5 hours) and minimize the produced effluent water. Collected samples were treated as previously described and concentration of atrazine in the effluent fluid was measured using the Atrazine Plate Kit (Beacon Analytical Systems Inc., USA) in accordance with the manufacturer's instructions.

2.3.5.3 Mechanical properties

Mechanical tests were performed on hemispherical beads (in triplicate) which were synthesized as previously described. A uniaxial testing machine was used with a 5 N load cell with 0.05 N resolution (Instron, Norwood, MA, USA). During testing, constant displacement rate was applied to the material until the material failed. Results were obtained in the form of a load-displacement curve.

2.3.5.4 Cell viability assay

Catalytic biomaterials were synthesized in scintillation vials, in triplicate. A 0.1 g aliquot of the material was pulverized using a mortar and pestle and the crushed material was suspended in 2 ml of sterile phosphate-buffered saline. The solution was serially diluted and spread-plated onto Luria-Bertani agar with 10 μg/ml chloramphenicol. Cell counts were determined based on the number of observed Colony Forming Units (CFUs) after overnight incubation.

2.3.5.5 Diffusivity assay

Trypan blue solution (0.4%) purchased from Sigma (Sigma-Aldrich Corp. St. Louis, MO, USA) was used to evaluate the diffusivity of the synthesized gels. Four hundred μL of gels without cells were synthesized in polystyrene cuvettes with 10x4 mm base dimensions. One hundred μL of Trypan blue solution was added on top of the gel and

progress of the dye diffusion in the gel was recorded by taking a picture every hour for 6 hours.

The diffusivity of the dye in the gel was evaluated by using the error function solution of the 1D diffusion problem with constant concentration boundary condition [49]:

$$C(x,t) = C_{BC} \times \mathrm{erfc}\left(\frac{x}{2\sqrt{Dt}}\right)$$

In this equation C is concentration, x is distance from the boundary, C_{BC} is fixed boundary condition concentration, t is time and D is diffusivity. To solve for D, we have used a 4 step image processing technique: (1) The images were converted to grayscale, (2) The intensity values of the pixels were averaged along the horizontal axis, (3) $C(x)/C_{BC}$ was determined from the ratio of the averaged intensity along a given horizontal axis at distance x over the averaged intensity at x_0 – averaged intensity at x_∞ (far enough from the boundary such that boundary condition has no effect), (4) x values corresponding to $C(x)/C_{BC}$ = 0.1, 0.2 and 0.3 were determined and obtained D values were averaged. All the image processing and computations were done using MATLAB.

2.3.5.6 Microstructure

Gel and encapsulated bacteria were examined by scanning electron microscopy (Hitachi S-4700). The encapsulated bacteria were fixed in 2% glutaraldehyde and then 1% osmium tetroxide in cacodylate buffer (0.1 M sodium cacodylate, pH 7.3). After fixation, the samples were gradually dehydrated in an up-grading series of ethanol (50, 70, 80, 95

and 100%). The samples were then dried in a Critical Point Dryer (Tousimis Model 780A) using liquid carbon dioxide as transitional fluid. Finally, the samples were sputter-coated with a thin layer of gold-palladium and examined under the SEM.

2.4 Results and discussion

In reporting the results, different gel formulations are denoted as SNP – SNP to crosslinker ratio (v/v) – Crosslinker type (example: HS40 – 3:1 – TEOS).

2.4.1 State of hydrolysis and condensation reactions of silicon alkoxide crosslinkers

After 1 hour of stirring, it was visually observed that the mixture became miscible in both TEOS and MTES solutions. This is due to destruction of water and production of ethanol during hydrolysis reactions. Based on the TEOS-water-ethanol ternary phase diagram, it is expected that ~85% of the water was destroyed at this point. [50] Fig 2.2 shows the collected IR spectra from samples in terms of normalized ratio of δ-OH bending peak of water to CH_3 bending peak (actual spectra shown on inset) between 1 to 3 hours at 15 minute intervals. In both TEOS and MTES solutions, the ratio initially decreased for 15 to 30 minutes, indicating continuing hydrolysis. Then the water content in the solution started increasing with respect to the total amount of CH_3, contributed from both silicon alkoxide and produced ethanol during hydrolysis reactions. This shows that hydrolysis was completed and condensation reactions were taking place, as expected based on the selected *r* and pH of the solution. It can also be seen that the ratio increased very slowly, indicating that condensation rate was low and the hydrolyzed silicon alkoxide solution was stable over time. It should be noted that while samples were being transferred to the BaF_2 windows, it is possible that minute volumes of ethanol have evaporated. This would increase the H_2O to CH_3 amplitude ratio and explain the variation in the data points.

Hence, it is possible that the increase is due to a combined effect of condensation reactions and ethanol evaporation, which means that silicon alkoxide solution is more stable than suggested by the data. Since we only seek to show temporal stability over the duration of encapsulation process, we have stopped FTIR analysis after 3 hours. Stability of the silicon alkoxide solution is also verified by leaving the hydrolyzed silicon alkoxide solution (both TEOS and MTES) in a scintillation vial without addition of SNPs. No gelation was observed within 2 days of storage at room temperature.

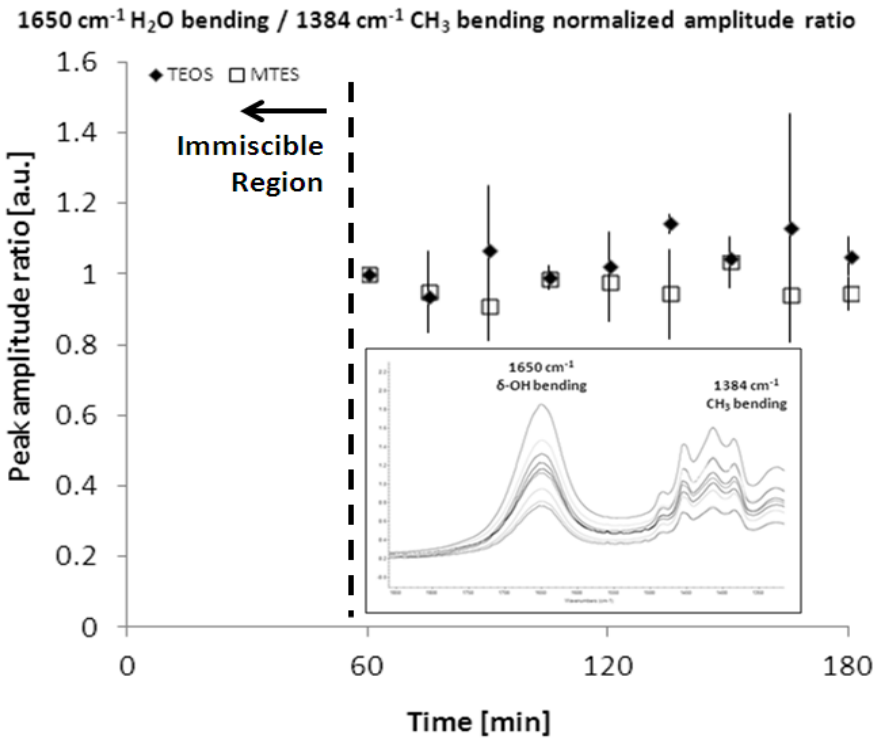

Figure 2. 2 Evaluation of the hydrolysis/condensation process by evolution of the peak amplitude ratio of δ-OH bending / CH3 bending

2.4.2 Silica gel: Gelation time, diffusivity, mechanical properties and microstructure

Materials were initially characterized by their time to gel, as shown in Table 2.3. Gels cross-linked by MTES gelled in the time-scale of hours, whereas gels with TEOS crosslinker gelled within seconds to minutes. It was also observed that increasing SNP size and SNP to crosslinker ratio increased gelation time. In fast gelation time formulations, insertion in an ice bath was sufficient to slow down crosslinking for molding. In the range of our experiments, the most prominent factor that affected gelation time was the functionality of the silicon alkoxide crosslinker. This result can be attributed to trifunctional MTES having less reactive sites for siloxane bond formation compared to tetrafunctional TEOS. This result is in accordance with the observations of Innocenzi *et al.*, [51] who observed an increase in gelation time of TEOS/MTES gels with increasing MTES content. Another result was that gelation time increased when SNP to crosslinker ratio increased and larger SNPs were used. This can be explained by the decrease in the total number of reactive sites per volume, as SNP content increases or nanoparticles get larger.

Table 2. 3 Gelation times for the catalytic biomaterials synthesized with selected parameters (Gelation times are given as: Seconds (Sec): t_{gel} < 1 min, Minutes (Min): 1 min < t_{gel} < 10 min, Hour (Hr): 10 min < t_{gel} < 2 hours and Hours (Hrs): t_{gel} > 2 hours)

SNP sol	Ludox HS40			Ludox TM40			Nexsil 85-40		Nexsil 125-40		
Crosslinker	TEOS		MTES	TEOS		MTES	TEOS	MTES	TEOS	MTES	
SNP to crosslinker ratio (v/v)	3:1 1:1	7:1	7:1 3:1 1:1	3:1 1:1	7:1	7:1 3:1 1:1	7:1 3:1 1:1	7:1 3:1 1:1	7:1 3:1 1:1	3:1 1:1	7:1
Approximate gelation time	Sec	Min	Hr	Sec	Min	Hr	Min	Hr	Min	Hr	Hrs

Effective diffusivity of the Trypan blue dye in the selected gels is shown in Fig. 2.3. It can be observed that the highest diffusivities were around 2.25 x 10^{-4} mm^2/s and were obtained with largest size (NS125 ~85 nm) nanoparticles. In all gels, diffusivity decreased with decreasing SNP size, except for HS40-3:1-MTES gel. Data from the 1:1-TEOS gels and HS40-3:1-TEOS gel are not shown due to observed rapid propagation of the dye through cracks within the gel due to gravitational force instead of diffusion. Dye diffusivity experiments show that the diffusivity of the gel can be controlled by varying the SNP size. It was also observed that the effect of SNP size on diffusivity is the most significant in 7:1-TEOS gels and least significant in 3:1-TEOS gels. This can be explained by SNP size having more effect on the microstructure in 7:1 SNP to crosslinker ratio gels as compared to 3:1 gels. This can also be observed in Fig. 2.4. In 12 nm SNPs (HS40), when SNP to crosslinker ratio was 7:1, SNPs were linked to each other with no observable crosslinker. However, when the ratio decreased to 1:1 (*i.e*. crosslinker content increased), SNPs were linked together with observable crosslinker. Note that the particles in 1:1 ratio appear slightly larger, because of crosslinker deposition on the surface before crosslinking. Similar effect of SNP to crosslinker ratio was observed for 50 nm SNPs (NS85). In 7:1 SNP to crosslinker ratio, particles were linked together with small area of contact. In 1:1 ratio, smaller aggregates of silica were observed along with the SNPs, formed by condensation reactions of the crosslinker. Note that even though the silicon alkoxide is stable in low pH conditions of the hydrolysis, when SNPs are introduced the pH of the solution rises and condensation reactions are unavoidable. Perullini *et al.* reported the effect of SNP content on diffusivity in sodium silicate + SNP gels, where

diffusivity of cationic dye Crystal Violet was used as a model. They reported that transport was faster when the gel was richer in SNPs. [38] We observed a similar trend only in TEOS cross-linked NS125-7:1 and NS85-7:1 gels. For MTES cross-linked gels, the effect of SNP to crosslinker ratio did not have a significant effect on gel diffusivity. The decreasing effect of larger SNP size on gel diffusivity was observed in all MTES gels, except for TM40 to HS40 transition in 3:1 gels. Encapsulated cells in silica gel are shown in Fig. 2.5.

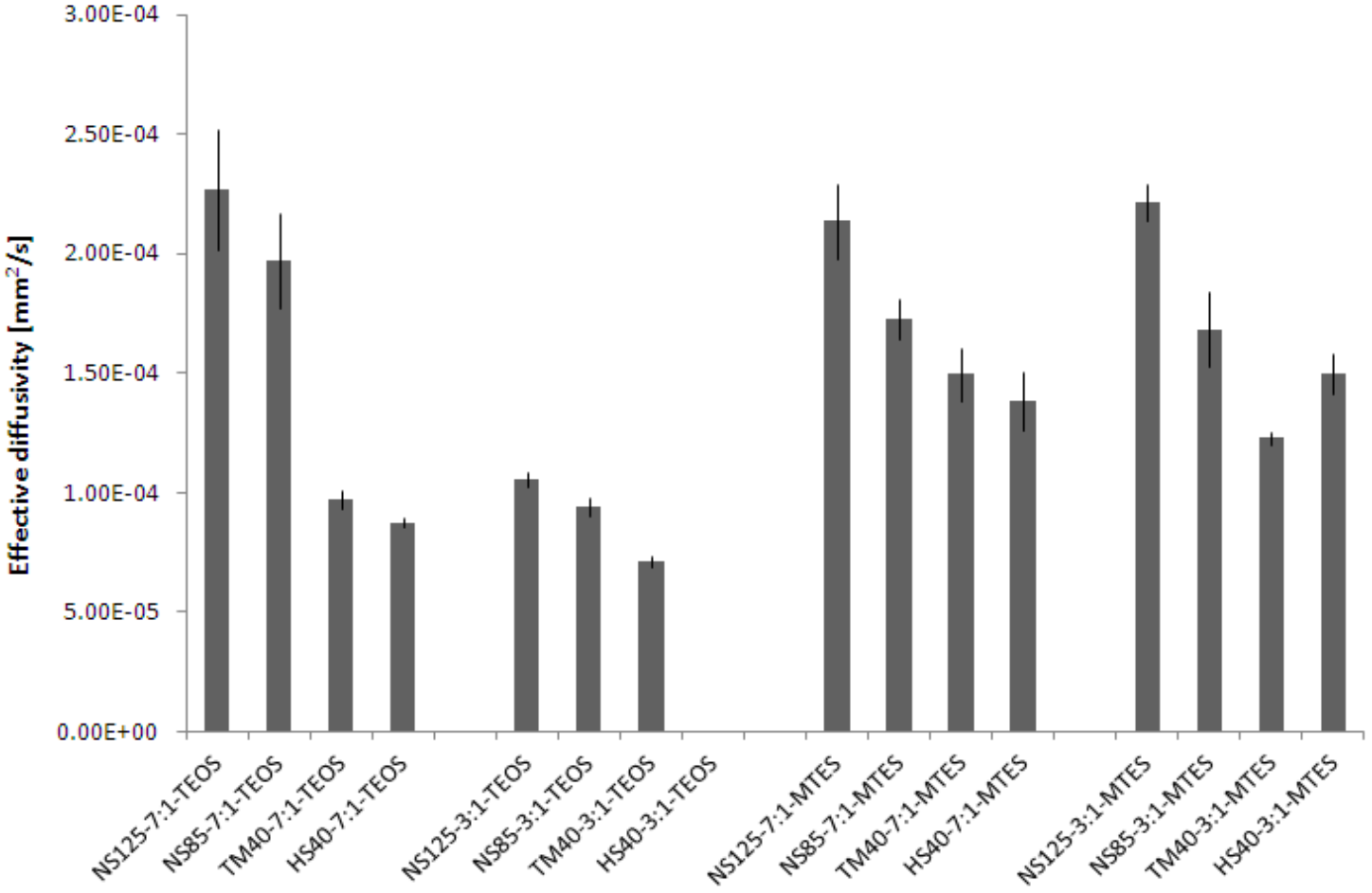

Figure 2. 3 Effective diffusivity of the selected gels

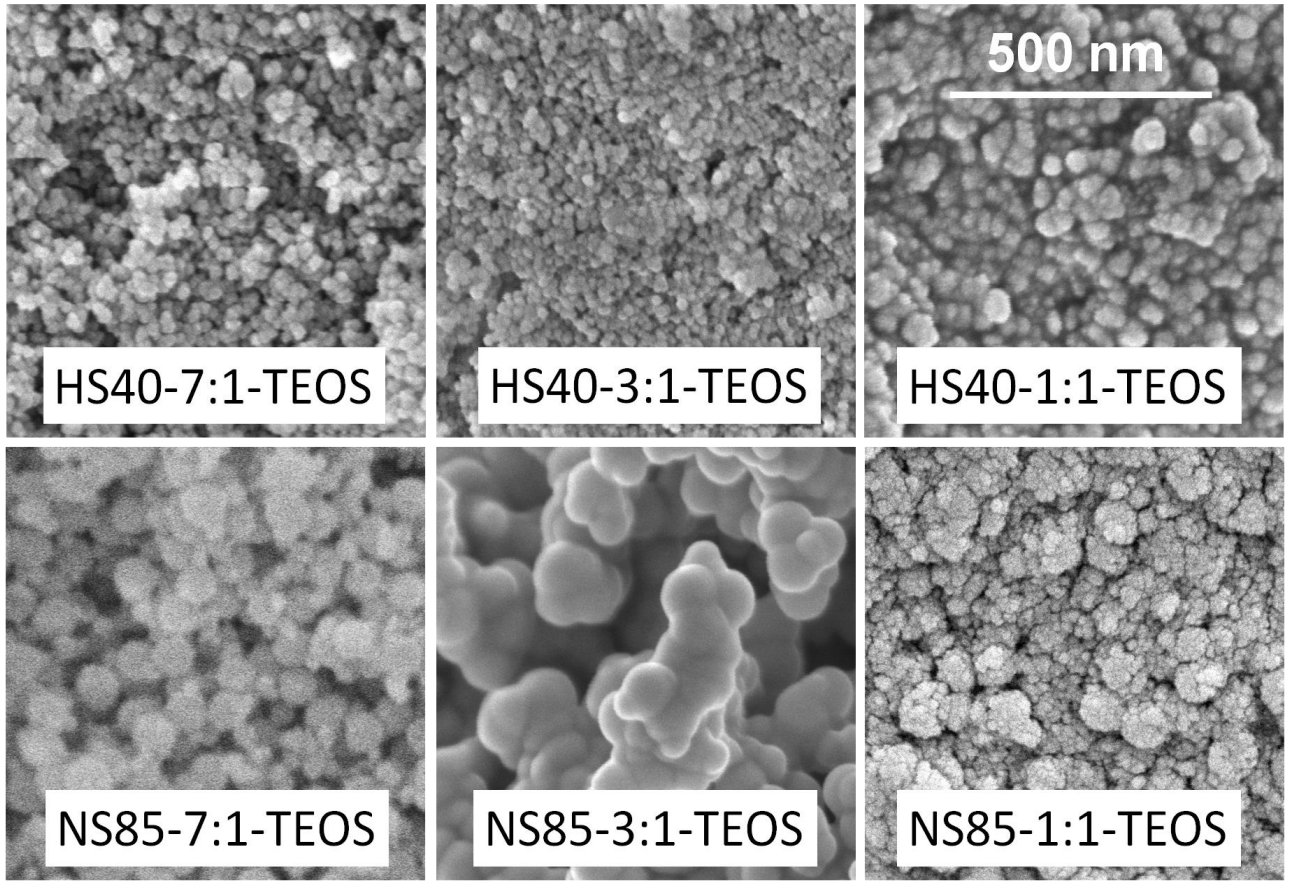

Figure 2. 4 Particle-scale SEM micrographs of TEOS cross-linked gels with different SNP sizes (HS40 ~12nm and NS85 ~50nm) and SNP to crosslinker ratios (the scale-bar is the same for all images)

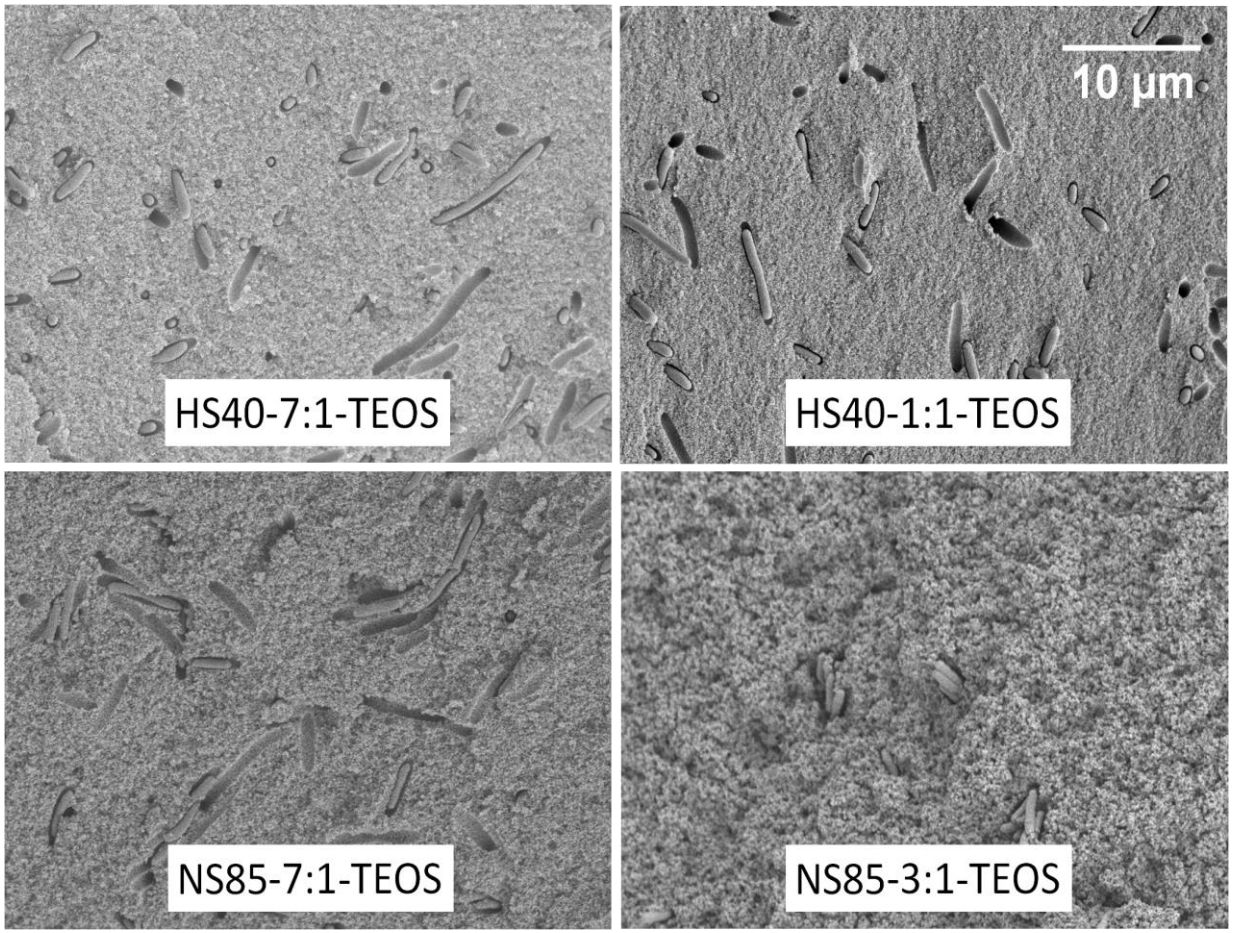

Figure 2. 5 Cell-scale SEM micrographs of TEOS cross-linked gels with different SNP sizes (HS40 ~12nm and NS85 ~50nm) and SNP to crosslinker ratios (scale-bar is the same for all images)

It should be noted that, a macroporous structure was observed in SEM micrographs of the NS85-3:1-TEOS gel. This was caused by excessive crosslinker deposition on the SNP surface and large SNP size. However, it is interesting that this macroporous structure was not conserved when SNP to crosslinker ratio was increased to 7:1 or SNP size was increased to ~85 nm (NS125 SNPs). One would expect to see increased diffusion rates of NS85-3:1-TEOS gel, with increased porosity seen in SEM images, however this was not the case as shown in Fig. 2.3. Therefore, microstructures of the gels (especially the conditions leading to the observed macroporous structure of NS85-3:1-TEOS gel) needs to be further investigated in future studies.

Mechanical properties of different samples were evaluated on the basis of load at compressive yield (Fig 2.6). In both TEOS and MTES cross-linked gels, best mechanical properties were obtained with the smallest size SNPs (HS40 and TM40 respectively) and there was a decreasing trend in load at compressive yield when SNP size was increased. When 12 nm size HS40 SNPs were used, decreasing the SNP to crosslinker ratio decreased the load at compressive yield of the gel. On the contrary, when 85 nm size NS125 SNPs were used, the effect was reversed. Independent from the crosslinker functionality, we observed a decreasing trend in load at compressive yield of 7:1 gels with increasing particle size. As seen in Fig. 2.4, for 7:1 gels, number of SNPs per volume increases when SNP size is decreased. Therefore, the number of crosslinking sites increased per volume which can explain the increase in compressive strength. MTES cross-linked gels had higher compressive strength than TEOS in TM40-7:1 and

NS125-7:1 formulations. However, a wider range of gel formulations need to be tested to evaluate the effect of crosslinker functionality on mechanical strength of the gels. We selected hemispherical beads for mechanical testing since they were utilized in the flow-through biocatalytic activity assays. However, we suspect that the geometry of the samples has contributed to variation in the results, due to non-perfect curvature of the samples.

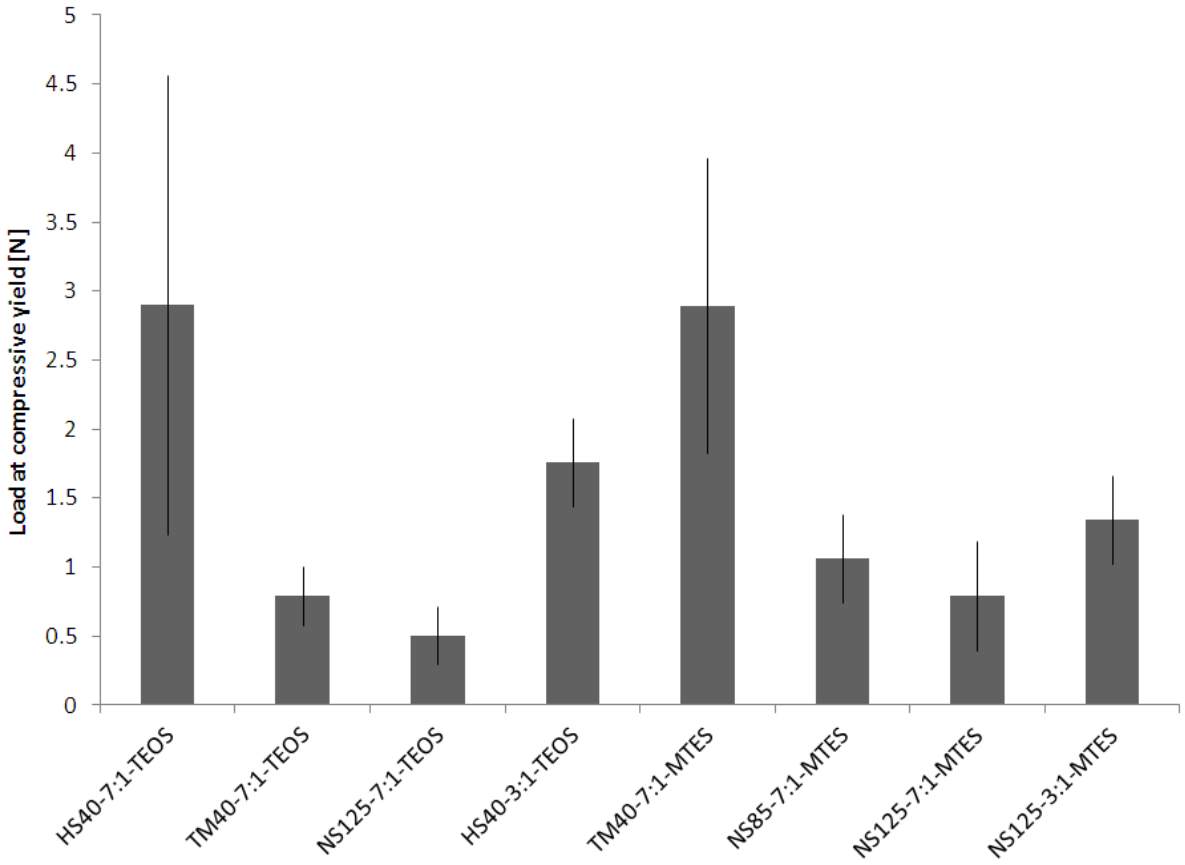

Figure 2. 6 Mechanical properties of the selected silica gels

In summary, it was observed that during gelation, silicon alkoxide crosslinkers can react with surface silanol groups of SNPs and deposit on the particles and/or form aggregates by condensation reactions. Note that even though the silicon alkoxide crosslinkers are stable after hydrolysis in low pH conditions, introduction of the SNPs in neutral pH catalyzes the condensation reactions. Therefore, it is unavoidable to obtain small aggregates of silica formed by silicon alkoxides. Higher SNP to crosslinker ratios favor microstructures dictated by SNP size as shown in Fig. 2.4 which also increases the diffusivity of the gel. However, the gels with higher diffusivity values (such as NS125-7:1-TEOS, NS125-7:1-MTES and NS125-3:1-MTES) have lower mechanical strength under compressive loading as can be seen in Fig. 2.6.

2.4.3 Bacterial biocatalyst: Cell viability and catalytic activity

Cell viability assay results are shown in Fig. 2.7. (Gel formulations with no viable cells on day 0 are not shown). On day 0, TEOS cross-linked samples with 7:1 and 3:1 SNP to crosslinker ratio had viable cells with comparable CFU counts, whereas 1:1 SNP to crosslinker ratio samples had no viable cells. MTES cross-linked samples had viable cells with 7:1 SNP to crosslinker ratio, but not with 3:1 SNP to crosslinker ratio. On day 4, only one of the TEOS cross-linked samples (HS40-7:1-TEOS) had viable cells. MTES-7:1 gels, however, had viable cells even though the CFU count has decreased 1-2 orders of magnitude on average. It is well known that ethanol is detrimental to the bacteria and time-scale of alcohol's detrimental effects is very rapid. Therefore, we expect that all the viability loss in day 0 is due to alcohol. However, alcohol does not explain the decrease

in viability after 4 day storage period. One possible explanation is the aging of the material and stiffening of the gel inducing increased mechanical stress on the cells. Another possible explanation is the desiccation of the bacteria due to lack of water. For either theory, we were unable to find evidence based on micrographs obtained after 4 days of storage (data not shown).

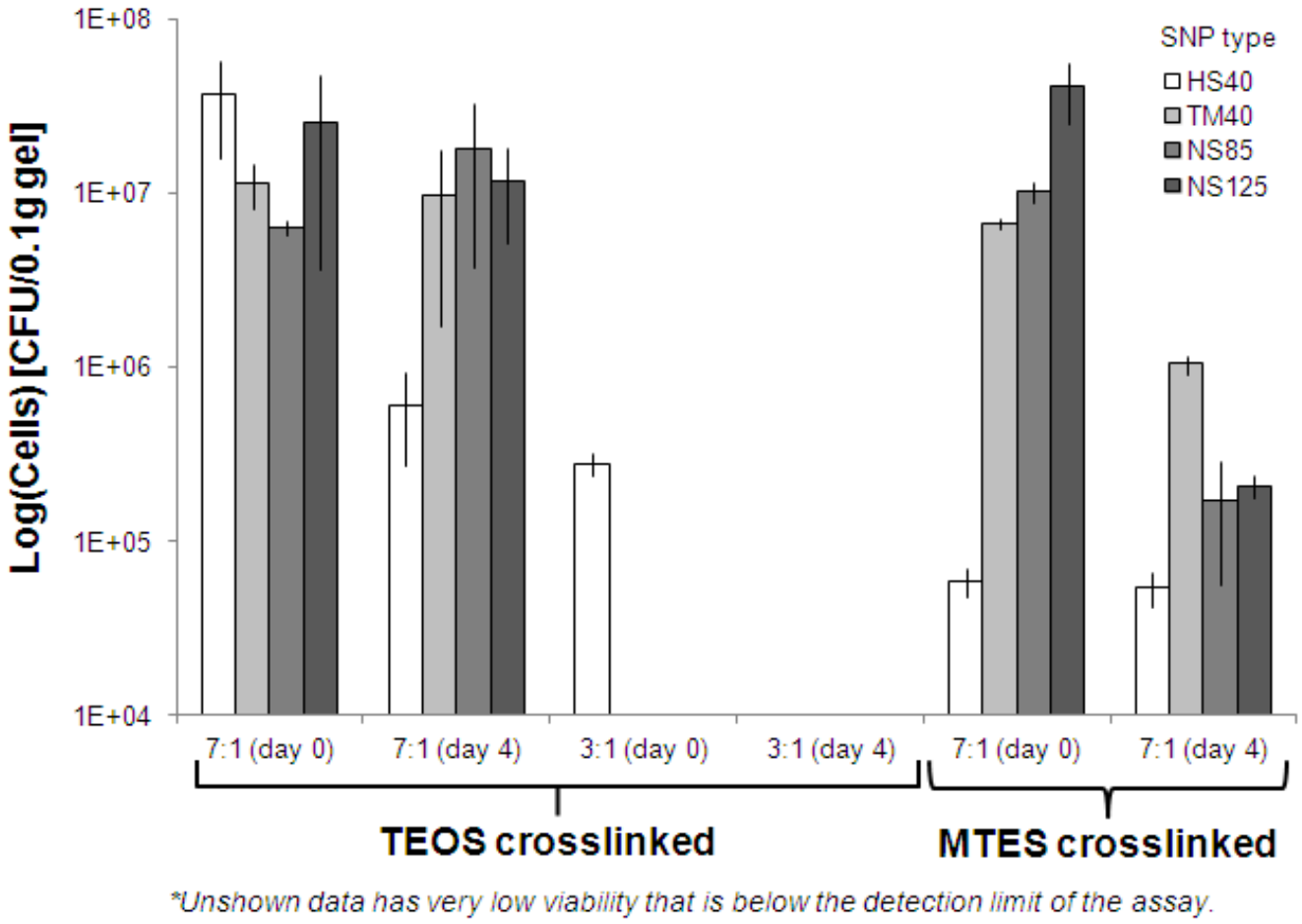

Figure 2. 7 *E. coli* viabilityin TEOS and MTES cross-linked biomaterials after encapsulation (day 0 and day 4)

Transient biocatalytic activity results show hydroxyatrazine (degradation product of atrazine by the encapsulated AtzA biocatalyst) concentration in the initially 150 μM (~32.4 ppm) aqueous atrazine buffer solution after an hour of incubation with the catalytic biomaterial. Results for TEOS and MTES cross-linked gels are shown in Fig. 2.8 (a) and (b). For TEOS cross-linked gels, the most prominent factor affecting biocatalytic activity was SNP to crosslinker ratio. On day 0, 7:1 and 3:1 samples had comparable biocatalytic activity for all SNP sizes; whereas 1:1 samples had significantly lower activity. On day 4, 7:1 samples retained 50 to 90% of their activity (except NS85) while 3:1 samples lost more than 50% activity. We did not observe a trend based on the SNP size. Based on these observations, we did not proceed with the 1:1 ratio for the MTES cross-linked gels. For MTES cross-linked gels, 7:1 and 3:1 samples had comparable biocatalytic activity for all SNP sizes on day 0, similar to the TEOS case. Likewise on day 4, 7:1 samples retained 60 to 90% of their activity (except HS40) while most of the 3:1 samples lost more than 90% of activity (except NS125). Unlike the previous case, we could observe an apparent trend based on the SNP size where activity increased slightly with increasing SNP size. MTES cross-linked gels had higher activity than TEOS gels on day 0 for all SNP sizes and SNP to crosslinker ratios. On day 4, most of the 7:1 gels with MTES crosslinker had higher activity (except HS40) and 3:1 gels with both TEOS and MTES had comparably low activity, except for NS125-3:1-MTES. We selected 8 gels out of 20 to proceed with the mechanical tests, based on their activity on day 4.

It was shown in a previous study that biocatalytic activity does not require cell viability [25] and MTES-3:1 results in Fig. 2.8 confirms this result. Based on the day 0 results in Fig. 2.7, three conclusions can be drawn:

(1) In most cases, SNP size did not significantly affect viability of the cells.

(2) When SNP to crosslinker ratio was decreased to 1:1, cell viability decreased to zero. Note that crosslinker content of the gel increases from 12.5% (7:1 ratio) to 25% (3:1 ratio) and 50% (1:1 ratio) as SNP to crosslinker ratio changes. Since hydrolyzed crosslinker solution also contains produced ethanol during hydrolysis reactions, ethanol content also doubles and quadruples respectively; which would explain the loss of viability.

(3) When the crosslinker with lower functionality was used (MTES), the cell viability diminished in 3:1 ratio, even though the alcohol content contribution from MTES is lower (assuming full hydrolysis, hydrolyzed MTES solution contains 25% less alcohol than TEOS) due to its lower functionality. Since MTES gels have longer gelation times, bacterial cell membranes are fully exposed to alcohol for longer durations, which can increase the detrimental effect of alcohol. Day 4 results show that all MTES cross-linked gels with 7:1 ratio had viability, whereas only HS40-7:1 gel had viable cells within TEOS cross-linked gels.

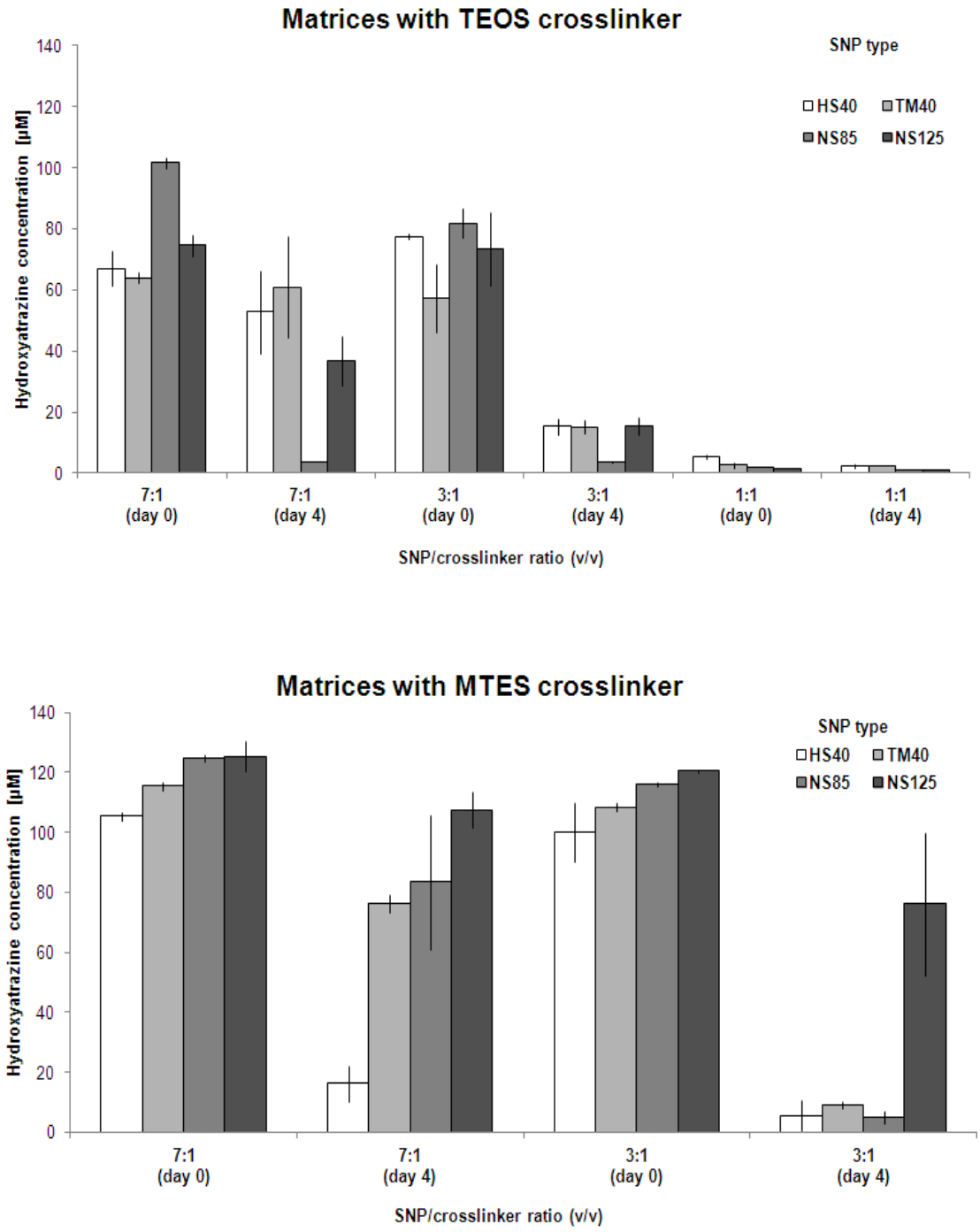

Figure 2. 8 Catalytic activity of TEOS (a) and MTES (b) cross-linked biomaterials measured by hydroxyatrazine (metabolite) concentration in solution after an hour of incubation with atrazine (day 0 and day 4)

The transient activity results show that biocatalytic activity is affected significantly by SNP to crosslinker ratio and crosslinker functionality, but not SNP size. The loss of activity with decreasing SNP to crosslinker ratio can be explained by chemical composition within the gel. When SNP to crosslinker ratio decreases, water content decreases and alcohol concentration increases and both parameters can hamper enzymatic activity. We have shown that by increasing SNP size, diffusivity of the gel increases. Therefore, we would expect SNP size to have an effect on activity if the overall reaction rate was limited by species transport in the gel. However, no correlation was observed between the catalytic activity rate of the biomaterial and its diffusivity. This result suggests that the reaction rate is either limited by the enzymatic reaction rate of AtzA or a larger transport resistance that occurs at the cell membrane or material/solution interface. It was previously reported that there is about 7% variation in the catalytic activity of free *E. coli* cells expressing AtzA [25]. Consequently, we believe that the variation in the activity of free biocatalyst contributes to the variation of activity results in encapsulated cells. In future studies, reaction kinetics studies should be conducted in both high and low concentrations of atrazine with free *E. coli* cells expressing AtzA to better understand the reaction/diffusion rate limitations on the overall catalytic activity rate. The effects of pH and alcohol content on the catalytic activity rate of the free cells should also be investigated.

Three formulations (HS40-7:1-TEOS, TM40-7:1-MTES, NS125-7:1-MTES) were selected for flow-through biocatalytic activity experiments based on the results of

transient activity assays and mechanical testing. We selected HS40-7:1-TEOS and TM40-7:1-MTES based on their sustained activity during storage (Fig. 2.3) and superior mechanical strength (Fig. 2.6), and NS125-7:1-MTES based on its superior biocatalytic activity on day 4 (Fig. 2.3). As a negative control, we used TM40-7:1-MTES gel without encapsulated cells. Long-term steady-flow biocatalytic activity assay results (Fig. 2.9) show that for all the selected gels, the effluent atrazine concentration was sustained below 30% of the influent concentration of 10 ppb for 2 months. It can be observed that effluent concentration of the reactor with the no-cell control gradually reached the influent concentration only after ~7 weeks, suggesting that some portion of atrazine was still being adsorbed by silica gel within that time frame. The difference in effluent concentrations between no cell material and encapsulated cells over the duration of the experiment shows that the removal of atrazine was mostly due to degradation rather than adsorption. Within the reported duration of the experiment, no significant variation in atrazine removal efficiency was observed amongst different gel formulations. Therefore, steady-flow performance of different formulations could not be evaluated. This is primarily due to the long residence time of atrazine solution within the bioreactors, concealing any performance difference between the gels. Higher flow rates need to be investigated in future studies to fully assess the limitations of the developed materials both in terms of their mechanical integrity and degradation activity.

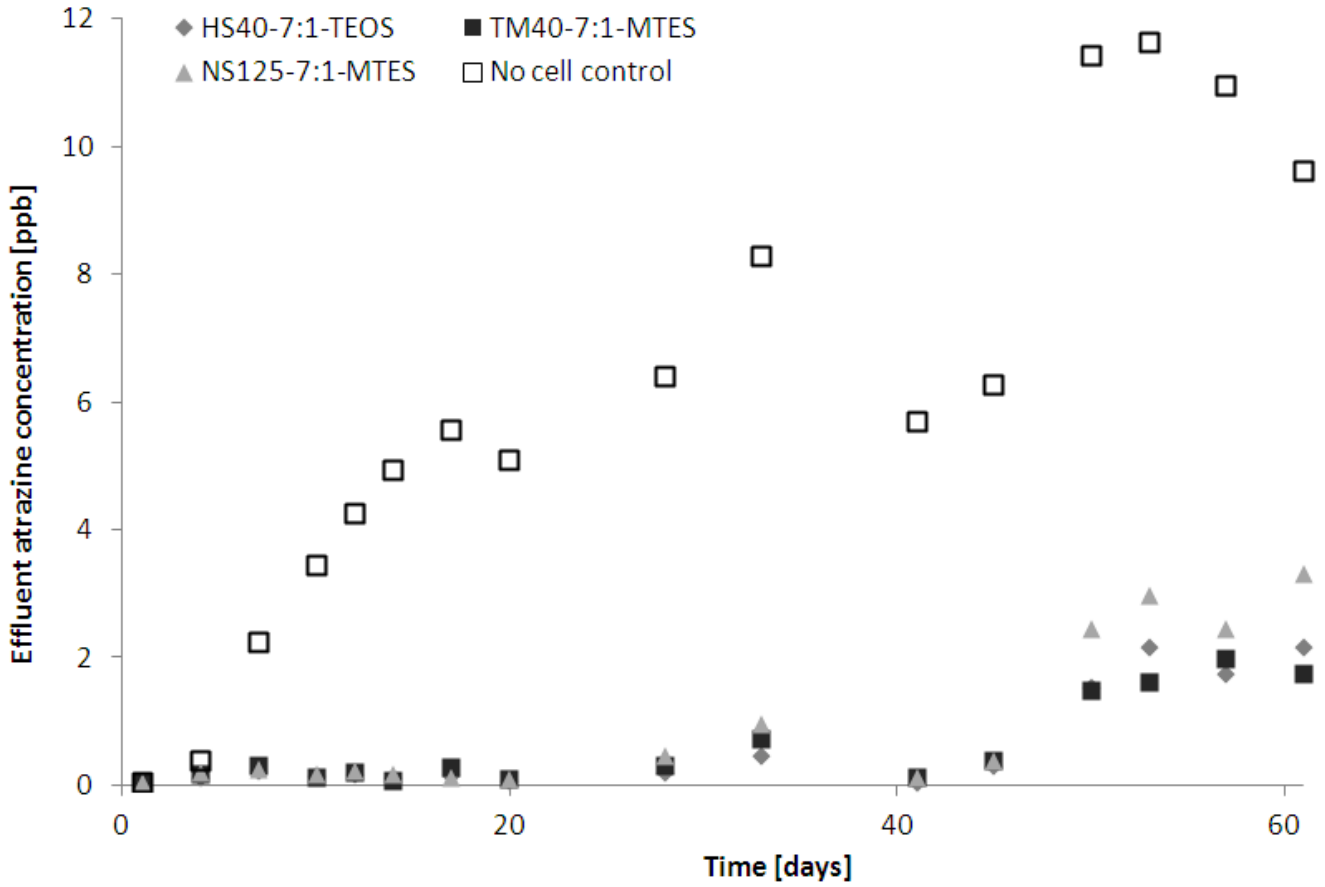

Figure 2. 9 Long term steady-flow biocatalytic activity of selected biomaterials as demonstrated by measuring effluent concentration of atrazine. The influent concentration was 10 ppb.

2.5 Conclusion

Sol-gel encapsulation of bacterial biocatalysts in silica gel requires a fine balance between obtaining good material properties (mechanical strength, structural integrity, permeability, etc.) and preserving biocatalytic activity of the cells. These constraints cause limitations on the design process, oftentimes leading to insufficient material properties or biocatalytic performance. Solving these problems usually involves incorporation of additives, which in turn increases the cost of the material. In this study, we show that by using silicon alkoxide cross-linked silica nanoparticle gels for encapsulation of bacterial biocatalysts, silica gel microstructure can be fine-tuned while preserving good biocatalytic activity. Use of SNPs as the major silica precursor and elimination of the additives significantly reduces the cost of the material, making it a suitable alternative for large scale water treatment applications.

Besides pesticides, other low concentration contaminants in drinking water supplies (pharmaceuticals, personal care products, endocrine disruptors, etc.) is also an increasing concern, and studies suggest that water treatment plants cannot completely remove these pollutants by conventional treatment methods [52]. Our results show that the developed catalytic biomaterials can be used to remove trace levels of atrazine in a flow-through packed bed reactor system with high removal efficiency for at least 2 months. Therefore, the developed encapsulation method in this study holds potential to be applied to different bacterial biocatalysts, and can be used for removal of other pollutants from drinking water supplies.

Acknowledgements

This research was supported by a National Science Foundation grant (CBET-0644784) to Alptekin Aksan, a research grant from Syngenta Crop Protection to Lawrence Wackett, Michael Sadowsky and Alptekin Aksan and a BioTechnology Institute grant to Alptekin Aksan and Lawrence Wackett.

2.6 Publication of thesis work

This research[53] was the result of the efforts of several individuals (listed as published): Baris R. Mutlu, Sujin Yeom, Ho-Wang Tong, Lawrence P. Wackett, and Alptekin Aksan

For this chapter, my contributions were: Literature searching and analysis, generating ideas, reviewing the manuscript, designing and performing experiments, and analyzing data including: growing and maintaining bacterial cultures, cell viability and catalytic activity measurements in batch experiments (Fig. 7 and 8), maintaining the flow-through system, collecting samples and performing catalytic activity measurements with Atrazne immunoassay kit from the samples in flow-through experiments (Fig. 9).

CHAPTER 3 Bacterial Cyanuric Acid Hydrolases for Water Treatment

3.1 Summary

Di- and trichloroisocyanuric acid are widely used as water disinfection agents but cyanuric acid accumulates with repeated additions and must be removed to maintain free hypochlorite for disinfection. This study describes the development of methods for using a cyanuric acid degrading enzyme contained within non-living cells that were encapsulated within a porous silica matrix. Initially, three different bacterial cyanuric acid hydrolases were compared: TrzD from *Acidovorax citrulli* strain 12227, AtzD from *Pseudomonas* sp. ADP, and CAH from *Moorella thermoacetica* ATCC 39073. Each enzyme was expressed recombinantly in *Escherichia coli* and tested for cyanuric acid hydrolase activity using freely suspended or encapsulated cell formats. Cyanuric acid hydrolase activities differed by only a two-fold range when comparing across the different enzymes with a given format. A practical water filtration system is most likely to be used with non-viable cells and all cells were rendered non-viable by heat treatment at 70^{o}C for 1 hour. Only the CAH enzyme from the thermophile *M. thermoacetica* retained significant activity under those conditions and so it was tested in a flow-through system simulating a bioreactive pool filter. Starting with a cyanuric acid concentration of 10,000 µM, more than 70% of the cyanuric acid was degraded in 24 hours, it was

completely removed in 72 hours, and a respike of 10,000 µM cyanuric acid a week later showed identical biodegradation kinetics. An experiment conducted with water obtained from municipal swimming pools showed the efficacy of the process, although cyanuric acid degradation rates decreased by 50% in the presence of 4.5 ppm hypochlorite. In total, these experiments demonstrated significant robustness of cyanuric acid hydrolase and the silica bead materials in remediation.

3.2 Introduction

Cyanuric acid is a high volume industrial chemical [54] and is not known to be a product of biosynthesis, but is nonetheless biodegradable [55]. Cyanuric acid is toxic in admixture with melamine, as was recently discovered when crude melamine containing cyanuric acid was added to pet food, and more than one thousand animals died from kidney failure [56, 57]. Cyanuric acid is also formed during the bacterial metabolism of *s*-triazine herbicides and as a by-product of disinfection processes [58]. In the latter example, di- or trichloroisocyanuric acids are frequently used to disinfect outdoor swimming pools and their decomposition leaves cyanuric acid [59], but high cyanuric acid impairs the disinfection process, leaving people vulnerable to viral, bacterial and protozoal infections. The cyanuric acid must be removed to sustain disinfection and there are currently no efficient means to accomplish this. A typical remedy is to drain and refill pools, leading to downtime for the pool, disposal issues and increased fresh water usage.

Cyanuric acid is very stable below 300°C [1], but it can be degraded at ambient temperature in soil and water via a specific enzyme that has been identified within a limited number of bacteria [60]. Those bacteria typically utilize cyanuric acid as their sole source of nitrogen and some have been shown to completely degrade the *s*-triazine ring to liberate all three of the nitrogen atoms as ammonia [55]. Complete degradation requires the consecutive action of cyanuric acid hydrolase, biuret hydrolase and allophanate hydrolase [61]. Of these, cyanuric acid hydrolase is the most well studied and found to be, along with the enzyme barbiturase, members of a rare protein family that is distinct from major hydrolase superfamilies [60]. The X-ray structures of two cyanuric acid hydrolases were recently determined and were found to have a protein fold unique to the cyanuric acid/barbiturase protein family [62, 63]. Characterized cyanuric acid hydrolases were all from bacteria, until a recent study described a homologous, isofunctional enzyme from a fungus [64].

Cyanuric acid hydrolases can be used to treat contaminated water, but the most economical system for large volumes of water would be to use whole cells expressing high levels of the enzyme immobilized within a matrix and contained in a flow-through bioreactor. Recent work with *s*-triazine herbicides [25] has shown that silica encapsulation provides an inexpensive, permeable matrix that stabilizes enzymes within bacterial cells. In that study, the *in vivo* enzyme was atrazine chlorohydrolase, and the cells were rendered completely non-viable, but the enzyme activity was maintained at initial levels for at least four months [25]. Cyanuric acid degradation is also initiated by a hydrolytic

enzyme, suggesting that a stable, even non-viable cell system could be effective for removing chlorinated isocyanurate disinfection by-products in pools, spas, and fountains. Cyanuric acid degradation by bacteria encapsulated in silica gels has not been studied previously.

In the present study, *E. coli* cells expressing three different cyanuric acid hydrolases were each studied for their ability to degrade cyanuric acid under conditions most likely to be used in a flow through system. The most well studied cyanurric acid hydrolases, TrzD from *Acidovorax avenae* subsp. *citrulli* [65], AtzD from *Pseudomonas* sp. strain ADP [46] and CAH from *Moorella thermoacetica* ATCC 39073[66] were chosen. The optimum enzyme for these purposes was found to be the cyanuric acid hydrolase from *M. thermoacetica*. A water-recycling, flow-through system was constructed and shown to be effective in removing 10,000 µM cyanuric acid, a concentration well above that encountered in real-world, disinfection processes.

3.3 Materials and Methods

3.3.1 Bacterial strains and culture conditions.

E. coli strains were grown at 37°C in LB medium with vigorous aeration. Three recombinant strains expressing the following cyanuric acid hydrolases were used (Table 3.1): AtzD, TrzD, CAH (*Moorella thermoacetica* cyanuric acid hydrolase, from open reading frame Moth_2120)). *E. coli* BL21(DE3)(pET28b+ CAH) were induced by adding 0.5 mM isopropyl-β-D-thiogalactopyranoside (IPTG) to the culture that had reached an optical density at 600 nm of 0.5. The induced cells were grown overnight at 37°C. When required, antibiotics were added at the following concentrations: 100 μg ampicillin mL^{-1} and 50 μg kanamycin mL^{-1}.

Table 3. 1 Strains, plasmids and primers used in this study

	Relevant markers and characteristics [a]	**Reference**
Strain		
DH5α	Δ*(lacZYA-argF)*U169 *(*Φ80*lacZ* ΔM15*)*	Lab stock
BL21(DE3)	F$^-$ *ompT hsdS$_B$* ($r_B^- m_B^-$) *gal dcm* (DE3)	Life
CAH	Strain DH5α harboring pUCMod *CAH*; Amp^R	Technologies
AtzD	Strain DH5α harboring pUCMod *atzD*; Amp^R	This study
TrzD	Strain DH5α harboring pUCMod *trzD*; Amp^R	This study
CAH-induced	Strain BL21(DE3) harboring pET28b+ *CAH*; Km^R	This study
		This study
Plasmid		
pUCMod	*rep* (pMB1), *bla* (Amp^R), constitutive *lac* promoter	
pUCMod CAH	pUCMod carrying the *Moorella thermoacetica* ATCC 39073 *Cyanuric Acid Hydrolase* gene	[67]
	pUCMod carrying the *Pseudomonas* sp. strain ADP *atzD* gene	This study
pUCMod AtzD	pUCMod carrying the *Acidovorax avenae* subsp. *citrulli trzD* gene	This study
pUCMod TrzD	pET28b+ carrying the *Moorella thermoacetica* ATCC 39073 *Cyanuric Acid Hydrolase* gene	This study
pET28+ CAH		[66]
Primer	**Sequence 5'–3'** [b]	
CAH-F	GAA TTC **AGG AGG** ATT ACA AAA TGC AAA AAG TCT TTC GTA TCC CAA CAG	
CAH-R	ATT ACC ATG GCT ACA CCC TGG CAA TAA CAG CAA TTG GG	
AtzD-F	ATT GAA TTC **AGG AGG** ATTA CAA AAT GTA TCA CAT CGA CGT TTT CCG AAT CCC TTG CCA C	
AtzD-R	ATT TAA TGC GGC CGC TTA AGC GCG GGC AAT GAC	
TrzD-F	ATT GAA TTC **AGG AGG** ATT ACA AAA TGC AAG CGC AAG TTT TTC GAG TTC C	
TrzD-R	ATT TAA TGC GGC CGC TTA AGC TGT GCG CGC GAT AAC	

[a] Amp^R, Km^R; resistance to ampicillin or kanamycin.

[b] Underlined letters indicate restriction enzyme recognition sites. Bold letters indicate a Shine-Dalgarno sequence.

3.3.2 Cloning procedures and plasmid construction.

To construct *E. coli* strains containing cyanuric acid hydrolase, pET28b+::Moth_2120, pET28b+::*atzD* and pET28b+::*trzD* were utilized as the PCR template [66]. The gene from *Moorella thermoacetica* ATCC 39073 was amplified from pET28b+::Moth_2120 with the primers CAH-F and CAH-R. The fragment of *CAH* was cloned into the *Eco*RI and *Nco*I cloning sites of the StrataClone PCR cloning vector (Agilent Technologies, Inc). The resulting plasmid was digested with the same restriction enzymes and the fragment released from the StrataClone plasmid was ligated into pUCMod, yielding pUCMod CAH (Table 1) [67]. The plasmid was introduced into MAX Efficiency *E. coli* DH5α Competent Cells (Life Technologies). CAH-induced strain was constructed by introducing the vector, pET28b+::Moth_2120 into One Shot® BL21(DE3) Chemically Competent *E. coli* (Life Technologies), thereby generating *E. coli* BL21(DE3)(pET28b+ CAH)(Table 1). The full lengths of *atzD* and *trzD* were amplified from pET28b+::*atzD* and pET28b+::*trzD*, respectively via PCR with the primers AtzD-F, AtzD-R, TrzD-F and TrzD-R. The fragments were then cloned into the *Eco*RI and *Not*I cloning sites of the pUCMod vector, yielding pUCMod *atzD* and pUCMod *trzD* (Table 1). The plasmids were introduced into *E. coli* DH5α by electroporation. *E. coli* DH5α competent cells were prepared by washing cells harvested at the exponential phase (OD_{600} ~ 0.5) with distilled water and a 10% (v/v) glycerol solution.

3.3.3 Encapsulation.

Silica-encapsulated cells were prepared either in molds, 20 mL glass scintillation vials or 4 mL glass tubes. Reagent grade tetraethyl orthosilicate (TEOS) was purchased from Sigma-Aldrich. NexSil 125-40 colloidal silica nanoparticles (SNP) was purchased from Nyacol Nano Technologies Inc. TEOS was hydrolyzed by stirring at a 1:5.3:0.0013 molar ratio of TEOS:water:HCl for 2 hours [53]. The pH of the Nexsil 125-40 SNP was adjusted to pH 7.0 by adding 1 M hydrochloric acid. After pH adjustment, an appropriate amount of cells suspended in phosphate buffered saline (PBS, pH 7.4) was added to the SNP solution to obtain a cell loading density of 0.125 g of wet cell mass/mL of the final gel. Gelation was started by adding hydrolyzed TEOS at a 7:1 volume ratio of SNP:TEOS to the mixture of SNP and cells at room temperature.

3.3.4 Cyanuric acid hydrolase activity assays.

Cells for assay were grown overnight, harvested by centrifugation, and resuspended into phosphate buffered saline (PBS) at a density of 0.3 g wet cell mass per mL. The reaction was initiated by either adding 0.03 g of resuspended cells or exposing 2 mL of silica gel containing encapsulated cells to 3 mL of 10 mM cyanuric acid solution in 0.1 M potassium phosphate buffer (pH 7.0). Samples were incubated with shaking at 120 rpm and collected after 30 min of incubation. The samples were filtered through a 0.2-μm pore size PTFE syringe filter. No detectable enzyme activity was found to be released from the silica gels during the course of the experiments.

To assay for the enzymatic conversion of cyanuric acid to biuret and then to ammonia, the biuret hydrolase from *Rhizobium leguminosarum* bv. *viciae* strain 3841 was purified as described previously [68] and coupled with the cyanuric acid hydrolase activity. One mole of biuret is transformed to one mole each of allophonate and ammonia by biuret hydrolase and ammonia was quantified using the hypochlorite-phenol reaction (Fig. 3.1) [68]. Enzyme assays were conducted for 30 min incubation with an excess of biuret hydrolase. Positive controls with known concentrations of biuret were conducted in parallel to ensure the all of the biuret was converted to ammonia.

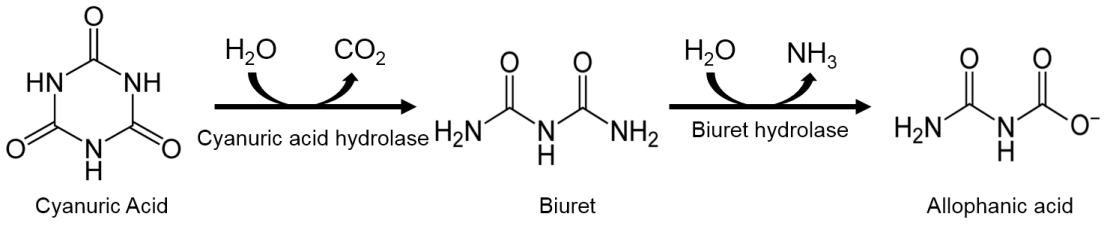

Figure 3. 1 Coupled assay for cyanuric acid hydrolase activity using biuret hydrolase and measuring stoichiometric formation of ammonia via the hypochlorite-phenol reaction described in the Materials and Methods section.

Cyanuric acid hydrolase activity was also determined by measuring cyanuric acid disappearance with the addition of 20 mM of melamine in 0.1 M phosphate buffer to form a 1:1 melamine-cyanuric acid complex that can be quantified by its turbidity by apparent absorbance (light scattering) at 600 nm. A standard curve of cyanuric acid

showed this method to be linear within the range used in these experiments. All incubations and assays were conducted at 22°C. All of the enzymes are significantly active at this temperature and their relative rates with heat treatment have been compared previously (16).

3.3.5 Inactivation of hydrolase-producing *E. coli* cells by heat treatment.

Two mL of encapsulated cells in a 20 mL glass scintillation vial (thickness = 3.5 mm and diameter = 24 mm) were used in these studies. For experiments with suspended cells, the cells were grown overnight and resuspended in 0.1 M phosphate buffer (pH 7.0) with a density of 0.01g of wet cell mass/mL in a 1.7 mL microcentrifuge tube. The samples were placed in a water bath adjusted to 60°C, 65°C, or 70°C, or left at 22°C as a control, for 1 hour and then placed on ice for 5 min. Suspended cells were pelleted by centrifugation and resuspended into the same buffer. Cyanuric acid hydrolase activity was measured as described previously with the cell density of 0.001g of wet cell mass/mL. Encapsulated cells were tested as gel plugs in the bottom of vials as previously described.

3.3.6 Oxygen consumption.

Cells were encapsulated in a 4 mL glass tube with the diameter of 6 mm as 200 μL cylindrical blocks. Measurements of oxygen consumption were conducted using a Hansatech Oxytherm system (Hansatech Instruments). Three mL of LB medium was pipetted into the chamber of the Oxytherm device. The chamber was sealed after the

encapsulated sample was placed inside. The data were exported to a computerized chart recorder (Oxygraph, Hansatech Instruments).

3.3.7 Stains for cellular membrane disruption.

One µL of each dye solution was added to 1 mL of cell suspension. Twenty mM of propidium iodide dissolved in dimethyl sulfoxide was one cell stain. The intensity of fluorescence was measured with a fluorescence spectrophotometer (Molecular Devices SpectraMax M2) using an excitation wavelength of 535 nm and an emission wavelength of 617 nm. BacLight Green Bacterial Stain (Invitrogen) was prepared according to the to manufacturer's instructions. The BacLight Green Bacterial Stain was measured at an excitation wavelength of 480 nm and an emission wavelength of 516 nm. All measurements were corrected by subtracting the small background fluorescence observed with a phosphate buffer control.

3.3.8 Cyanuric acid degradation measurement with the flow-through system.

Cells were encapsulated as hemispherical silica beads (1.0 – 1.5 mm in diameter) in molds as previously described (18). 6.6 g of the beads were placed in the bioreactors. One L of 10,000 µM cyanuric solution in 0.1 M potassium phosphate buffer (pH 7.0) was the influent solution to the bioreactors and was circulated at 360 mL/h flow-rate. Four days after completion of the first experiment, the channels were flushed with 0.1 M phosphate buffer (pH 7.0) for 1 hour and then the treatment of a fresh 1 L 10,000 µM cyanuric acid solution commenced. One-half ml samples were collected and tested for cyanuric acid

degradation using biuret hydrolase and the hypochlorite-phenol method as previously described.

3.3.9 Pool water degradation.

Pool water samples were taken from three different swimming pools in the Twin Cities area and tested for pH, hypochlorite and cyanuric acid levels. One g of 1 mm spherical silica beads containing CAH-induced cells were incubated in 200 mL pool water at room temperature with shaking at 120 rpm. A buffered water, 20 mM sodium phosphate, 137 mM NaCl, 2.7 mM KCl at pH 7.6, was used as a positive control. Cyanuric acid concentrations were determined by measuring the formation of melamine-cyanuric acid complex as described previously. Hypochlorite concentrations were measured by the *N*,*N*-dimethyl-*p*-phenylenediamine (DPD) colorimetric method (20). A DPD solution (3.9 mM) was prepared by dissolving 16 mg of DPD in 25 mL water (pH 2.0). A freshly opened 5.25 % sodium hypochlorite solution was used to prepare a standard curve. The oxidation of DPD by hypochlorite was monitored at 550 nm on a Beckman DU 640 spectrophotometer (Beckman Coulter, Fullerton, CA).

3.4 Results and Discussion

3.4.1 Use of a sensitive enzyme-coupled assay for cyanuric acid hydrolase activity.

Previous studies assaying cyanuric acid hydrolase activity used a direct spectrophotometric measurement of substrate disappearance at 214 nm. This assay was ineffective in the present studies because even minor impurities from the cells, glassware or tubing strongly contributed to absorbance at 214 nm. Cyanuric acid and biuret can be analyzed with high-pressure liquid chromatography but the present study demanded a large number of assays to be conducted rapidly. In that context it was found here to be most effective to measure cyanuric acid hydrolase activity by converting the product of the reaction, biuret, stoichiometrically to ammonia with purified biuret hydrolase [68]. Degradation as low as 5 nmole per mL could be determined this way and this was at least twice as sensitive as other methods. Water samples without cyanuric acid were run as a control and ammonia leakage from cells was found to be negligible. This method was compared to directly measuring cyanuric disappearance in water by adding melamine and measuring precipitation the extent of the 1:1 melamine:cyanuric acid precipitant as described in the methods section. Both methods gave consistent results, but the biuret hydrolase coupled assay was more sensitive and thus used routinely in this study (Fig. 3.2).

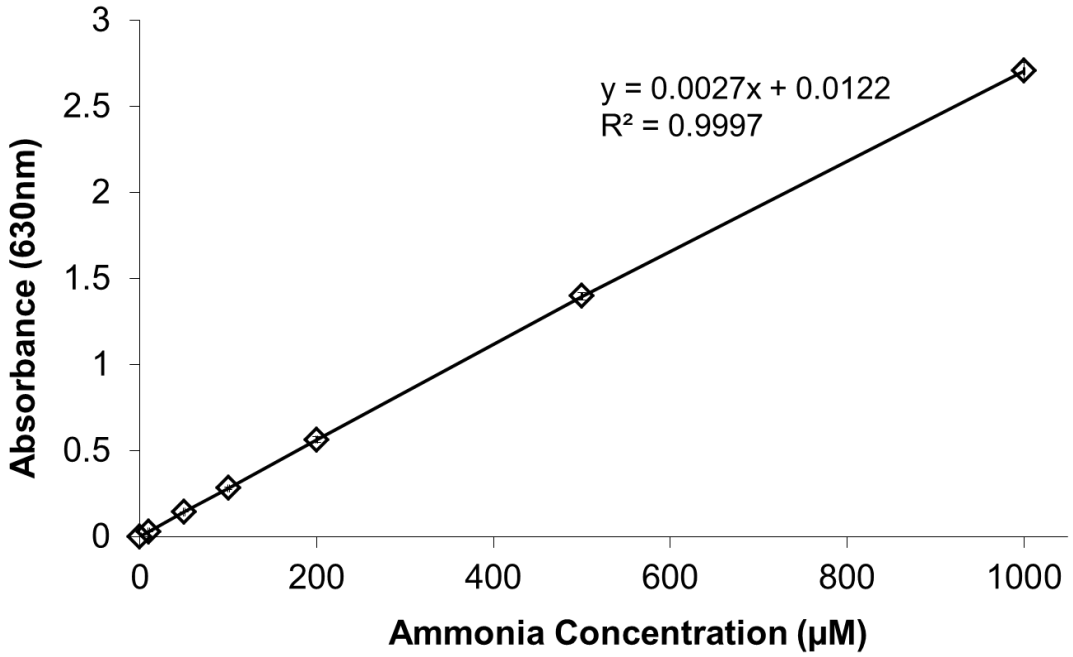

Figure 3. 2 Standard curve of a coupled assay for cyanuric acid hydrolase activity.

3.4.2 Comparison of cyanuric hydrolase activity in whole cells.

The three cyanuric acid hydrolases, TrzD, AtzD, and CAH, were expressed in the same *E. coli* cell background so diffusion through cell membranes, expressions levels, and other interacting proteins and other cell properties would be the same. Each enzyme was expressed constitutively with the same expression system. SDS-PAGE gels confirmed that the expression levels of the enzymes were similar and the majority of each respective cyanuric acid hydrolase was found in the soluble fraction of cell lysates. (Fig. 3.3). Our previous studies with cyanuric acid hydrolases expressed in *E. coli* also did not encounter problems with inclusion body formation [66].

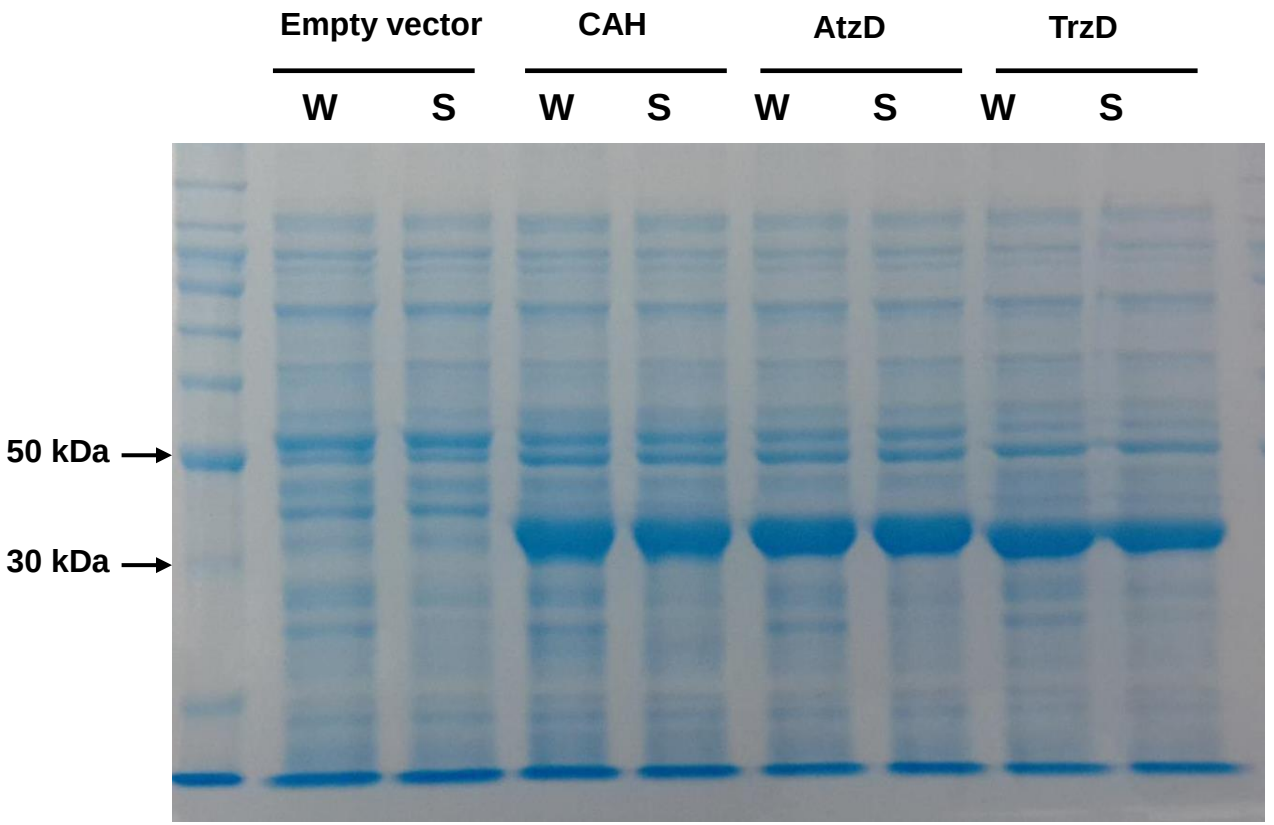

Figure 3. 3 Protein expression level. SDS-PAGE was carried out using a 10 % polyacrylamide gel to check the level of protein expression. Soluble lysate fractions were obtained by centrifugation of sonicated whole lysates for 30 min at 10,000 × *g*. 30 µg of protein was loaded in each lane. *DH5α* (pUCMod empty vector) was run as a negative control. W, whole lysate; S, soluble fraction. The size of CAH, AtzD, and TrzD are 38.9 kDa, 38.2 kDa and 39.4 kDa, respectively.

In an *in vivo* comparison of the three enzymes, TrzD showed the highest activity (Fig. 3.4A). This result is consistent with a previous report that TrzD showed approximately a two-fold higher k_{cat}/ K_m compared to AtzD and CAH [60]. This increase was attenuated when using cells encapsulated into silica gels (Fig. 3.4B), due to the diffusion limitation imposed by the silica gel matrix (13, 18). This limitation also causes an order of magnitude difference between the activity rates of suspended and encapsulated cells (compare Fig. 3.4A and B). Rate limiting effect of diffusion in an encapsulated cell system can be reduced by decreasing the size of the material [69]. Since the focus of this study was to compare the relative activities and stabilities of different cyanuric acid hydrolases *in vivo* when encapsulated, the diffusion properties of the gels were not optimized.

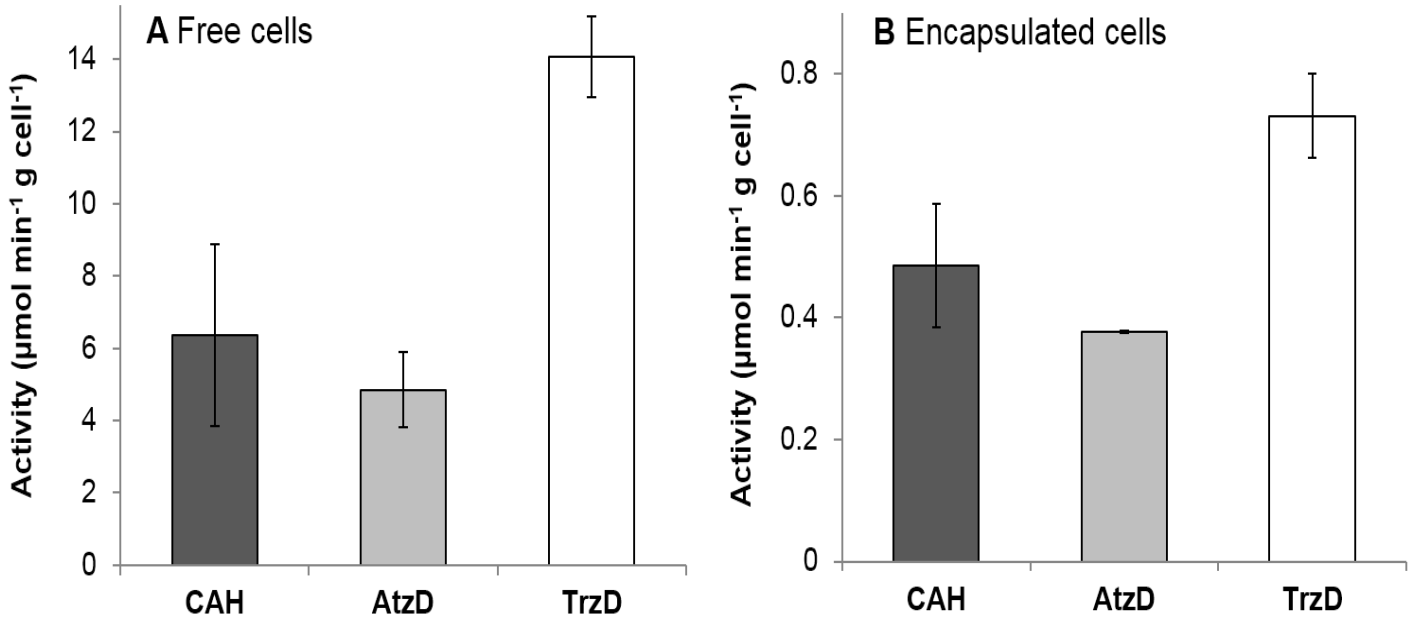

Figure 3. 4 A comparison of in vivo activity for different cyanuric acid hydrolases expressed in *E. coli* : (A) whole cells in suspension (Free cells); (B) whole cells encapsulated in silica gels. *E. coli* cells were encapsulated as 2 mL cylindrical blocks (3.5mm thickness and ~570 mm^2 surface area). Activities are reported as the mean values from triplicate determinations.

3.4.3 Viability and inactivation of hydrolase-producing *E. coli* cells by heat treatment.

The use of encapsulated cells in a disinfection-treatment system would be most acceptable if the cells could be rendered non-viable while retaining all or nearly all cyanuric acid hydrolase activity. It is possible to have activity in non-viable cells because the enzyme is a hydrolase, it does not require cofactors and, in that regard, it resembles atrazine chlorohydrolase which has been shown previously to remain fully active for over four months in non-viable *E. coli* cells [25]. Non-viability is defined as the inability to replicate and/or when cells have disrupted membranes that allow molecules to freely diffuse in and out, as typically shown with dyes [70-72]. Moreover, the equilibrium for the cyanuric acid hydrolase reaction is completely in the direction of product formation. We previously showed that the reaction is essentially irreversible due to rapid and spontaneous decarboxylation of the enzyme product, carboxybiuret, that leads to the stoichiometric formation of the stable product, biuret [60].

In the first experiment, *E. coli* cell suspensions were heated to temperatures (T > 60°C) known to induce 100% cell death [73]. Treatment at 60°C, 65°C and 70°C resulted in no viable cells, confirmed by plating heat-treated cells on rich media plates. We next tested cell viability/permeability using commonly-accepted methods. The two fluorescent dyes, propidium iodide (PI) and BacLight Green, are known to give increased fluorescence when cells become non-viable or show loss of membrane integrity [74, 75]. In the present study, we treated cells at 22°C, 60°C, 65°C and 70°C and the fluorescence went up

dramatically between 22°C and 60°C, suggesting that the cell membranes became permeable by heat treatment (Fig. 3.5A). This is consistent with the plate-counting results showing a complete loss of *E. coli* cell replication ability between 22°C and 60°C.

To determine the viability of encapsulated cells, the silica matrix was pulverized to a fine powder using a mortar and pestle and the released cells were suspended in sterile PBS. Cell counts were determined based on the number of observed Colony Forming Units (CFUs) after overnight incubation on rich medium plates (Fig. 3.6). By this measure, no cell viability was observed at 60°C, 65°C or 70°C. However, the plate-counting method could underestimate cell viability in silica-gel because encapsulated cells may not become fully separated from the silica matrix during the grinding process. To further investigate viability, we tested for metabolic activity by looking for oxygen consumption in the presence of a rich, oxidizable substrate mix with an Oxygraph. Encapsulated cells at room temperature consumed about half of the dissolved oxygen within 15 min whereas encapsulated cells heated to 60ºC or higher showed no discernible oxygen consumption (Fig. 3.5B).

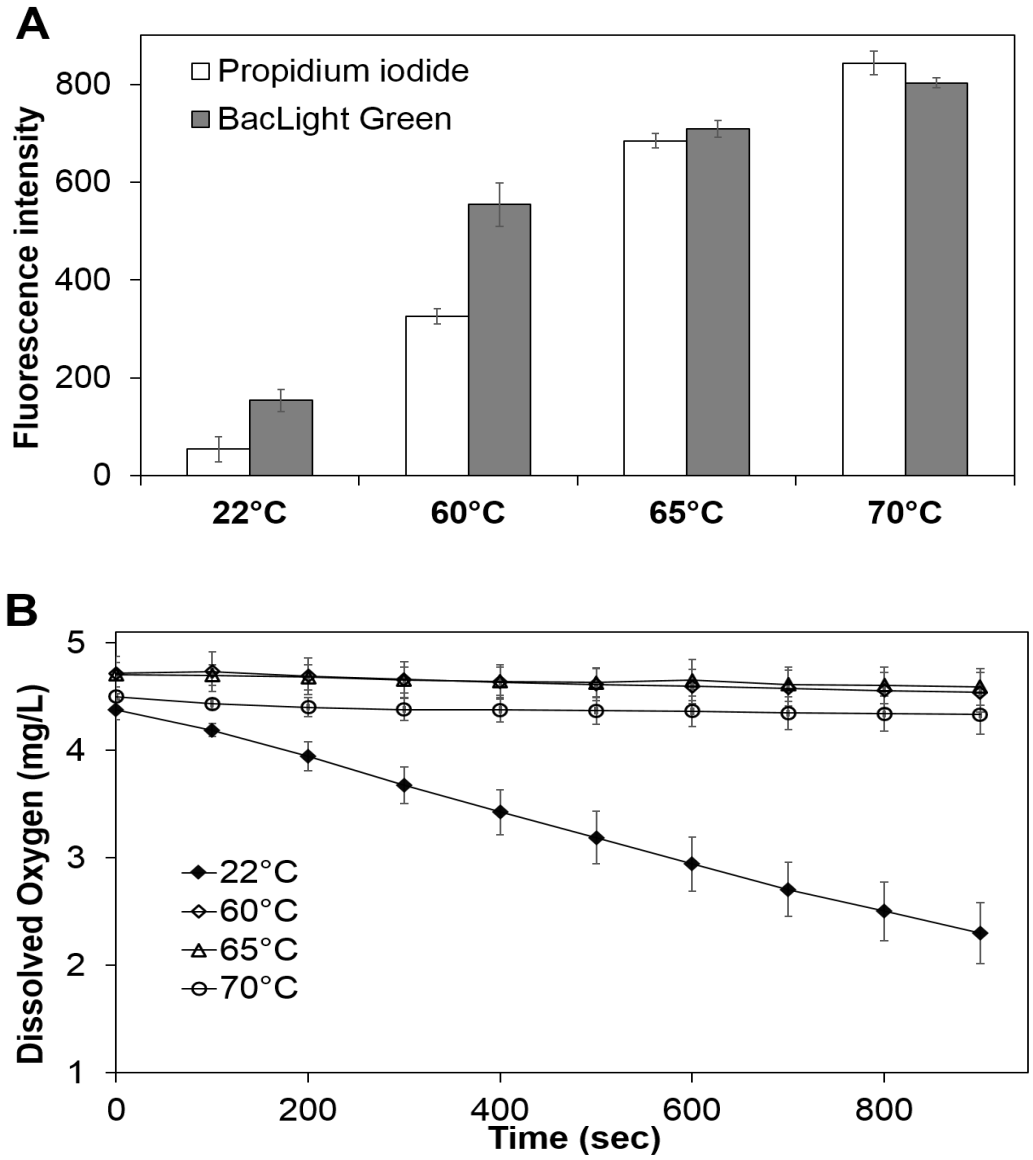

Figure 3. 5 The effect of heat-treatment on *E. coli* cells in suspension and encapsulated in silica blocks. (A) Cells in suspension at different temperatures exposed to fluorescent dyes testing for cell non-viability/permeability as labelled in the figure; (B) Viability of encapsulated cells (200 µL cylindrical blocks with thickness of 6 mm and surface area of ~30 mm^2) at different temperatures as determined by total loss of metabolic activity shown by oxygen consumption. Data are reported as the mean values from triplicate determinations.

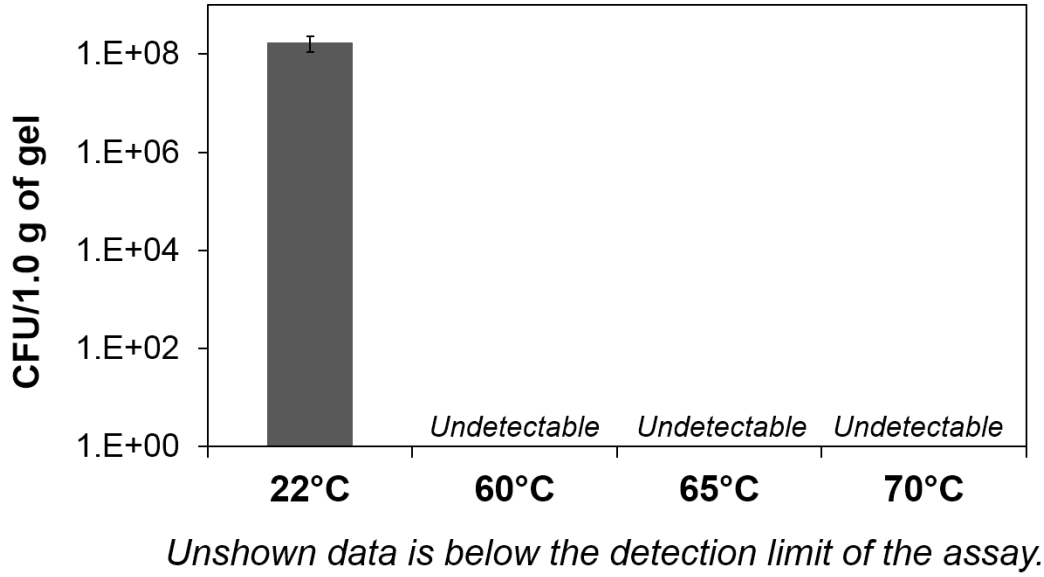

Figure 3. 6 Cell viability. Viability of the encapsulated cells were monitored using the serial dilution and plate-counting method. A 0.1 g aliquot of the material was pulverized using a mortar and pestle and the crushed material was suspended in 2 mL of sterile PBS. The solution was serially diluted and spread-plated onto LB agar with 100 µg ampicillin mL^{-1}. Cell counts were determined based on the number of observed Colony Forming Units (CFUs) after overnight incubation. Data marked "undetectable" were below the detection limit of the assay.

3.4.4 Cyanuric acid hydrolase activity measurements post heat treatment.

In the next set of experiments, cyanuric acid hydrolase activity was determined following heat treatment at 60°C, 65°C or 70°C for one hour and cooling back down to assay temperature. All of the cells showed an increase in activity following treatment at 60°C, presumably due to membrane disruption that led to greater substrate diffusion into the cell (Fig. 3.7A). It has been reported that heat treatment at 55°C and above causes vesiculation and blebbing in the outer membrane of *E. coli* [76]. The loss of lipopolysaccharide (LPS), that poses a significant barrier to substrate entry into cells, was also observed in other studies [77, 78]. However, at 65°C and 70°C, the cyanuric acid hydrolase activity for cells expressing TrzD dropped precipitously, whereas AtzD and CAH remained consistent (Fig. 3.7A). At 70°C, CAH activity remained at the same level following the 60°C and 65°C heat treatments. These results are consistent with *in vitro* studies comparing CAH to AtzD and TrzD in which CAH was shown to be more thermally stable [60]. CD spectroscopy has shown that the thermal denaturation temperature of purified CAH in buffer was above 70°C [62].

When examining the heat stability of cyanuric acid hydrolase activities in silica encapsulated cells, the trend was similar but the greater stability of CAH compared to TrzD and AtzD was even more dramatic (Fig. 3.7B). The increase in the activity above 100% (the activity was normalized to that measured prior to heat treatment) was likely due to membrane damage leading to increased permeability to cyanuric acid. However, this effect at 65°C or 70°C was more than nullified with TrzD and AtzD by the

inactivation of the enzymes. It is currently unclear why the encapsulated enzyme showed an even greater sensitivity to heat treatment than enzyme in non-encapsulated cells. However, at 65°C, the CAH activity remained more than 250% that observed prior to heat treatment, making CAH very attractive for obtaining high cyanuric acid degradation activity while rendering bacteria non-viable.

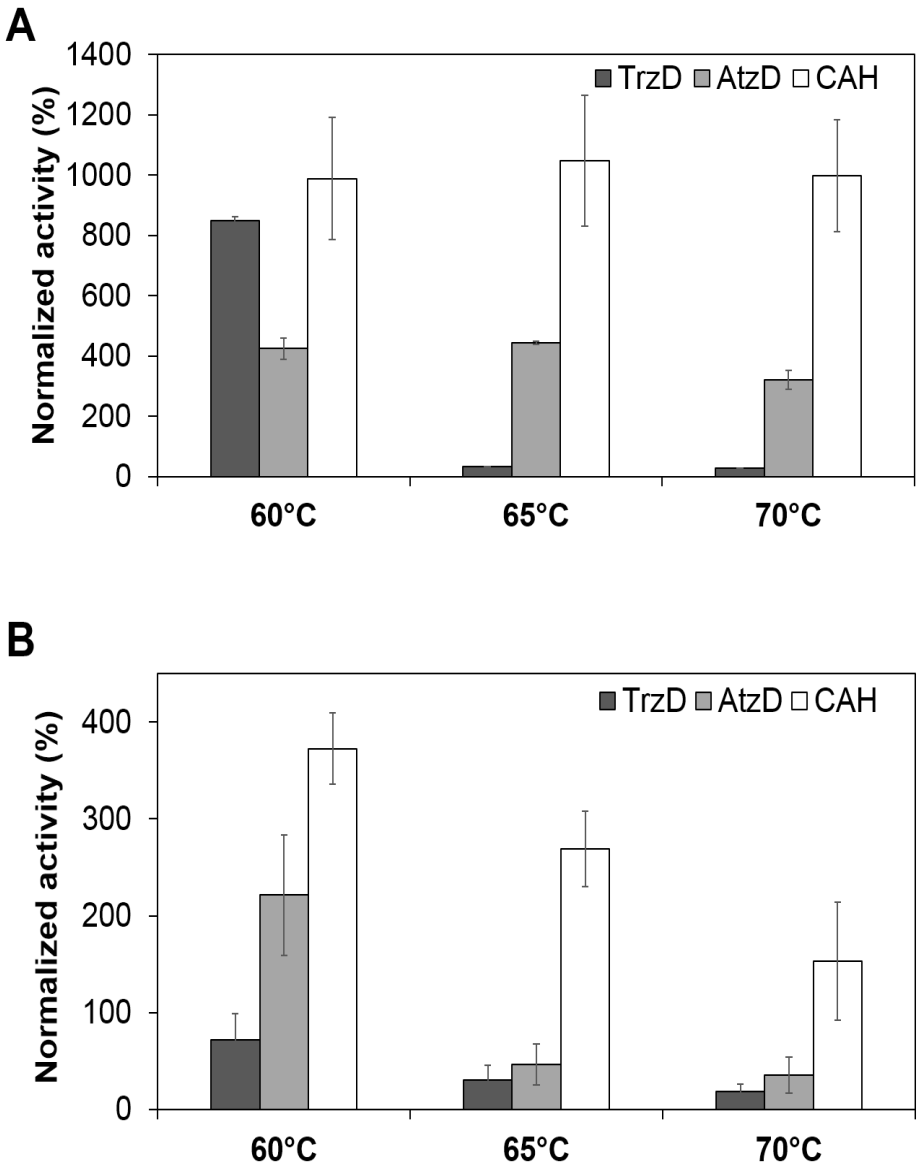

Figure 3. 7 The effect of heat-treatment on cyanuric acid hydrolase activity with (A) non-encapsulated cells; (B) encapsulated cells. *E. coli* cells were encapsulated as 2 mL cylindrical blocks. Data were normalized by setting the activity prior to heat treatment as 100%. Activities were measured in triplicate and the mean values are represented.

Several approaches have been employed in whole-cell enzyme applications to render cells more permeable; for example, using organic solvents or detergents [79-81]. The present data suggest that heat treatment with cells encapsulated in silica, and containing a thermostable enzyme, can be used to reduce substrate permeability barrier while also rendering cells non-viable, which is a desirable feature for water treatment applications.

3.4.5 Storage stability of encapsulated cells.

In order to evaluate storage stability, encapsulated cells were subjected to no heating, or heating at 60°C, 65°C or 70°C, and then maintained at room temperature. No special treatment was made, nor stabilizing agents added. Individual stored gels were sampled at the time points indicated in Figure 5 and assayed for cyanuric acid hydrolase activity. When encapsulated cells were maintained at room temperature at all times, the cyanuric acid activities with AtzD, TrzD and CAH all increased substantially with CAH increasing the most to more than 400% of the original activity (Fig. 3.8A). Note that encapsulated *E. coli* cells expressing atrazine chlorohydrolase activity also showed an increase upon storage for two weeks although it was less than 200% of the original activity which had been attributed to a time-dependent disruption of the cell membrane allowing greater permeability of the substrate [25].

The effect of heat-treatment on stability of cyanuric acid hydrolase activity was also investigated. With TrzD, the measured activity after heat treatment and one day of storage increased at 60°C and 65°C, but the activity decreased to 20% of the untreated,

non-stored level after heat treatment at 70°C and storage for one day (Fig. 3.8B). Upon long-term storage (14 days), all of the heat-treated and stored samples showed a decrease in activity to at best around the level of non-heated, non-stored encapsulated TrzD cells. The results with AtzD were qualitatively similar to those with TrzD cells (Fig. 5C). After long-term storage, all samples showed less than original levels of activity.

The CAH encapsulated cells showed a much more robust response (Fig. 3.8D). The initial gains in activity upon storage were modest, <150% of the starting activity, but the level of activity remained quite constant thereafter. These results are significant because a product for treatment of pools and spas will likely require shelf storage for weeks and months and the present data suggest that the formulation containing the CAH enzyme is best able to meet those criteria.

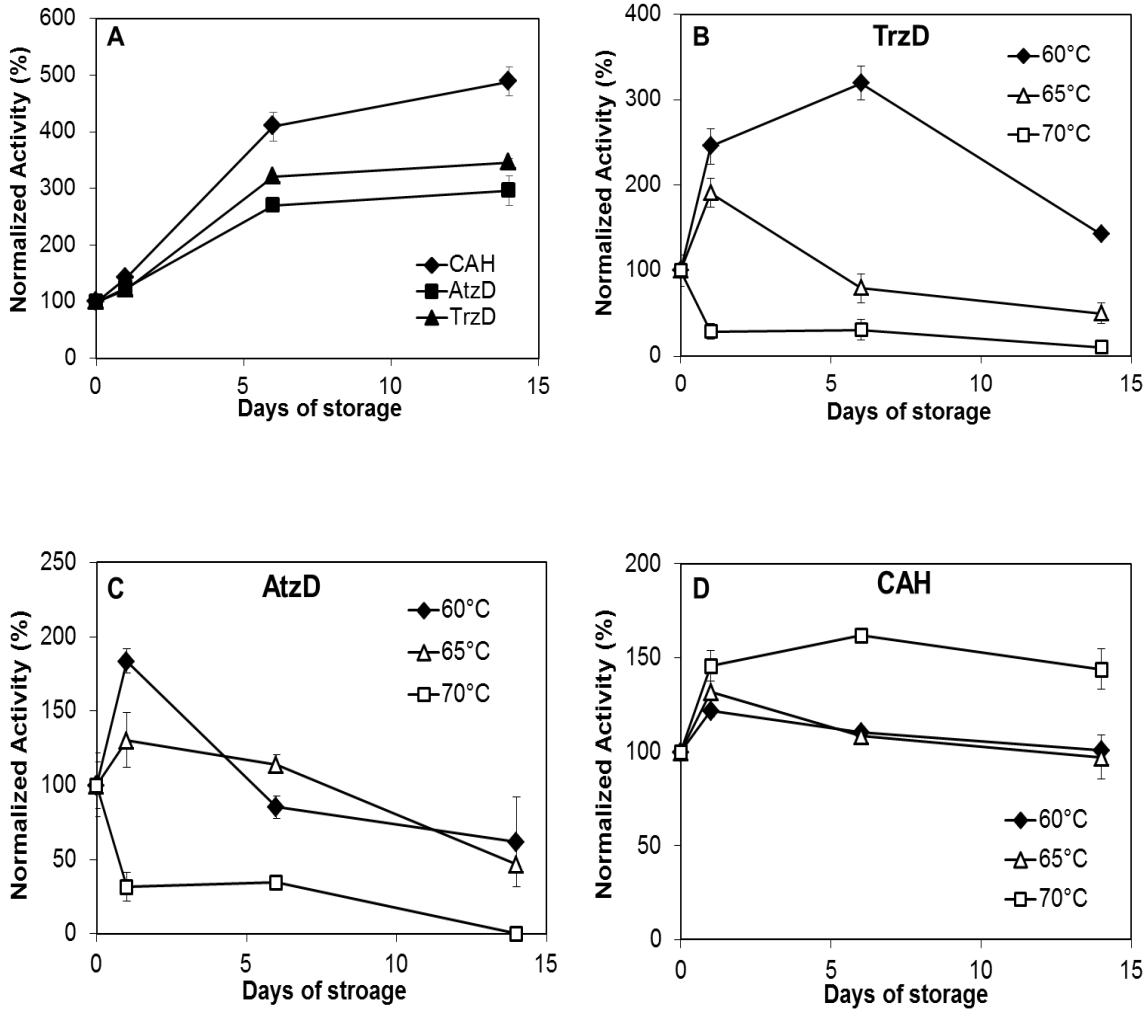

Figure 3. 8Cyanuric acid hydrolase activity in *E. coli* cells encapsulated in 2 mL cylindrical blocks that had been subjected to different heat treatments and then stored at room temperature for up to 2 weeks. (A) No heat treatment prior to storage. (B, C, and D) Each enzyme as indicated (TrzD, AtzD, CAH) was heat treated as described in the Methods section and then stored at room temperature. Data are normalized with respect to the initial activity at time zero for each set of encapsulated cells. Assays were conducted in triplicate at indicated times and the mean value is represented.

3.4.6 Flow-through cyanuric acid treatment.

In light of the storage and thermal stability of the CAH activity, *E. coli* expressing CAH was chosen to test for practical applications simulating a flow-through pool water treatment system. In this experiment, silica beads with a 1.0 – 1.5 mm diameter were used. There were four packed columns, two with active CAH enzyme *in vivo*, one with beads alone and one empty column (Fig. 3.9A). Each column was treated by pumping buffer containing 10,000 µM cyanuric acid through the column. The 1 L of cyanuric acid solution was pumped at a 6 mL/min flow-rate through over 24 cycles. From the control experiment with beads alone, we could determine that the amount of ammonia release from cells unrelated to cyanuric acid hydrolase activity could at most account for 0.5% of the observed degradation. It was shown that over 7,000 µM cyanuric acid was removed in 24 hours and the complete degradation of cyanuric acid was observed in 72 hours (Fig. 3.9B). To further test the longevity of the system, after the column system had been at room temperature for a week, the identical experiment was run. Fig. 3.9B shows that the cyanuric acid degradation activity was virtually indistinguishable. This further indicates that the CAH enzyme is highly stable, as there was not even slight loss of degradation activity under operating conditions and over the course of one week.

The observed decrease in cyanuric acid was plotted to determine if it followed first or second order kinetics and the fit was much better with a first order model. A least-squared fit for the first-order linear plot of the logarithm of cyanuric acid concentration versus time yielded an R^2 value of 0.99 (Fig. 3.9B, inset). A plot of the data assuming a

second-order model yielded a much poorer fit to a straight line, with an R^2 value of 0.74 (data not shown). Thus, a first-order decay of cyanuric acid is indicated over the entire range of cyanuric acid concentration, from 10,000 µM to the final concentration of essentially 0 µM after 72 hours.

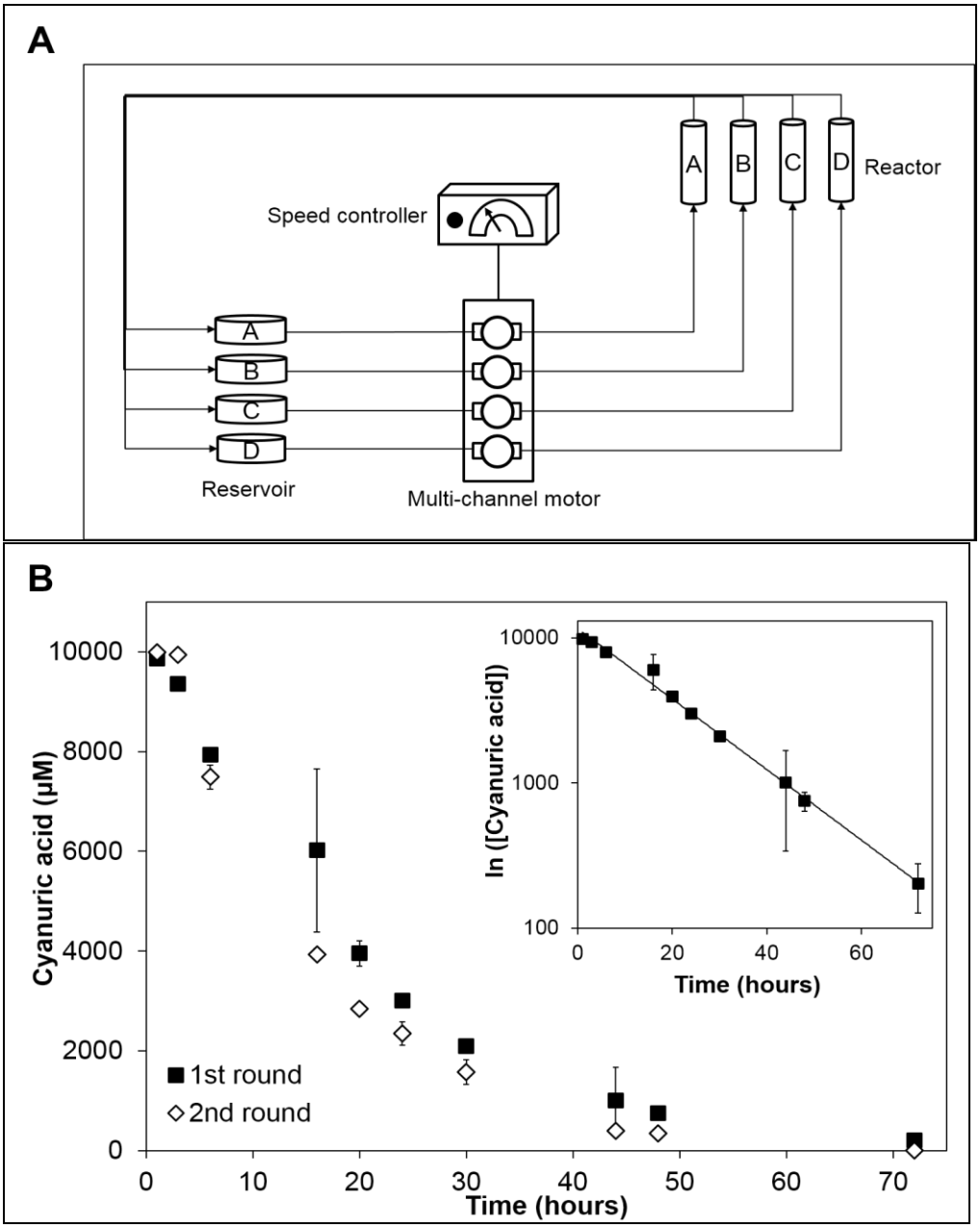

Figure 3. 9 Cyanuric acid degradation by *E. coli* cells expressing CAH enzyme encapsulated in hemispherical silica beads (1.0 – 1.5 mm in diameter) contained within a glass cylindrical column of bead dimensions 2.0 cm (diameter) and 3.0 cm (height) operating in a flow-through, recirculating mode. (A**) Shows a schematic diagram of the system. Channel A, empty reactor; Channel B, beads with no cell; C and D, beads with encapsulated cells; controls showed no degradation (**B**) Plots the determined concentration of cyanuric acid in the reservoir with beads containing encapsulated cells, as a function of time. The 2nd round was the same bioreactor with the same cells and beads tested with a fresh cyanuric acid solution one week later. The inset graph shows the same data for the 2nd round plotted as the logarithm of cyanuric concentration versus time. All data shown are the average of triplicate determinations.**

The observed first-order biodegradation of cyanuric acid with encapsulated cells can be contrasted with what would be expected with isolated purified enzyme in solution for which the K_M has been determined to be 110 µM [66]. The time course of cyanuric acid degradation by the isolateµd enzyme can be calculated by solving for substrate concentration as a function of time with the integrated Henri-Michaelis Menton equation. If the enzyme were put into a 10,000 µM cyanuric acid solution, the degradation of the substrate would proceed in an essentially zero order fashion for greater than 95% of the substrate disappearance, in contrast to what was observed in Fig. 3.9B. This large difference in the kinetics for the isolated enzyme and the encapsulated whole cells suggests either that the *in vivo* enzyme has a K_M orders of magnitude higher than the *in*

vitro enzyme as tested [66], or that the *in vivo* cyanuric acid concentration is very low, such that first order kinetics hold. The latter explanation is more plausible given that the cell membranes, the silica matrix surrounding the cells, and the concentration gradient likely formed throughout the length of the column can all lead to a low effective concentration of cyanuric acid in the cell cytoplasm where the enzyme is expressed. Several observations are consistent with this hypothesis. First, the activity of the cells increased up to 5-fold over the first 2 weeks of storage. Similar observations were made with *E. coli* cells expressing another hydrolytic cytoplasmic enzyme, atrazine chlorohydrolase, and that was shown to correlate with changes in the membranes that led to increased entry of the substrate into the cell [25]. In other studies, the silica matrix was directly tested for chemical diffusion and shown to impose rate limitations over lengths more than 0.1 mm [69] and the current beads ranged from 1.0 – 1.5 mm in diameter, consistent with a significant diffusional barrier imposed by the matrix.

While the diffusional barriers of cell membranes and silica matrix likely impose slower degradation rates compared to purified enzymes, a commercial treatment system for a swimming pool will need to meet certain requirements of cost that make the use of purified enzyme prohibitive. Moreover, the silica matrix can be rendered more porous, to enhance diffusion, but this will cause a corresponding decrease in mechanical strength causing beads to disintegrate in flow systems, as has been previously described [69]. The silica beads used in the flow-through experiments maintained mechanical integrity throughout the two tests.

3.4.7 Test of encapsulated *E. coli* expressing CAH with swimming pool waters.

There may be additional chemicals present in actual swimming pool waters that would affect the *in vivo* CAH activity and so this was tested directly. Recently opened swimming pools from the Twin Cities metropolitan area were sampled in mid-June, 2015. Because it was early in the season, the addition of chlorinated isocyanuric acids were relatievly low, and so we spiked with additional cyanuric acid to make it up to a level that would require treatment (> 100 ppm or 775 μM). Otherwise the waters were not modified and were of similar pH of 7.3-7.4 but contained differing levels of hypochlorite. The silica encapsulated cells with CAH were gently shaken in each of the three swimming pool waters, along with a water control (no hypochlorite).

The pool waters all showed substantial reductions in cyanuric acid over a 20 h period but there was a difference observed as a function of the hypochlorite concentration (Fig. 3.10). Without hypochlorite, or at a concentration of 0.9 ppm (17 μM), the initial cyanuric acid was at undetectable levels at 15 h. At 1.8 ppm (34 μM) and 4.5 ppm (85 μM) hypochlorite, there was still residual cyanuric acid at 10 (194 μM) and 20 ppm (388 μM), respectively, after 20 h. The initial rates of cyanuric acid degradation were plotted as a function of hypochlorite concentration and this showed a significant effect of chlorine, decreasing the rate approximately 50% at the highest level of hypochlorite (4.5 ppm) compared to the no hypochlorite control. Swimming pools generally contain < 5ppm (97 μM) hypochlorite to avoid irritation to swimmers, so the levels tested here go to near the highest accepted levels and show that the encapsulated *E. coli* cells expressing

the *Moorella* cyanuric acid hydrolase still function at that level, albeit at a diminished rate.

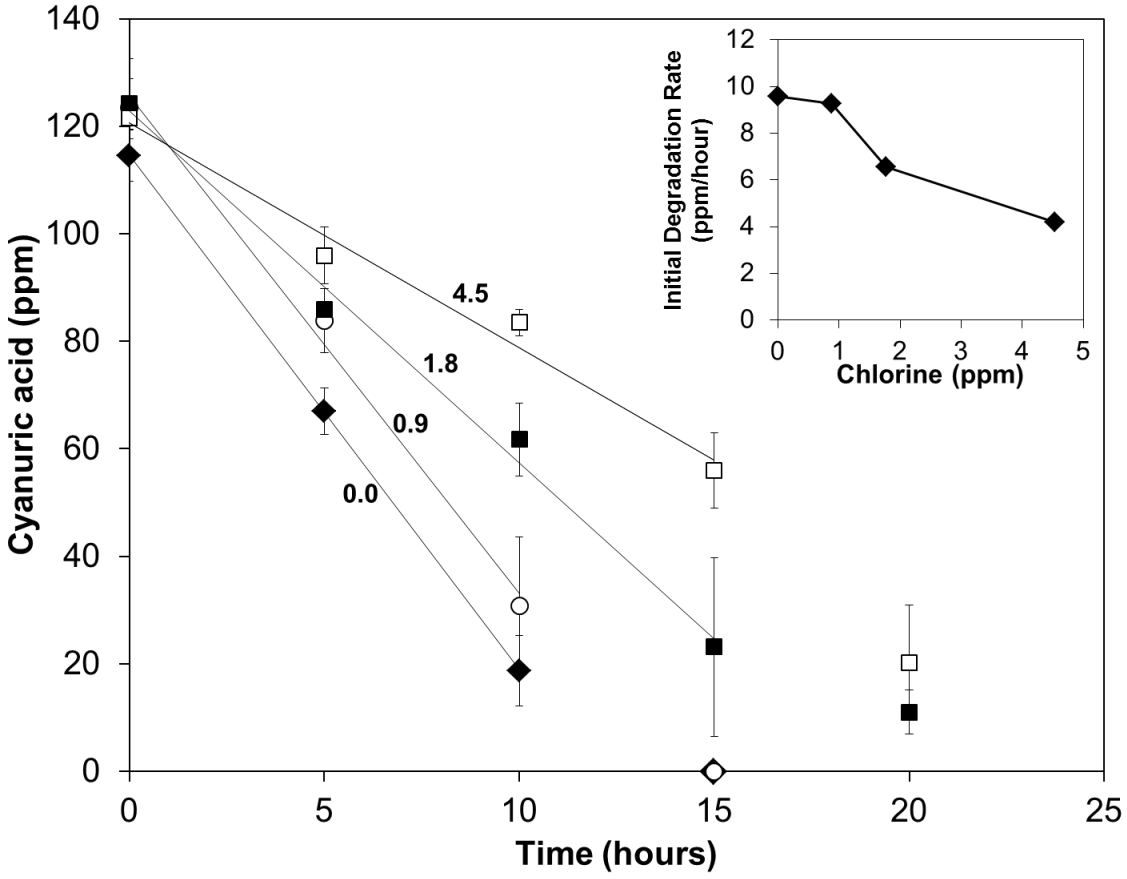

Figure 3. 10 Cyanuric acid degradation by *E. coli* cells expressing CAH and enapsulated in 1 mm spherical silica beads tested with swimming pool waters from three different sites containing different levels of hypochlorite. The hypochlorite, pH and cyanuric acid levels were determined as described in the Methods section. Since the pools had only recently been opened, cyanuric acid levels were relatively low and so they were spiked to a level > 100 ppm at which pools need to be treated. The hypochlorite levels were as follows: control water from lab with 0.0 ppm (♦); pool

containing 0.9 ppm (○); pool containing 1.8 ppm (■); pool containing 4.5 ppm (□). For clarity, the numbers denoting the hypochlorite concentration in ppm are adjacent to the respective line generated from waters with those values. The data are obtained from triplicate samples run in parallel and the mean value is plotted. The inset graph shows the same data plotted as the initial rate of cyanuric acid degradation versus chlorine concentration. The rate curves show a fit of $R^2 = 0.99$ except for the 4.5 ppm water where the $R^2 = 0.98$. The last points at or near the baseline were not plotted as they are not initial rate points as the cyanuric acid had been depleted.

In general, the use of silica-encapsulated cells containing the *Moorella* cyanuric acid hydrolase (CAH) offers a good trade-off with significant rates, activity maintenance during storage and use, heat stability allowing cell killing with heat, and overall mechanical stability in a flow-through system. In a swimming pool, it is generally desirable to diminish cyanuric acid concentrations from levels of 120 ppm (930 μM) to approximately 40 ppm (310 μM). In the present experiments with the flow through system and without hypochlorite, 13 ppm (101 μM) cyanuric acid was removed within ~1 h. In swimming pool waters, the presence of hypochlorite was observed to diminish rates significantly. Further studies are warranted to investigate the effects of hypochlorite, develop mitigation strategies, and to deliver cost-effective, microbial enzymatic systems for swimming pool treatment.

Acknowledgements

We thank Mr. Joey Benson for expert assistance in making silica beads and Dr. Anthony G. Dodge for constructing the CAH strain. The pUCMod vector was kindly provided by Dr. Claudia Schmidt-Dannert. This research was supported by an NSF-IIP/PFI Grant (#1237754), a MnDRIVE-OVPR grant and a MnDrive fellowship (to BRM) from the BioTechnology Institute at the University of Minnesota.

Disclaimer

Drs. Lawrence Wackett and Alptekin Aksan own equity in and are entitled to royalties from, Minnepura Technologies, Inc., a company involved in the development, commercialization and marketing of patented encapsulated biological platforms for water treatment. The University of Minnesota also has equity and royalty interest in Minnepura. These interests have been reviewed and managed by the University of Minnesota in accordance with its conflict of interest policies.

3.5 Publication of thesis

This research[82] was the result of the efforts of several individuals (listed as published): Sujin Yeom, Baris R. Mutlu, Alptekin Aksan, and Lawrence P. Wackett.

For this chapter, my contributions were: Literature searching and analysis, generating ideas, designing and performing all the experiments, analyzing data, and writing the paper. The second author, Baris R. Mutlu, contributed significantly in the construction of the flow-through.

CHAPTER 4 Silica Ecosystem for Synergistic Biotransformation

4.1 Summary

Synergistical bacterial species can perform more varied and complex transformations of chemical substances than either species alone, but this is rarely used commercially because of technical difficulties in maintaining mixed cultures. Typical problems with mixed cultures on scale are unrestrained growth of one bacterium, which leads to suboptimal population ratios, and lack of control over bacterial spatial distribution, which leads to inefficient substrate transport. To address these issues, we designed and produced a synthetic ecosystem by co-encapsulation in a silica gel matrix, which enabled precise control of the microbial populations and their microenvironment. As a case study, two greatly different microorganisms: *Pseudomonas* sp. NCIB 9816 and *Synechococcus elongatus* PCC 7942 were encapsulated. NCIB 9816 can aerobically biotransform over 100 aromatic hydrocarbons, a feat useful for synthesis of higher value commodity chemicals or environmental remediation. In our system, NCIB 9816 was used for biotransformation of naphthalene (a model substrate) into CO_2 and the cyanobacterium PCC 7942 was used to provide the necessary oxygen for the biotransformation reactions via photosynthesis. A mathematical model was constructed to determine the critical cell

density parameter to maximize oxygen production, and was then used to maximize the biotransformation rate of the system.

4.2 Introduction

Pure cultures of naturally-occurring or recombinant microorganisms are used for biotransformation of chemicals at large scale [83-85], most prominently in renewable energy [86], pharmaceutics [87, 88], agriculture [89], and environmental remediation industries [90]. More recently, applications of mixed bacterial populations are being sought for commercial use, drawing on the ability of communities to perform a larger variety of more complicated tasks than individual species [91]. A major challenge in utilizing multiple bacterial species cooperatively in a complex chemical transformation reaction is to establish temporal population stability and to preserve the spatial distribution characteristics within the system [92, 93]. In consortia or mixtures, interspecies competition may lead to an imbalance in population distribution, reducing efficacy and yield, and may even result in a complete termination of the process if one of the species is eradicated.

Aromatic hydrocarbons are major industrial feedstock chemicals and also environmental pollutants, therefore their biotransformation is important for both chemical synthesis and remediation applications. Aromatic hydrocarbons are oxidized to higher value products (*e.g.* phenols, benzoates, phthalates, quinones, hydroquinones, dyes), and biotransformation has a higher conversion efficiency than chemical transformation. However, the higher oxygenation demand of biotransformation makes it economically

unfavorable for synthesis of these products. On the other hand, aromatic hydrocarbons with polycyclic rings (PAHs) are prominent carcinogens and EPA priority pollutants [94], and therefore are top targets for water or soil remediation. Bioremediation of PAHs is shown to be feasible using *Pseudomonas sp.* NCIB 9816 [95], but the process requires continuous oxygenation via mechanical aeration. Aeration can account for more than 50% of the overall energy consumption in a typical bioremediation processes [96], making bioremediation economically less feasible.

In this communication, we designed and produced a synthetic self-sustaining ecosystem where cyanobacteria, *Synechococcus elongatus* PCC 7942, provided the necessary oxygen for NCIB 9816 to biotransform aromatic hydrocarbons, eliminating external oxygenation requirement. PCC 7942 and NCIB 9816 were encapsulated in an optically transparent, highly porous, and mechanically sturdy silica gel for synergistic biotransformation of naphthalene to CO_2 (Figure 41a). Silica gel encapsulation of whole cells (eukaryotes and prokaryotes) has been studied in the literature, and is proven to be an effective tool for utilizing and studying cells in physical confinement, as summarized in review articles [36, 97]. NCIB 9816 is known to aerobically transform over 100 aromatic hydrocarbons [98], thus has a wide range of potential applications in chemical synthesis and remediation.

We engineered the system to maximize the combined activity of NCIB 9816 and PCC 7942 populations, while ensuring ease of integration into existing industrial processes. In

almost all bioencapsulation systems, cells constitute the major proportion of the overall cost. Thus, encapsulated cell densities were optimized to maximize the biotransformation rate while minimizing the required amount of cells. The silica gel was further optimized for mechanical stability, cytocompatibility and optical transparency. Light attenuation (due to absorption and scattering effects of the encapsulating gel and the cells within) in the silica gel matrix was modeled, and experimentally verified by measuring the oxygen generation rates of the encapsulated PCC 7942 at various cell densities. This model was used to determine the geometry-dependent critical cell density parameter, which maximized total oxygen generation rate. Using this parameter, loading density of NCIB 9816 was optimized and the biotransformation performance of the system was experimentally verified. The developed ecosystem was able to sustain biotransformation reactions after the dissolved oxygen in the medium was depleted. Furthermore, it was shown that photosynthetic oxygenation via co-encapsulated PCC 7942 in very close proximity to NCIB 9816 was more efficient than external aeration due to micron scale diffusion length-scale between the co-encapsulated cells. Confocal microscopy was used to verify homogeneous distribution of the cells within close proximity.

4.3 Methods

4.3.1 Materials

Reagent grade tetraethyl orthosilicate (TEOS, 98%) and Ludox HS-40/TM-40 colloidal silica nanoparticles (SNP) were purchased from Sigma-Aldrich (Sigma-Aldrich Corp. St. Louis, MO, USA.). NexSil 85-40/125-40 silica nanoparticles were purchased from Nyacol (Nyacol Nano Technologies Inc., Ashland, MA, USA). All chemicals were used without further purification. Ultrapure water (UPW) was used in all the experiments, which was prepared by filtering distilled water through a Milli-Q water purification system (Millipore, Billerica, MA, USA) to a final electrical resistance of > 18.2 MΩ/cm.

4.3.2 Bacterial strains and growth conditions

Synechococcus elongatus PCC 7942 was obtained from the Pasteur Culture Collection of Cyanobacteria, France. *S. elongatus* PCC 7942 was grown at 28 °C in BG-11 medium [99] and was contiguously bubbled with air. The cultures were incubated at an average light intensity of 50 µmol photons m^{-2} s^{-1}. Cell growth was monitored by measuring OD730 on a Beckman DU 640 spectrophotometer (Beckman Coulter, Fullerton, CA). When the culture reached OD730 of 0.8, it was harvested by centrifugation at 8,000 rpm for 20 min at 22 °C. Cultures of *Pseudomonas sp.* NCIB 9816-4 were grown on Luria Broth (LB) at 30°C for about 8 h and used to inoculate minimal salts buffer (MSB) at OD600 of 0.01. MSB was prepared following previously discussed methods [100], with the following substitutions (Hutner's Metals): 318 mg of $Na_2EDTA \cdot 2H_2O$, 24 mg of $CoSO_4 \cdot 7H_2O$,

17.7 mg of $Na_2B_4O_7 \cdot 10H_2O$. The MSB was supplemented with 1 g naphthalene per 300 mL media. Cultures were grown in 2 L shake flasks (at 230 rpm) for 18 h at 25°C with vigorous aeration. Cultures that reached a final OD600 of 1.5–2.5 were filtered through glass wool to remove any naphthalene crystals remaining in the solution prior to harvest. Cells were harvested by centrifugation at 5,000g for 10 min. All cells were re-suspended at approximately 0.5 g wet mass/mL in phosphate buffered saline (PBS) for encapsulation. The OD730 of the cell suspensions were 1.2 after a 100-fold dilution.

4.3.3 Silica gel synthesis and encapsulation of bacteria

Tetraethyl orthosilicate (TEOS) was hydrolyzed by stirring 2 h at a 1:5.3:0.0013 molar ratio of TEOS:water:HCl. The pH of the SNPs was adjusted to 7.4 by adding 1M hydrochloric acid. After pH adjustment, PBS was added to further stabilize the pH of the SNPs and improve overall cytocompatibility of the solution. Bacteria suspension was added to SNP/PBS solution, and hydrolyzed TEOS was added to the SNP/PBS/bacteria solution by pipetting a few times to obtain a homogeneous sample. The final product was placed in glass vials or 96-well plates (depending upon the experiment) for gelation. Final volume of the gels consisted of 40% of silica precursors (TEOS + SNP) and 60% of (PBS + Bacteria suspension). Gels were named based on the volumetric ratio (α) of TEOS to (TEOS + SNP) in the gel formulation. For instance, SNP/α = 0.25 gel with 10% [v/v] cells had 300 µL of SNP, 100 µL of hydrolyzed Si alkoxide, 100 µL of cell suspension and 500 µL of PBS per mL of gel.

4.3.4 Mechanical property measurement

Gels were synthesized in cylindrical molds (diameter = 12.5 mm, height = 12.5 mm). After gelation, samples were removed from the molds and placed briefly into PBS to keep them hydrated until testing. The samples were tested by axial compression until failure at a loading rate of 1 mm/min using an MTS QT10 mechanical testing machine (MTS Systems, Eden Prairie, MN). The stress at failure was reported as is, and elastic modulus was calculated from the linear-elastic region of the stress–strain curve using Matlab (Mathworks, Inc., Natick, MA).

4.3.5 Oxygen generation/consumption and biotransformation rate measurement

Oxygen generation and consumption rates of the silica gel encapsulated bacteria were measured by using an Oxygraph Oxytherm System (Hansatech Instruments Ltd., United Kingdom). Silica gels were made into cylindrical 200 µL test pieces by mixing the reagents and bacteria suspension in a 96-well plate. After gelation, a thin copper wire was used to extract the test pieces (radius = 0.32 cm and height = 0.62 cm) and suspend them in the reaction chamber during measurement. For oxygen production measurements with cyanobacteria containing gels, 3 mL of PBS was added to the chamber and the LED was turned on to provide light to the cyanobacteria. The light intensity in the chamber was 89 µmol photons m^{-2} s^{-1} (estimated using pixel intensity and calibration from a light meter). For oxygen consumption measurements with NCIB 9816 containing gels, 3 mL solution of PBS saturated with naphthalene was added to the chamber.

For biotransformation rate measurements, NCIB 9816 and PCC 7942 were mixed gently via vortexing prior to encapsulation. Silica gels with co-encapsulated cells were synthesized (500 µL volume, height = 0.15 cm) in septa sealed, glass vials. After gelation, 9 mL of saturated naphthalene + BG-11 solution was added on top of the gel, ensuring that the vial was completely filled before sealing (except for the samples with additional 4 mL of headspace). Then, the samples were placed on a shaker setup and incubated at an average light intensity of 98 µmol photons m^{-2} s^{-1}. Naphthalene concentrations in the solution were measured intermittently using gas chromatography–mass spectrometry, as described in a previous report [95].

4.3.6 Confocal imaging of co-encapsulated cells

NCIB 9816 were incubated with BODIPY R6G fluorescent dye (ThermoFisher Scientific, MA, USA) before encapsulation. PCC 7942 were encapsulated without addition of a fluorescent dye because of their auto-fluorescence. Samples were prepared by pipetting 20 µL gel volume on a glass slide and were sealed using an adhesive spacer and a cover slip. Confocal images were taken using a Nikon A1Rsi inverted confocal microscope (Nikon Instruments Inc., Melville, NY), using a 488 nm laser.

4.4 Results and Discussion

4.4.1 Material design and characterization

Silica gels were synthesized using two precursors: Tetraethyl orthosilicate (Si alkoxide) and aqueous silica nanoparticles (SNPs). The volumetric ratio of the two silica precursors (α = Si alkoxide / (Si alkoxide + SNP)), and the diameter of the SNPs were varied to optimize the mechanical and optical properties of the silica gels. Optical properties of the silica gels varied considerably with the size of SNPs used. Gels made with HS40 (12 nm in diameter) and TM40 (22 nm) SNPs were visibly transparent, while NS85-40 (55 nm) and NS125-40 (85 nm) gels were opaque, independent of α. Since optical transparency is crucial for efficient oxygen generation, NS85-40 and NS125-40 gels were excluded from the study. Transparent gels synthesized with HS40 and TM40 SNPs were further characterized using UV-Vis spectrophotometry (Figure 4.1b). In the entire photosynthetically active spectral range (PAR, 400-700 nm), transmittance (ratio of transmitted light to received light) in the gels synthesized with smaller (HS40) SNPs was higher than that of gels synthesized with larger (TM40) SNPs. The wavelength of 680 nm was selected for characterization studies as it is the maximum absorption wavelength for Photosystem II [101], where oxygen evolving complex is located in cyanobacteria. It was further observed that transmittance of TM40 gels decreased gradually as α decreased, while that of HS40 gels were unaffected (Figure 4.1b). This was attributed to formation of silica aggregates by the Si alkoxide during gelation [53]. These aggregates were smaller than the TM40 SNPs but comparable in size to the HS40 SNPs, thus they did not affect the optical properties of the HS40 gels.

The gel with the best mechanical properties (HS40/α = 0.5) had an elastic modulus of 8.79 ± 0.72 MPa and a stress at failure of 380 ± 34 kPa (Figure 4.1c-d). HS40 gels had higher mechanical properties as compared to the TM40 gels, for all α values tested, which is due to the higher crosslinking density of the smaller nanoparticles. HS40 gels were also superior to TM40 gels in terms of optical transparency, thus TM40 gels were not further investigated. Mechanical properties (elastic modulus and stress at failure) of the gels declined as α decreased. This is in accordance with previously reported results that increasing Si alkoxide content of the gel improves its mechanical properties, albeit reducing the viability of the encapsulated biocatalytic bacteria [53]. In that system the encapsulated bacteria were recombinant *Escherichia coli* overexpressing a catalytic enzyme, and cell viability was not essential. However, in this system NCIB 9816 and PCC 7942 must both be viable to carry out biotransformation and photosynthesis, respectively. Thus, we proceeded with measuring their post-encapsulation biological activity with respect to α.

Activity of encapsulated PCC 7942 was evaluated by measuring its oxygen generation rate. The rate increased significantly when α decreased from 0.5 to 0.25, and plateaued around 4.4 ± 0.1 nmoles/min (Figure 4.1e). Conversely, activity of the silica gel encapsulated NCIB 9816 was evaluated by measuring oxygen depletion in the supernatant due to biotransformation of a saturated naphthalene solution. The naphthalene-dependent oxygen consumption rate of encapsulated NCIB 9816 increased significantly from α = 0.5 to 0.25, and a maximum of 45.3 ± 6.6 nmoles/min was

achieved at $\alpha = 0.16$ (Figure 4.1e). These results verified that a compromise was necessary between the cytocompatibility and the mechanical properties of the gel. HS40/$\alpha = 0.25$ gels had very small loss in oxygen generation (with PCC 7942) and biotransformation (with NCIB 9816) activity, and maintained better mechanical properties as compared to the other cytocompatible ($\alpha = 0.16$ and 0.12) gels. While the mechanical properties of all the tested silica gel formulations were sufficiently high for our experiments, we opted to use HS40/$\alpha = 0.25$ gel for modeling and optimization purposes to facilitate its potential use in a scaled-up biotransformation application.

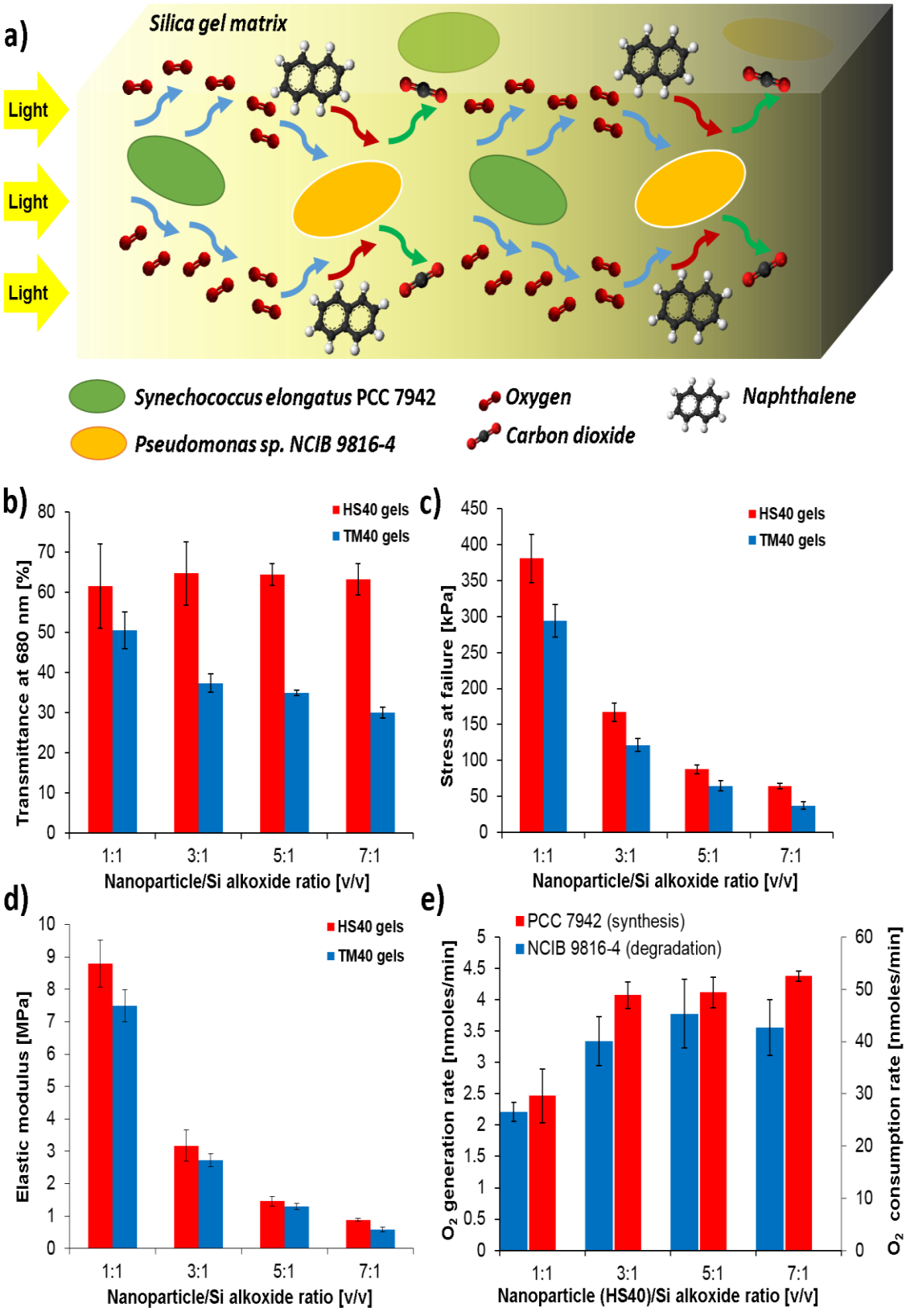
a)
Silica gel matrix
Light
Light
Light
Synechococcus elongatus PCC 7942
Pseudomonas sp. NCIB 9816-4
Oxygen
Carbon dioxide
Naphthalene
b)
HS40 gels
TM40 gels
Transmittance at 680 nm [%]
Nanoparticle/Si alkoxide ratio [v/v]
c)
HS40 gels
TM40 gels
Stress at failure [kPa]
Nanoparticle/Si alkoxide ratio [v/v]
d)
HS40 gels
TM40 gels
Elastic modulus [MPa]
Nanoparticle/Si alkoxide ratio [v/v]
e)
PCC 7942 (synthesis)
NCIB 9816-4 (degradation)
O2 generation rate [nmoles/min]
O2 consumption rate [nmoles/min]
Nanoparticle (HS40)/Si alkoxide ratio [v/v]

Figure 4. 1 Silica gel matrix optimization based on its optical and mechanical properties, and the post-encapsulation activity of PCC 7942 and NCIB 9816. Four different α values (0.5: Highest Si alkoxide, to 0.12: Lowest Si alkoxide in gel formulation) and two different nanoparticle sizes (HS40: 12nm, TM40: 22 nm) were tested. a) **Schematic of the biotransformation system illustrating the silica gel encapsulated bacteria, and the transport of substrates between cells** b) **Optical transmittance of the gels at 680 nm and 1 cm pathlength,** c) **Stress at failure,** d) **Elastic modulus,** e) **Oxygen generation rate of encapsulated PCC 7942 (in PBS) and oxygen consumption rate of encapsulated NCIB 9816 during biotransformation of naphthalene in saturated naphthalene solution** ***(All error bars indicate standard deviation with n ≥ 3).***

4.4.2 Modeling of oxygen generation and consumption

A mathematical model was constructed to analyze oxygen generation by encapsulated PCC 7942 as a function of cell density (ρ) and distribution of light intensity (I) in the silica gel. Light intensity varies through the gel as both the silica gel and the encapsulated bacteria within contribute to light attenuation (At) via absorption and scattering. Spatial attenuation in one dimensional solutions in photobioreactors (where bacteria are freely suspended in media) has been extensively studied [102], and is typically modeled by the Beer-Lambert law:

$$At(\rho, x) = C_1 \rho x \quad (1a)$$

where attenuation coefficient C_1 represents the contribution of cells to light attenuation, ρ is the cell density (of the photosynthetic bacteria), and x is the pathlength of light in the cell suspension. This model can be modified for silica gel encapsulated PCC 7942 as follows:

$$At(\rho, x) = (C_1 \rho + C_0(1 - \rho))x \quad (1b)$$

where attenuation coefficient C_0 represents the contribution of the gel to light attenuation, and x is the distance from the gel surface.

Coefficients of Equation (1b) were determined experimentally by measuring light transmittance through HS40/α = 0.25 gels with encapsulated PCC 7942 at different cell densities, as well as with free PCC 7942 in suspension (Figure 4.2a). It was observed that light attenuation through free and encapsulated cell volumes were very similar, indicating that the optical transparency of the designed gel (C_0 = 0.089 1/cm) was sufficiently high

and the major contribution to light attenuation in the gel was due to cells (C_1 = 116.42 mL/(mL cells-cm)). Thus, the cell density and light penetration are inversely correlated and contribution of each bacterium to overall oxygen generation decreases along the pathlength (due to increased attenuation), potentially reaching zero at a critical distance from the surface. Using Equation (1b), transmittance (T) at a distance x from the gel surface for encapsulated PCC 7942 was determined as:

$$\frac{I(\rho_C, x)}{I_0} = T(\rho, x) = exp(-At) = exp(-(C_1\,\rho + C_0(1-\rho))x) \quad (2)$$

Note that I_0 is the light intensity at the gel surface, which depends only on the light source characteristics. Since the light source in the experimental setup was fixed, light transmittance profile ($T = I/I_0$) was used instead of the absolute light intensity (I) in the calculations, for simplicity.

Based on Equation (2), two volume elements (Figure 4.2b) for cells encapsulated in a silica gel of uniform cross-section (UCS) and non-uniform (cylindrical) cross-section (NUCS) were defined. The UCS volume element was used for the derivation of a general analytical solution for the critical cell density parameter and optimization of the cell densities for the synergistic biotransformation study. The NUCS volume element was used for the characterization of oxygen generation in the Oxygraph chamber, where cylindrical samples were used. For UCS, a differential volume can be defined as:

$$dV = A\,dx$$

where A is the uniform cross-sectional area (the differential volume definition and the derivation of the following equations for NUCS is provided in the supplemental

information). Oxygen generation rate of cyanobacteria is known to be linearly correlated with light intensity up to a saturation limit where photo-inhibition effects start damaging the oxygen evolution complex [102]. The system was designed to operate below the saturation limit, so the net oxygen generation rate ($d\dot{q}$) in the differential volume was defined as:

$$d\dot{q} = (k_{gen}\rho_C T(\rho_T, x) - k_{con}\rho_C - k_{deg}\rho_N)dV \quad (3)$$

Table 4. 1 Oxygen generation rate model parameters

Sym-bol	Definition	Value	Units	Notes
k_{gen}	O_2 generation rate constant per unit volume of PCC 7942 per s at 100% light intensity	721.73	nmoles/ (min-mL cells)	Evaluated by fitting experimental data into the developed model
k_{con}	O_2 consumption rate constant per unit volume of PCC 7942 per s	22.1 ± 1.7	nmoles/ (min-mL cells)	Experimentally measured via Oxygraph
k_{deg}	O_2 consumption rate constant during naphthalene transformation per unit volume of NCIB 9816 per s	~18,000	nmoles/ (min-mL cells)	Adapted from Sakkos *et al.* [103]
ρ_T, ρ_C, ρ_N	Cell density (T: Total, C: PCC 7942, N: NCIB 9816)	Varies	mL cells/ (mL (gel) volume) % [v/v] *	ρ_C, ρ_N: Known $\rho_T = \rho_C + \rho_N$
C_0, C_1, C_s	Constants for contribution of cells (C_0), silica gel (C_1), and back-scattering effects (C_S) to light attenuation	$C_0 = 0.089$, $C_1 = 116.42$, $C_s = 1.88$	[1/cm], [mL/(mL cells-cm], [dimensionless]	C_0, C_1: Experimentally measured via UV-Vis spectroscopy C_S: Evaluated using the model

*****Cell volume (mL cells) was equal to the volume of PBS suspended cells. See methods for details of wet cell mass in a given cell volume.

All the parameters used in Equation (3) are summarized in Table 4.1. The net oxygen generation rate in the volume was then obtained by integrating Equation (3) over the whole volume, and incorporating the consumption by the NCIB 9816, as shown in Equation (4):

$$\dot{Q} = \int_{x=0}^{x=L} \underbrace{(k_{gen}\rho_C T(\rho_T, x)}_{I} \underbrace{-k_{con}\rho_C}_{II} \underbrace{-k_{deg}\rho_N)}_{III} A\, dx \ (\text{UCS})(\mathbf{4})$$

In Equation (4), *(I)*, *(II)* and *(III)* represent the oxygen generation by PCC 7942, oxygen consumption by PCC 7942, and oxygen consumption during aerobic transformation by the NCIB 9816, respectively. Note that in the case when only PCC 7942 was encapsulated, Equation (4) simplified to:

$$\dot{Q} = \int_{x=0}^{x=L} (k_{gen}\rho_C T(\rho_C, x) - k_{con}\rho_C) A\, dx \ (\text{UCS})(\mathbf{5})$$

Critical cell density was evaluated by differentiating Equation (5) with respect to ρ_C:

$$\rho_{cr} = \frac{A.ln\left(\frac{k_{gen}}{k_{con}}\right)}{C_1 V} = \frac{ln\left(\frac{k_{gen}}{k_{con}}\right)}{C_1 L}$$

This result showed that critical cell density, ρ_{cr}, was inversely proportional to the attenuation coefficient of the cells (C_1) and path length of the light (L), as expected. ρ_{cr} thus yielded an upper limit for the net oxygen generation rate of the system. Critical cell density for NUCS geometry was numerically solved.

The results obtained from the mathematical model were verified experimentally using an oxygen electrode as shown in Figure 2c. Cell density (ρ_C) was varied from 1% to 30%

[v/v] in the silica gel with PCC 7942 to determine how ρ_C affected oxygen generation rate (the contribution of the thin copper wire to light attenuation in the samples is assumed to be negligibly small). The net oxygen generation rate of the whole gel increased with increasing ρ_C up to a certain point, then slightly decreased (Figure 4.2d). The maximum oxygen generation rate of 3.7 ± 0.7 nmoles/min was achieved at ρ_C = 20% [v/v]. Base oxygen consumption rate constant of PCC 7942 (k_{con}) was measured in the absence of light (in the absence of oxygen generation) as 22.1 ± 1.7 nmoles/(min.mL-cells). Incorporating k_{con} and other known experimental parameters for encapsulated cells into Equation S3, k_{gen} was determined by least-squares regression with the experimental data. This yielded a k_{gen} value of 1228.6 nmoles/(min.mL-cells) for a fit as shown in Figure 2d (blue line), and a ρ_{cr} value of 7.82% [v/v]. It was shown in the literature that cells receive some back-scattered light from other cells, which can also contribute to photosynthesis [104]. Thus, back-scattering contributions were incorporated into Equation (1b) with a coefficient C_S, as follows:

$$At(\rho, x) = \frac{-(C_1 \rho + C_0(1-\rho))}{C_S} x \quad (6)$$

When back-scattering effects were accounted for k_{gen} was 721.74 nmoles/(min.mL-cells), ρ_{cr} was 12.1% [v/v], and C_s was 1.88 with a fit as shown in Figure 4.2d (red line). It is evident that the model, which incorporated back-scattering fit the experimental data and predicted the value of ρ_{cr} significantly better. The modified model was then used to optimize the relative densities of the co-encapsulated cells for naphthalene biotransformation.

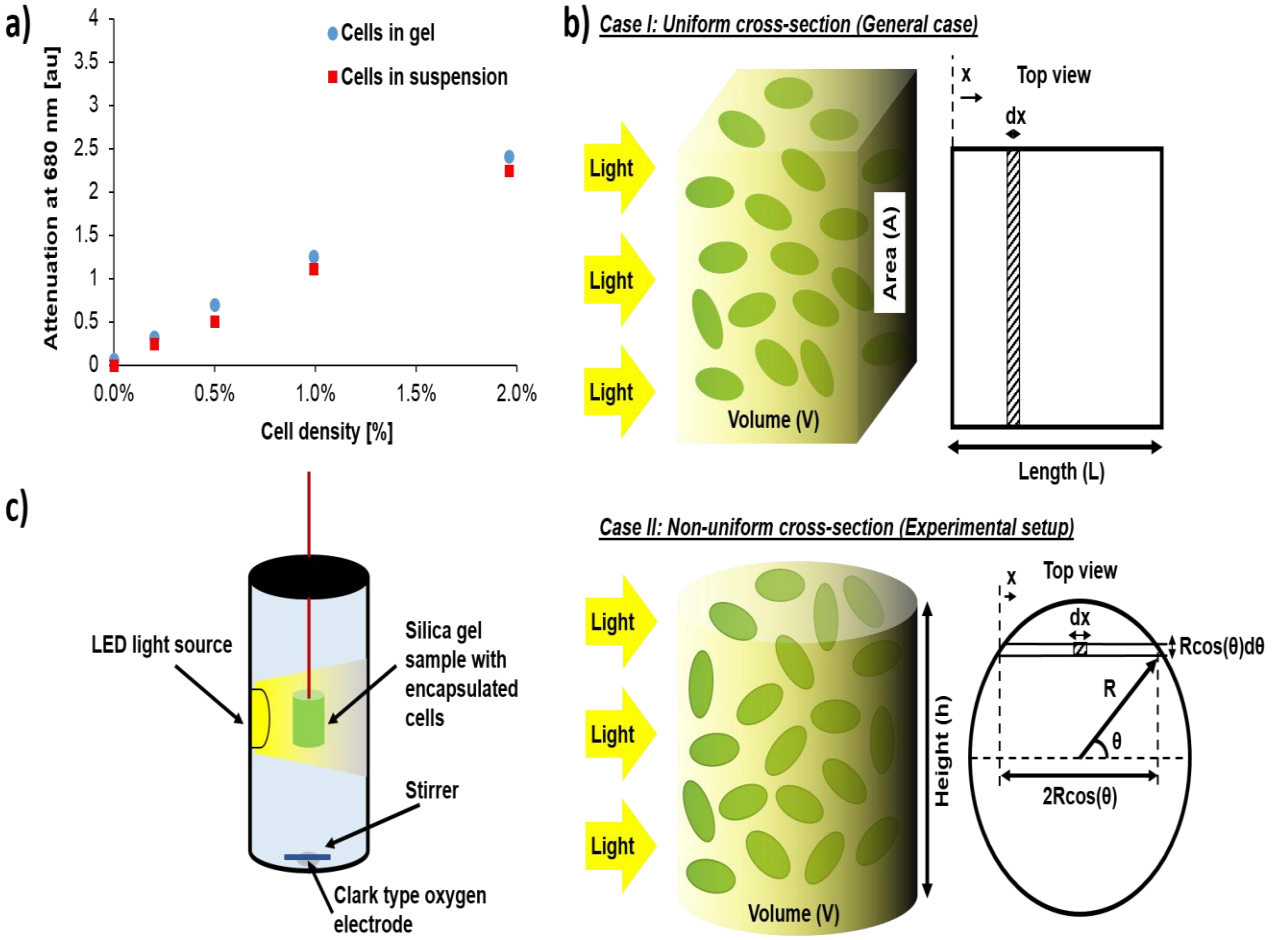
a)
Attenuation at 680 nm [au]
Cells in gel
Cells in suspension
Cell density [%]
0.0%
0.5%
1.0%
1.5%
2.0%
b)
Case I: Uniform cross-section (General case)
Light
Light
Light
Area (A)
Volume (V)
x
Top view
dx
Length (L)
c)
LED light source
Silica gel sample with encapsulated cells
Stirrer
Clark type oxygen electrode
Case II: Non-uniform cross-section (Experimental setup)
Light
Light
Light
Height (h)
Volume (V)
x
Top view
dx
Rcos(θ)dθ
R
θ
2Rcos(θ)

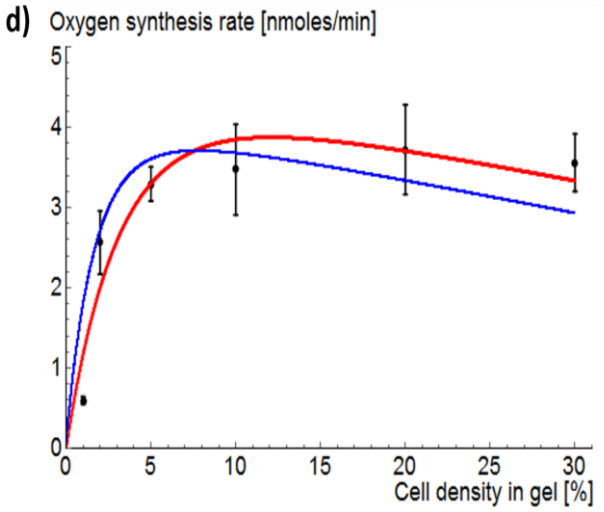

Figure 4. 2 Modeling the oxygen generation rate of the silica gel encapsulated PCC 7942. Light attenuation in the matrix by the silica gel material and encapsulated cells was characterized using UV-Vis spectroscopy. Modeling results were experimentally verified by measuring oxygen generation rate of the encapsulated cells at varying cell density. a) **Light attenuation in cells suspended in PBS (red) and silica gel encapsulated cells (blue),** b) **Schematic for the model in two different gel geometries with encapsulated cells,** c) **Schematic: Experiment setup (Oxygraph) used for oxygen generation or consumption rate measurements with encapsulated cells, Image: Silica gel samples with encapsulated PCC 7942. Oxygen (synthesized via photosynthesis) bubbles are clearly visible on the supporting wires (indicated with white arrows),** d) **Experimental measurements of oxygen generation rate of silica gel encapsulated PCC 7942 (black diamonds), and model results with (red curve) and without (blue curve) light back-scattering effects** ***(All error bars indicate standard deviation, n > 3).***

4.4.3 Optimization of the co-encapsulation matrix and synergistic biotransformation study

In mechanical aeration, oxygen partitions into water at the air interface, diffuses through the bulk of the liquid and the encapsulation matrix and reaches the biotransforming bacteria. On the other hand, encapsulated PCC 7942 generated oxygen in close vicinity of the biotransforming bacteria, NCIB 9816, minimizing transport barrier, enhancing the activity of the system developed here. Homogeneous distribution and micron-scale proximity of co-encapsulated cells in the gel matrix are illustrated by confocal microscopy images taken at two different ratios of PCC 7942 and NCIB 9816 (10%:10% [v/v] and 10%:1% [v/v]) (Figure 4.3a).

The goal of the optimization study was to maximize the biotransformation rate of naphthalene to CO_2 while minimizing the required amount of cells. We proposed that under optimal operating conditions, the system is to have neither an oxygen surplus (*i.e.* excess PCC 7942) nor an oxygen deficit (*i.e.* excess NCIB 9816). This design requirement was satisfied by solving Equation (4) for $\dot{Q} = 0$, which yielded a non-linear ρ_C vs. ρ_N curve (Figure 4.3b). It can be seen that ρ_C increased with increasing ρ_N, up to ρ_N = 0.4% [v/v] where a ρ_{cr} value of 40% [v/v] was reached. If ρ_N is increased beyond this critical point, additional PCC 7942 cannot provide more oxygen for the biotransformation reactions, yielding an oxygen deficit ($\dot{Q} < 0$).

Model analysis (in the previous section) showed that maximum oxygen generation rate was achieved at a critical PCC 7942 cell density: $\rho_C = \rho_{cr}$. It is clear that in order to maximize the biotransformation rate of the system, the density of PCC 7942 should be set to ρ_{cr}, and based on the optimization study the density of NCIB 9816 should be at $\rho_{N,}$ which yields $\dot{Q} = 0$. It should be noted that the solution which maximizes the biotransformation rate is not the most cost-effective point to operate the system, due to the non-linearity of the $\dot{Q} = 0$ curve. Decreasing ρ_C and ρ_N (*i.e.* moving left on the $\dot{Q} = 0$ curve) would increase the cost-effectiveness of the system, but also reduce the biotransformation rate, which may not satisfy the performance requirements.

Based on the experimental parameters selected, the optimal volumetric ratio of NCIB 9816 to PCC 7942 were approximately 1/100 = 0.01. The efficiency of oxygenation can be calculated by considering a hypothetical case with no light attenuation in the gel (either by the gel or cells), where all the PCC 7942 generate oxygen at the maximum rate (k_{gen}). In such a case, the NCIB 9816 to PCC 7942 cell ratio would be equal to k_{gen}/k_{deg} = 0.04. Since 0.04 is the highest that this ratio can be, an efficiency factor can be calculated as: η = 0.01/0.04 = 25%. This result means that if the cells were co-encapsulated in an extremely thin gel with a single cell layer, one fourth of the encapsulated PCC 7942 would be sufficient to supply the same amount of oxygen. In our experiment setup, the strong hydrophilic interactions between the gel and the glass surface made it difficult to obtain a very thin gel with uniform thickness. Thus, experimental parameters were kept constant despite the low oxygenation efficiency.

Naphthalene biotransformation experiments with silica gel co-encapsulated cells were conducted as shown in Figure 4.3c. Four cases were tested: (I) No cells: Silica gel without cells, (II) NCIB 9816: Silica gel encapsulated NCIB 9816, (III) NCIB 9816 with air: Silica gel encapsulated NCIB 9816 with additional headspace which provides additional oxygen for biotransformation reactions and (IV) NCIB 9816 with PCC 7942: Silica gel co-encapsulated NCIB 9816 and PCC 7942. Based on oxygen consumption experiments of a scaled-down system, the point where the dissolved oxygen concentration in the solution was expected to be depleted was approximately 4 hours. Thus, the time points were selected as 4 and 24 hours for the naphthalene biotransformation experiment. In Case I, naphthalene concentration decreased only slightly over 24 hours (Figure 4.3d), verifying that the disappearance of naphthalene due to effects other than biotransformation was minimal. For cases II, III and IV, naphthalene concentrations were comparable after 4 hours at 52.3 ± 4.1%, 49.8 ± 10.9% and 43.9 ± 7.6% respectively. These values indicated that when a sufficient amount of dissolved oxygen was present in the solution, oxygen generation by encapsulated cyanobacteria did not make a difference. At 24 hours, the naphthalene concentrations in cases II and III were still comparable, whereas the naphthalene concentration for case IV was measured as 16.3 ± 2.3%, which was significantly lower than cases II and III. This indicated that dissolved oxygen was depleted in solution sometime between 4 and 24 hours, and after the depletion of dissolved oxygen, PCC 7942 provided oxygen to further drive the biotransformation reactions.

Experimental results also verified that oxygenation via co-encapsulated PCC 7942 (Case IV) was more efficient than providing oxygen externally (Case III). Oxygenation of a bioreactor using photosynthetic microorganisms was previously tested in spatially unstructured environments [105-107], but was shown to limit the biotransformation rate. In our system, we observed the opposite result due to the optimized and stabilized cell densities, as well as close spatial distribution of the cells. It should be noted that an aeration system which provides air directly into the solution could perform better than Case III, since it eliminates the partitioning limitation of oxygen from air to solution. However, this condition was not tested since naphthalene is a very volatile chemical and ensuring that it would stay in the solution in an open system was not feasible. In our experiment, approximately 60% to 70% of the naphthalene was transformed with the amount of dissolved oxygen in water (Case II, Figure 4.3d). Dissolved oxygen in water at room temperature (260 μM) can be utilized to transform approximately 15% of a saturated (246 μM) naphthalene solution into CO_2 (based on 7.5 moles of O_2 per mole of naphthalene as previously reported [103]). This suggests that some partial transformation of naphthalene to intermediate species occurred without complete transformation.

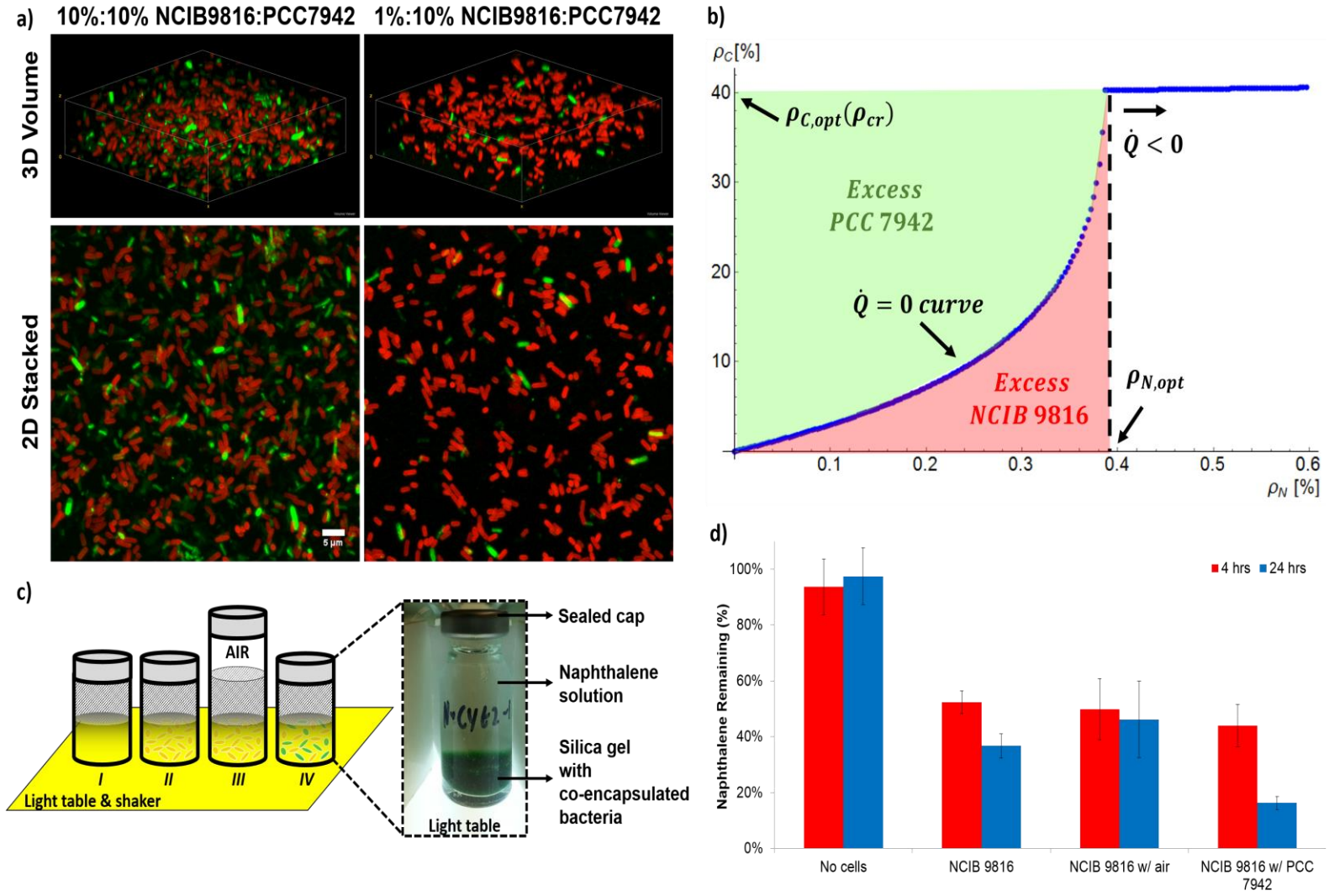
a)
10%:10% NCIB9816:PCC7942
1%:10% NCIB9816:PCC7942
3D Volume
2D Stacked
5 µm
b)
ρ_C[%]
40
30
20
10
$\rho_{C,opt}(\rho_{cr})$
$\dot{Q} < 0$
Excess
PCC 7942
$\dot{Q} = 0$ curve
Excess
NCIB 9816
$\rho_{N,opt}$
0.1
0.2
0.3
0.4
0.5
0.6
ρ_N [%]
c)
AIR
I
II
III
IV
Light table & shaker
Light table
Sealed cap
Naphthalene solution
Silica gel with co-encapsulated bacteria
d)
4 hrs
24 hrs
Naphthalene Remaining (%)
100%
80%
60%
40%
20%
0%
No cells
NCIB 9816
NCIB 9816 w/ air
NCIB 9816 w/ PCC 7942

Figure 4. 3 Synergistic biotransformation by silica gel co-encapsulated NCIB 9816 and PCC 7942. a) **Confocal images of silica gel co-encapsulated PCC 7942 (red) and NCIB 9816 (green) cells. Both species are homogeneously distributed in the silica gel matrix and positioned in micron-scale proximity.** b) **Cell densities of PCC 7942 (ρ_C) and NCIB 9816 (ρ_N) optimized for the experimental setup of the biotransformation experiment.** $\dot{Q} = 0$ **curve indicates the optimal operation conditions where the system has neither an oxygen deficit or surplus. The maximum biotransformation rate is achieved at $\rho_C = \rho_{cr}$ and corresponding ρ_N on the** $\dot{Q} = 0$ **curve** c) **Schematic of the experiment setup used for biotransformation of naphthalene. Four cases were tested: I) No cells (Negative control), II) NCIB 9816 (Oxygen is limited to the dissolved oxygen in solution), III) NCIB 9816 with headspace (Supplemental oxygen is provided via the air in the headspace), IV) NCIB 9816 with PCC 7942 (Oxygen is provided by the co-encapsulated PCC 7942)** d) **Results of the naphthalene biotransformation experiment. NCIB 9816 with co-encapsulated PCC 7942 achieved the highest biotransformation ratio *(All error bars indicate standard deviation, n = 3)*.**

Densities of PCC 7942 and NCIB 9816 were optimized based on their activity immediately after encapsulation, thus the biotransformation activity of the system was measured in a short time period (24 hours). It is known that the activity of encapsulated bacteria can vary over time, even when cell growth in the encapsulation matrix is restricted [108]. In addition, in our particular case a mutualistic relationship is expected to form between PCC 7942 and NCIB 9816, since CO_2 is essential for carbon fixation by PCC 7942. Thus, oxygen generation by PCC 7942 will be regulated by the biotransformation rate of NCIB 9816, and vice versa. It is expected that due to the temporal changes in activity and formation of a mutualistic relationship, the optimal cell densities can change during long-term use of the system. However, cell densities can still be optimized using the tools presented in this study, depending on the specific biotransformation (e.g. synthesis yield, degradation rate, etc.) goals of the application.

In summary, in this study we developed a synthetic ecosystem via 3D co-encapsulation of two bacterial populations in a silica gel matrix for synergistic biotransformation. This technology has various immediate applications in chemical synthesis and environmental remediation, but could also be used in biomedical or biosensing applications. The potential to use silica gel encapsulated bacteria as biosensors is reported in the literature [109, 110], and co-encapsulation of multiple species can amplify this potential. We expect that co-encapsulated species could either act as a supporting organism to the primary sensory species, or work successively to biotransform a sensory input (*e.g.* chemical) into a signal (*e.g.* light). This technology could also be utilized as a platform to study

fundamental microbial behavior. It has been long known that bacteria can act as a community via quorum sensing, and more recently interspecies quorum sensing was reported [111]. A synthetic ecosystem could provide a unique method to study this communication by enabling precise adjustment of bacterial communities' volume and proximity.

4.5 Publication of thesis work

This research[112] was the result of the efforts of several individuals (listed as published): Baris R. Mutlu, Jonathan K. Sakkos, Sujin Yeom, Lawrence P. Wackett & Alptekin Aksan.

For this chapter, my contributions were: Literature searching and analysis, generating ideas, obtaining *Synechococcus elongatus* PCC 7942 from the Pasteur Culture Collection of Cyanobacteria, optimizing methods for growing, harvesting, maintaining, and preserving of bacterial cultures, discussing experimental design and analyzing data for Fig. 1 and 3, and reviewing the manuscript.

CHAPTER 5 *s*-Triazine Adsorption and Biodegradation Using Hydrophobic Bio-Silica

5.1 Summary

s-Triazines are broad-spectrum herbicides used to control weeds in agriculture, and atrazine is the most widely used *s*-triazine in the United States. Accidental spills happen rarely, but such situations are best handled by immobilization of the herbicide coupled with biodegradation to ultimately destroy it. In the present study, adsorption and biodegradation were combined by designing bio-silica particles comprised of tetraethoxysilane (TEOS) and phenyltriethoxysilane (PTES) and *Arthrobacter aurescens* TC1, an *s*-triazine-degrading bacterium. A molar ratio of 3:1 TEOS:PTES was found to be optimum for binding atrazine and subsequently biodegrading the bound *s*-triazines. During the biodegradation of a limited starting concentration of atrazine, hydroxyatrazine, *N*-isopropylammelide, and cyanuric acid were quantitatively determined by HPLC and a mass balance was attained. The silica material, with and without attached cells, were characterized by light-scattering, optical microscopy, and scanning electron microscopy. That revealed nearly spherical silica particles, with a majority showing diameters of 1-3 µm. When the silica spheres were prepared in the presence of *A. aurescens* TC1 expressing green fluorescent protein, the green cells appeared to coat the silica particles that were highlighted by the hydrophobic stain Nile red. In total, these studies show feasibility for treating spills such that s-triazines can be adsorbed, the adsorption surfaces bioremediated, and further adsorption can occur.

5.2 Introduction

Atrazine is one of the most widely used herbicides to control broadleaf weeds, especially for corn, sorghum and sugarcane. It has also been used as a nonselective herbicide on non-cropped lands such as railroad ballast and highway shoulders. Once in the environment, atrazine may migrate out of soil and diffuse into a water body as it is mobile due to its low absorptivity by most soils[113, 114]. Atrazine has been detected in groundwater due to leaching and runoff[4, 5, 115]. In spill situations, larger, transient concentrations of atrazine are present in soil. The goal then is to prevent atrazine leaching into groundwater or being carried by runoff to surface water bodies. Currently, available methods for dealing with spills are to remove and dispose of contaminated soil at a landfill or incinerator. However, these methods are costly in money and energy.

Several studies have explored the use of biodegradation of to deal with high concentrations of atrazine in soil such as might occur via accidental spillage[116-121]. Although these studies showed efficacy in the laboratory, they were generally limited with respect to practical application, due to the large volumes of bacterial cultures required that would lead to an unacceptable cost. The efficiency and cost might be improved by combining physical and biological methods. In an ideal spill treatment system, atrazine would be rapidly removed by adsorption and then biodegraded by microorganisms, rendering the chemicals harmless and regenerating binding sites for adsorbing more atrazine.

The previously reported biodegradative materials for atrazine removal in our group have been prepared via the sol-gel process, starting with tetraethoxysiloxane (TEOS) or tetramethoxysiloxane (TMOS), but those suffer from being too hydrophilic[25, 53, 69]. Atrazine is considered to be hydrophobic (log k_{ow}=2.71)[122], and so a new method was developed here using organically functionalized silica that is more hydrophobic. Organically functionalized silica materials have been reported to adsorb larger amounts of organic chemicals than inorganic silica materials[123-125]. Organically functionalized silica materials have attracted increasing attention due to their ease of preparation and tunability for controlling physic-chemical properties. The hydrophobicity of materials can be tuned within a certain range by the choice of the organic groups[126].

In the present study, silica materials were prepared via co-condensation of tetraethoxysilane (TEOS) with phenyltriethoxysilane (PTES) in a one-step sol-gel procedure. *Arthrobacter aurescens* TC1, an *s*-triazine-degrading bacterium, was mixed with the two silica precursors to make a material that can serve both as an adsorbent and biodegradation catalyst. The hydrophobic materials synthesized with *A. aurescens* TC1 were characterized in terms of adsorption and biodegradation abilities. Our results showed strong absorptivity for atrazine and selective binding over the degradation products indicating that the prepared materials are reusable when adsorption sites are regenerated by biodegradation process. The biodegradation experiments of the particles showed that the material is regenerated during the biodegradation process without any additional manipulations.

5.3 Materials and Methods

5.3.1 Bacterial strains and growth conditions

Arthrobacter aurescens TC1[127] was grown in R minimal medium[128] at 30°C, with shaking. Starter cultures were made by inoculating 5 mL of R minimal medium containing 5 mM $(NH_4)_2SO_4$ as a nitrogen source and 0.2 % glucose as a carbon source with an isolated colony and incubating for 24 hours. Cell production flasks were inoculated with 1% (v/v) of starter cultures and grown in R minimal medium containing 2,000 mg/L of atrazine in powder form as a sole source of carbon and nitrogen conditions. When required, kanamycin was added to a final concentration of 200 μg kanamycin mL^{-1}.

5.3.2 Cloning procedures

The plasmid, pART2::GFP[129], was purified from *E. coli* DH5α using a QIAGEN mini-prep kit. To prepare electrocompetent cells, 100 mL of LB medium was inoculated with an overnight culture of *A. aurescens* TC1 to give a starting OD600 nm of 0.05-0.01 and incubated with shaking (250 rpm) at 28 °C. When the culture had grown to an OD600 nm = 0.5, the culture flask was incubated on ice for 15 min and then the cells were harvested at 5000 x *g*. The supernatant was removed and the cells were washed sequentially with 40, 20, and 10 ml aliquots of ice-cold sterile 10% glycerol. After the final wash, the cells were resuspended in 1 ml of cold sterile glycerol. A 200 μL aliquot of competent cells was combined with 1 μg of purified pART2::GFP in a microcentrifuge tube and incubated on ice for 10 min. After incubation, the mixture was transferred to a chilled 2.0

mm gap electroporation cuvette (Fisher) and pulsed at 2.5 kV in an Eppendorf Electroporator 2510. The cells were recovered with 0.8 mL of LB, transferred into a 14 mL Falcon tube, and incubated on a 28 °C shaker for 2 h. To select for transformants, the recovered cells were spread onto LB plates with 400 μg/mL kanamycin and incubated at 28 °C until colonies grew.

5.3.4 Silica particle preparation

All particle preparation steps were carried out at room temperature. The two silica precursors used in the synthesis of the particles, tetraethoxysilane (TEOS: $Si(OC_2H_5)_4$, 98%) and phenyltriethoxysilane ($C_6H_5Si(OC_2H_5)_3$, 98%), were purchased from Sigma-Aldrich and Acros Organics, respectively. The hydrophobic silica particles were synthesized by co-hydrolysis and co-condensation of precursors. Hydrolysis reactions of the silica precursors were controlled by adjusting the molar ratio of (TEOS+PTES):water:HCl to 1:5.3:0.0013 as previously described[53]. The mixtures prepared were stirred for 20 hours. The final particles were prepared by adding 100 μL of the hydrolyzed cross-linker solutions described above to 2 mL of 0.1 M phosphate buffer (pH 7.0). When preparing the bio-silica particles, the hydrolyzed cross-linker was added to a 2mL of bacterial cell suspension in the same phosphate buffer. Particles prepared with only TEOS served as a negative control, and the hydrophobic particles were synthesized by partially replacing TEOS with different molar ratios of PTES. The molar ratio of PTES to TEOS in the synthesized particles varied from 0 to 0.818. In reporting the results, a crosslinker ratio is denoted as Numeric number %, a PTES molar amount

that has replaced the TEOS control. The same molar amount of crosslinkers was added in preparing all alkoxide solutions, and the total molar amount of crosslinkers was considered 100%. For example, particles denoted as 0% were prepared by adding TEOS only (0% of PTES and 100% of TEOS), and particles denoted as 45% consisted of 45% of PTES and 55% of TEOS.

5.3.4 Adsorption experiments

Batch adsorption experiments were performed in a 20 mL glass scintillation vial. 5 mL solutions of 150 µM atrazine solution in 0.1 M phosphate buffer (pH 7.0) were added to 2 mL of particles prepared as described above and vials were placed on a rotary shaker. Samples were collected by filtration through a 0.2 µm pore size PTFE syringe filter to remove particles. The time-dependent adsorption profile of atrazine binding to the particles was measured using parallel samples for each time point and every time point was determined by triplicate samples.

5.3.5 HPLC analysis of atrazine and metabolites

HPLC analyses were performed by using a Hewlett-Packard HP1100 liquid chromatograph system (Agilent technologies, Santa Clara, CA) equipped with a photodiode array detector. Atrazine, hydroxyatrazine, and *N*-isopropylammelide were separated using an analytical C18 reverse-phase Agilent column with an acetonitrile (CH_3CN) gradient in water as previously described.[130] The concentrations of cyanuric acid were determined using an Alltima Amino column with an isocratic mobile phase

containing a mixture of acetonitrile and 5 mM potassium phosphate buffer (pH 7.2) in the ratio of 78%/22%.

5.3.6 Particle Size Analysis

The size distributions of particles were determined with a Microtrac S3500 particle analyzer (Microtrac Inc., PA). The particles in solution were introduced to the analyzer by pipetting. The samples were diluted with distilled water to a concentration determined by the instrument. Tests were performed in triplicate at room temperature. Particle distribution with different sizes was presented as % channel after the measurements. The percentage of each sizes (% channel) was presented relative to the total area of the chromatogram.

5.3.7 Biodegradation experiment

The changes in the culture concentrations of atrazine were continuously monitored using HPLC analysis. When the atrazine was fully utilized, *A. aurescens* TC1 cells were harvested by centrifugation at 8,000 x *g* for 20 min at 4 °C, washed twice in 0.1 M phosphate buffer (pH 7.0) and resuspended in the same buffer. Bio-silica particles were prepared by adding 100 µL of the hydrolyzed cross-linker solutions described above to 2 mL of cell suspension. 150 µM of atrazine solutions (5 mL) were added to the bio-particles prepared and placed on a rotary shaker. Samples were collected by filtration through a 0.2 µm pore size PTFE syringe filter to remove particles. The biodegradation

of the bio-particles was measured using parallel samples for each time point and analyzed by HPLC (UV). Every time point was determined by duplicate samples.

5.3.8 Fluorescence microscopy imaging

Fluorescence images were obtained on a Leica DM4000 B LED microscope equipped with a Leica DFC3000 G camera. Nile Red was added to the particles synthesized with *A. aurescens* TC1(pART2::GFP) to a concentration of 1 µg/mL to probe the hydrophobic particles. Nile red fluorescence was measured in the 570-610 nm range with an excitation wavelength of 545 nm. GFP fluorescence was measured in the 512-542 nm range with an excitation wavelength of 480 nm.

5.3.9 Scanning electron microscopy imaging

The hydrophobic particles with *A. aurescens* TC1 cells were prepared as described above. 20 µL of the mixture was deposited onto a small aluminum slide and left to dry for 2 minutes. The slides were then dipped in 2.5% gluteraldehyde for 3 h and dehydrated by a series of ethanol washes (25, 50, 75, and 100% ethanol). The ethanol was evaporated overnight in a hood. The dried samples on the slides were coated with a thin layer of iridium. The SEM images were taken with a Hitachi S4700 machine (Schaumburg, IL, USA).

5.4 Results and discussion

5.4.1 Hydrophobic silica particle preparation

The hydrophobic silica particles were prepared using a direct synthesis method where tetraethoxysilane (TEOS) condenses with phenyltriethoxysilane (PTES) as a co-precursor. The prepared hydrophobic silica particles were opaque and white (Fig. 5.1). The sol-gel transition occurred in the samples of 5% and 10% as PTES did not induce phase separation (Fig. 5.1a), indicating that the particle morphology was controlled by the initial sol composition. Because a significant phase separation was observed in 45%, the molar ratio of PTES to TEOS is greater than 1 was not investigated. Irregular materials in size and shape formed in samples where the PTES ratio was higher than 25% (Fig. 5.1b, arrows).

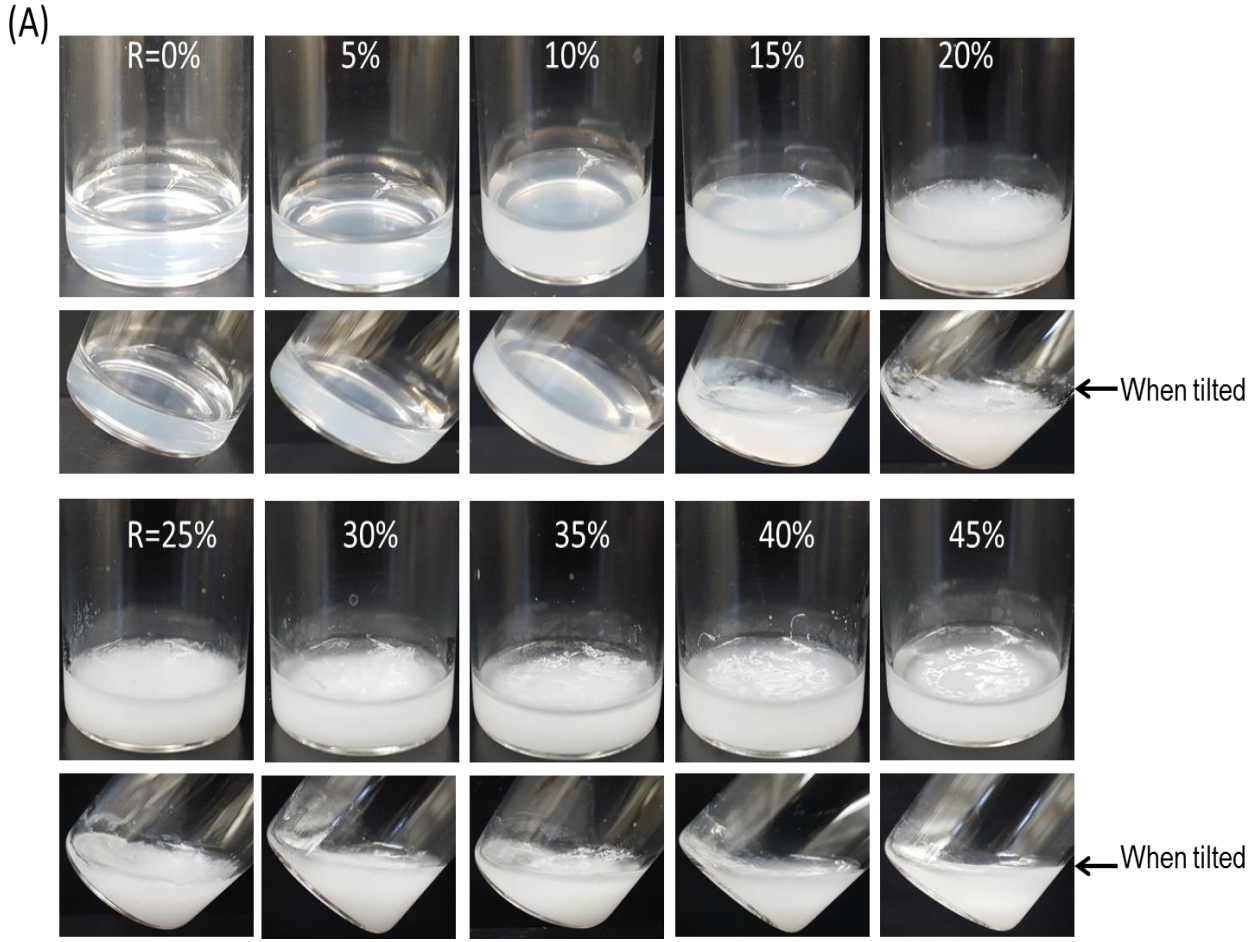
(A)
R=0%
5%
10%
15%
20%
When tilted
R=25%
30%
35%
40%
45%
When tilted

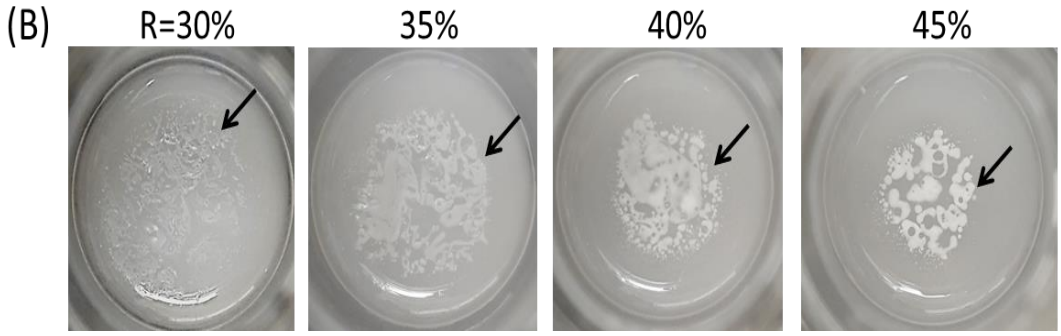

Figure 5. 1 Samples of gels and particles synthesized by the co-condensation of TEOS and PTES, as described in the method section. (a) Images taken from the side. (b) Images taken from the top.

5.4.2 Size distribution of particles

The hydrophobic particles were first characterized with respect to their size distribution profile. Particle size distribution was affected by the amount of PTES, as measured by a laser particle size analyzer (Fig 5.2). Samples where the sol-gel transition had taken place (5% and 10%) were not investigated. The mean diameter of particles gradually decreased with increasing the amount of PTES added, indicating that PTES accelerates the formation of smaller particles. Twenty-five % yielded the smallest and most homogeneous particles in size, where the mean diameter was 1.41 μm with the smallest standard deviation (Table 5.1). The mean diameter increased slightly as the PTES ratio increased further. This could be due to the early phase separation induced by PTES. The earlier the phase separation occurred before the sol-gel transition, the larger the particles were[131, 132]. The size distribution data indicates that PTES plays an important role in the phase separation and size control of the hydrophobic silica particles.

Table 5. 1 Mean diameter and standard deviation of the hydrophobic silica particles

PTES %	Mean diameter (μm)	Standard Deviation
15	19.73	9.39
20	7.41	3.88
25	1.41	0.31
30	1.78	0.78
35	1.75	0.66
40	2.88	1.23
45	3.17	1.55

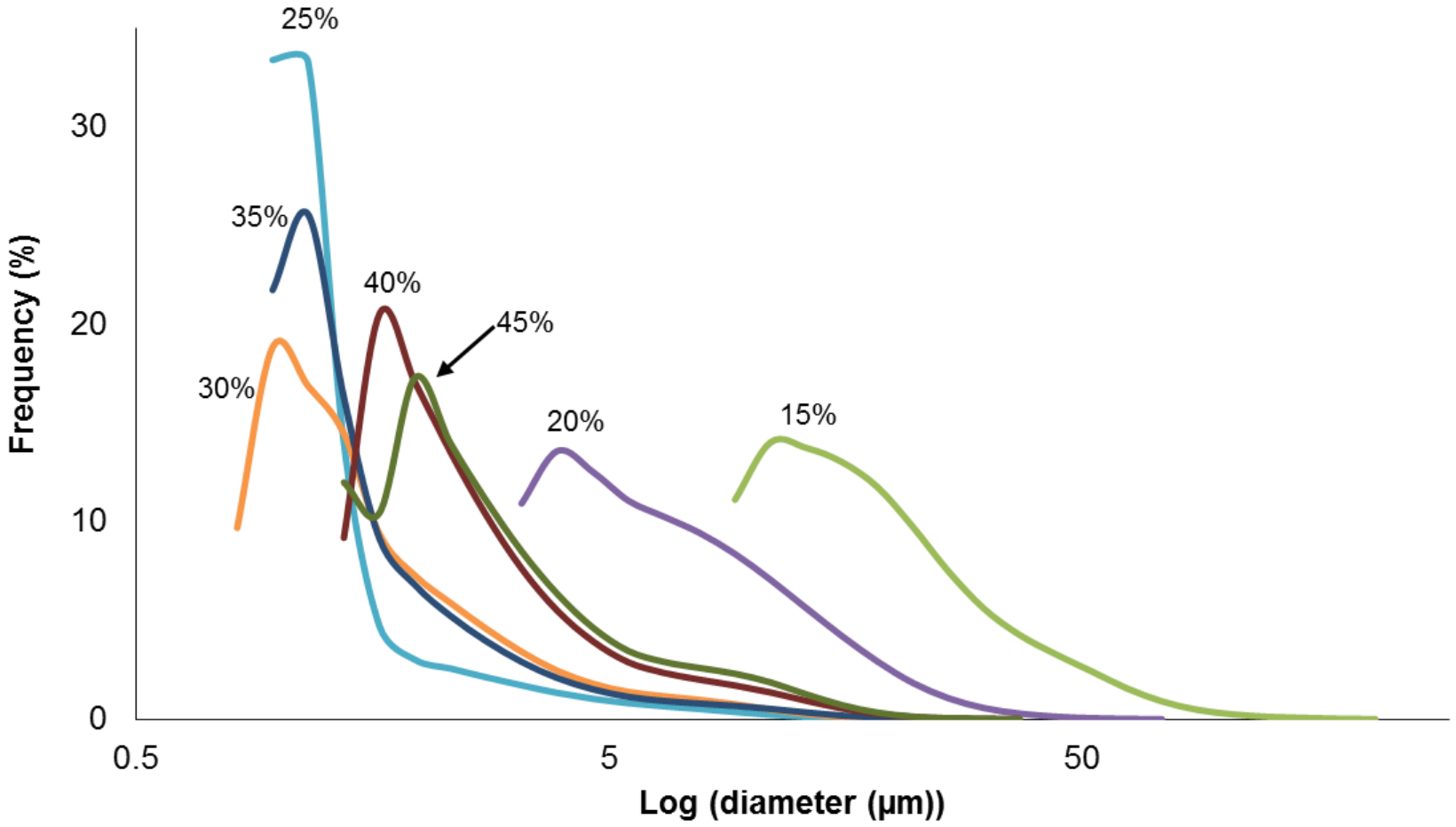

Figure 5. 2 Variation in the size distributions of the hydrophobic silica particles in solution as a function of phenyl content

5.4.3 Adsorption of atrazine to the phenyl functionalized particles

The hydrophobic particles were further characterized in terms of their adsorption properties in comparison with TEOS particles that had been investigated previously. Measurements of atrazine adsorption to the particles is shown in Figure 5.3. Immediately after atrazine solutions had been added to the prepared particles, the samples were collected. During this step, filtration of the particles took about 10 seconds. All hydrophobic particles (5% ≤ PTES ≤ 45%) adsorbed higher concentrations of atrazine than the TEOS particles, PTES = 0%. The instant adsorption of atrazine increased with the amount of PTES, and peaked with 25%, which has a molar ratio of PTES to TEOS at 1:3 to increase in hydrophobicity[133]. There was a 50% instant decrease in atrazine concentration in the solution within seconds in 25% PTES. A negative correlation of PTES amounts and adsorption was observed where PTES > 30%. This can be explained by particle size data, where particle size was found to increase as the PTES molar ratio was greater than 25%. The adsorption capacity likely decreased with an increase in the particle size because the effective surface area available for adsorption was diminishing.

Atrazine adsorption to the particles when measured over 24 hours showed a trend similar to that of instant adsorption, with adsorption increasing gradually (5% ≤ PTES ≤ 30%) and decreasing as the amount of PTES increases (35% ≤ PTES ≤ 45%).

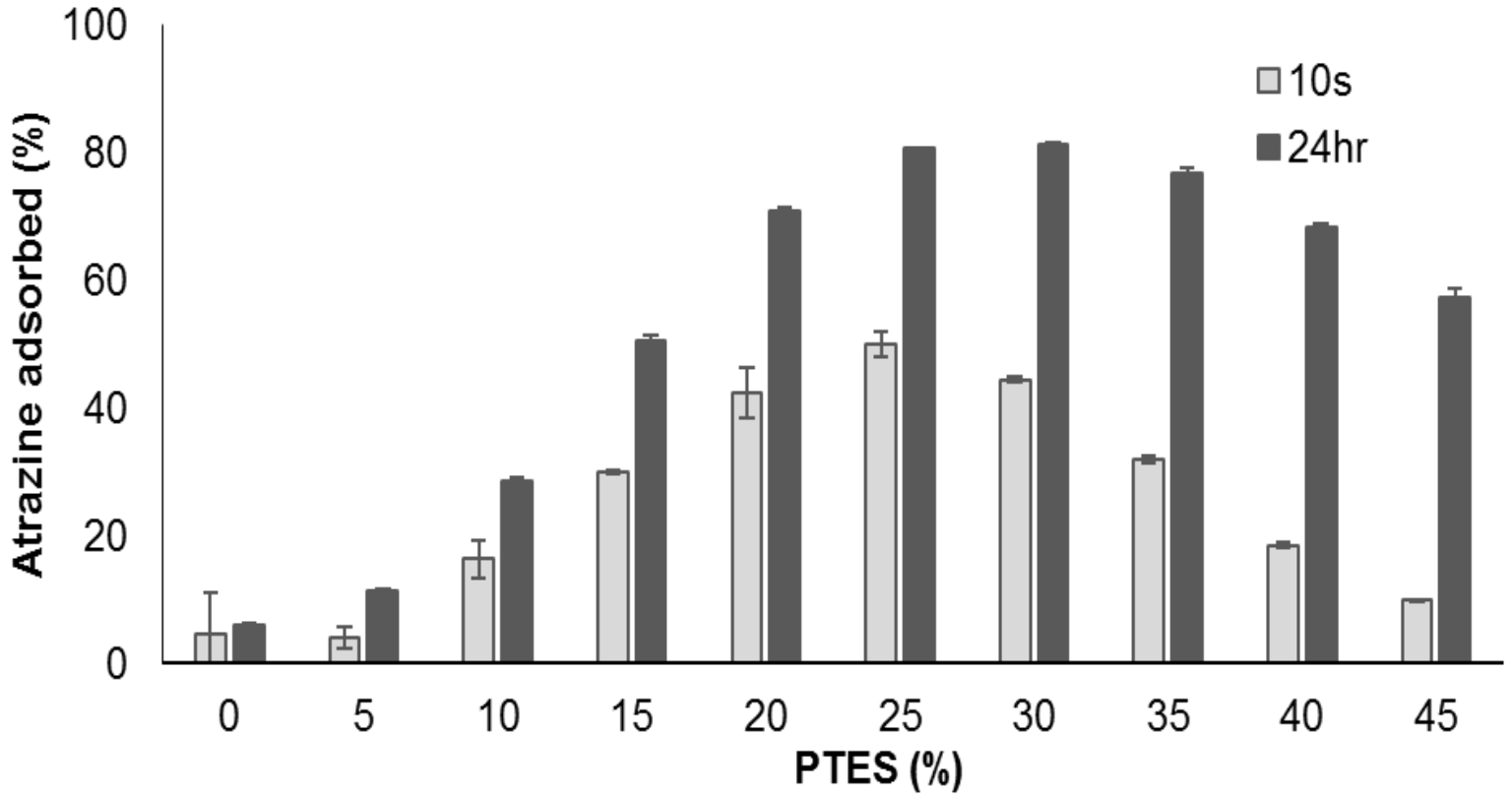

Figure 5. 3 Adsorption of atrazine to the hydrophobic silica particles as a function of phenyl content. Adsorption was evaluated after 10 seconds (Light grey bars) and 24 hours (Dark grey bars) of the addition of a 100 µM aqueous solution of atrazine to the particles, presented as a percentage adsorbed out of the initial concentration.

5.4.4 Characterization of 25% particles

In light of the results from particle size distribution and atrazine adsorption to hydrophobic particles, the 25% particles were selected for further studies to develop a material for remediation purposes. To investigate the morphology of the 25% particles, they were imaged using fluorescent microscopy and scanning electron microscopy (Fig 5.4 and 5.5). Figure 5.4 demonstrated that the silica particles were spherical, and a certain degree of aggregation occurred. Imaging via SEM also showed a similar range of particle sizes (1-3µm). Florescent microscopy revealed that the particles were observed to be stained by the hydrophobic dye Nile red that only fluoresces in hydrophobic environments[134, 135]. The fluorescent images showed that the bacteria physically associate with the hydrophobic particles (Fig. 5.5).

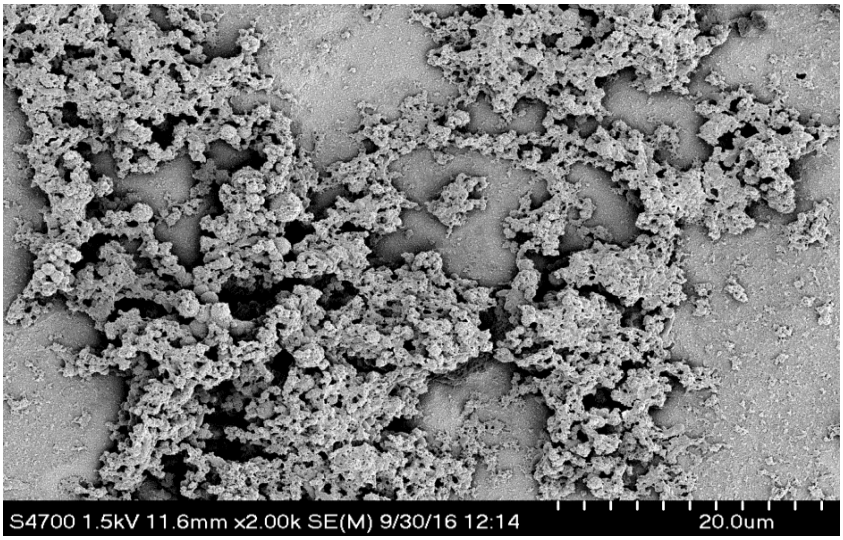

Figure 5. 4 SEM Images of 25% particles synthesized with *A. aurescens* TC1. The particles were synthesized as described in the method section in the presence of 0.01 g wet mass of *A. aurescens* TC1. The approximate ratio of particles to cells by weight is 7:1 (Scale bar = 20 µm).

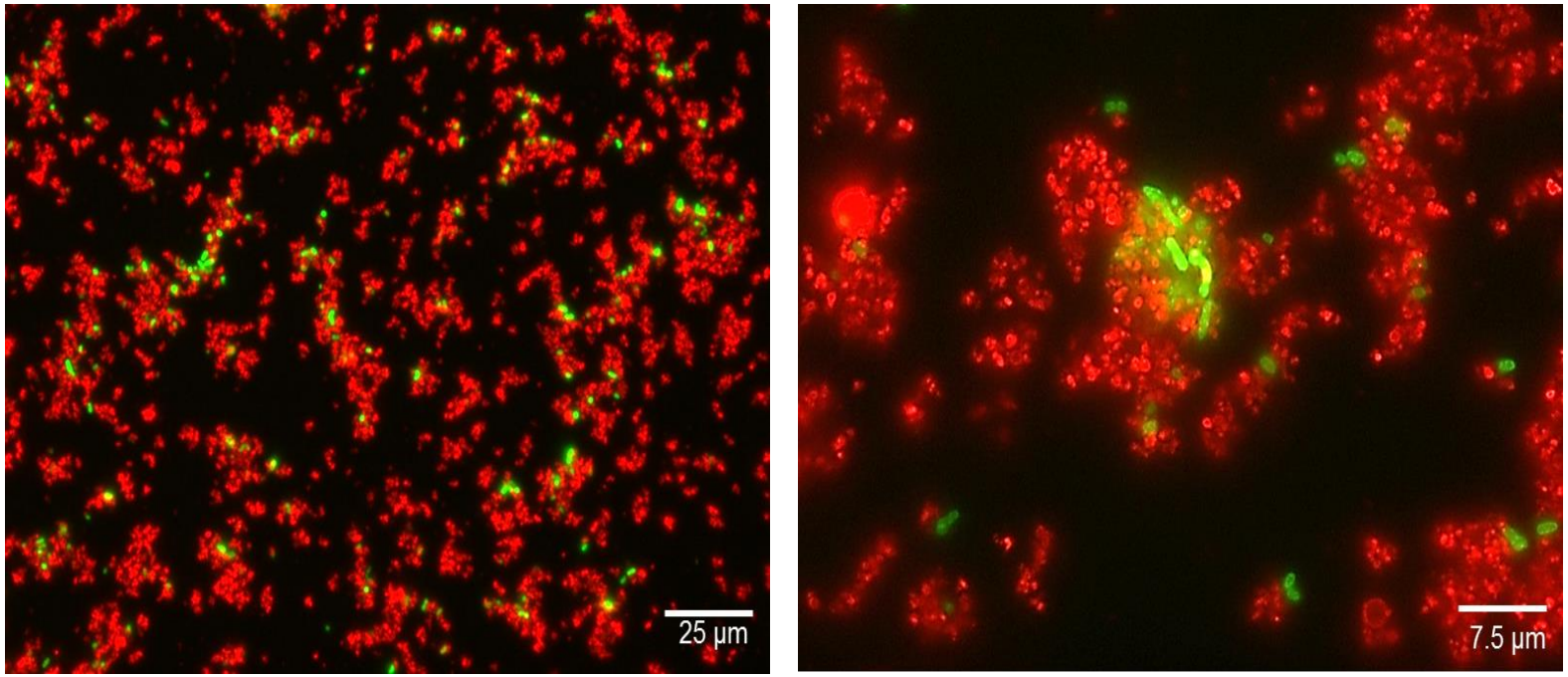

Figure 5. 5 Fluorescent images of 25% particles synthesized with *A. aurescens* TC1. The particles were synthesized as described in the method section in the presence of 0.01 g wet mass of *A. aurescens* TC1. The approximate ratio of particles to cells by weight is 7:1 Red: Silica particle stained with Nile red, Green: *A. aurescens* TC1 expressing GFP. The scales are given on each image.

Next, the kinetics of atrazine adsorption by R = 25% particles was evaluated (Fig. 5.6, ♦). The amount of atrazine adsorbed was found to depend on contact time where other parameters (pH and temperature) are kept constant. In Figure 5.6, which shows the effect of contact time on percentage removal of atrazine, it can be seen that atrazine removal continuously increases with increasing contact time. Approximately 50% of atrazine is removed within 10 sec, and the maximum adsorption is attained in about 5 hours, at which point the adsorption equilibrium is reached. Adsorbed atrazine on the particles reached 70% of the corresponding equilibrium value almost instantly. When the adsorption was combined with biodegradation, the atrazine removal by the particles was accelerated as A. *aurescens* TC1 removes atrazine by biodegradation (Fig. 5.6, ■ and▲).

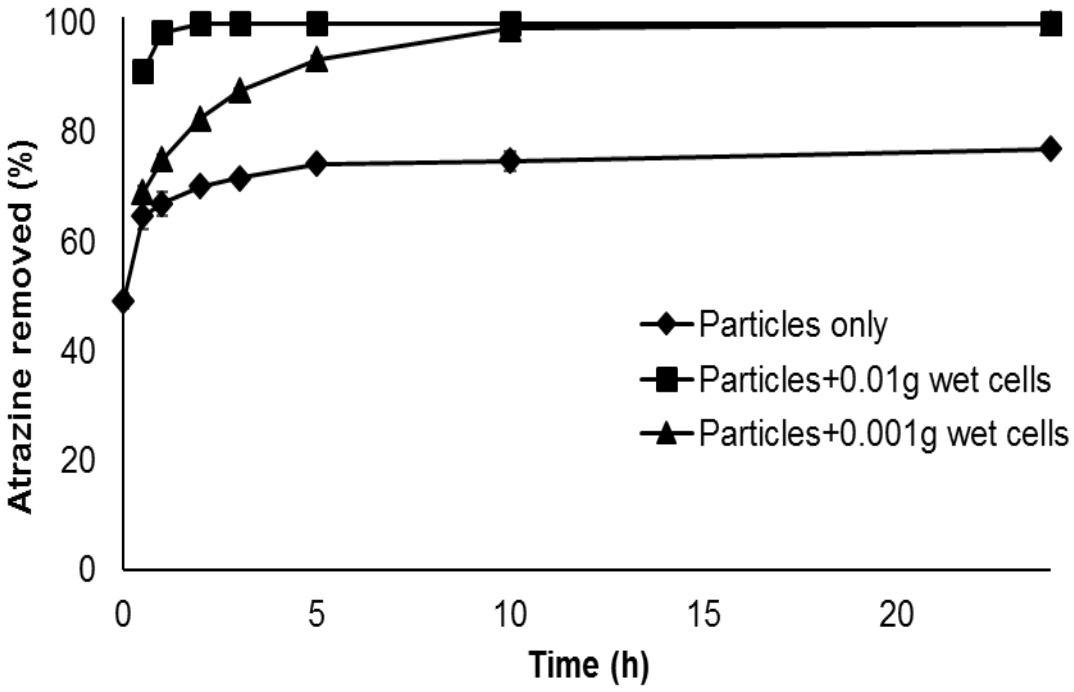

Figure 5. 6 Kinetics of atrazine removal by the hydrophobic silica particles, presented as a percentage adsorbed out of the initial concentration. ♦; the hydrophobic particles were prepared without *A. aurescens* TC1, ■; the hydrophobic particles were prepared in the presence of 0.01g wet mass of *A. aurescens* TC1, and ▲; the hydrophobic particles were prepared in the presence of 0.001g wet mass of *A. aurescens* TC1

Arthrobacter aurescens TC1 is a naturally occurring organism isolated from a contaminated soil [127]. As such, it does not require any genetic modifications for removing atrazine and, thus, can be used in any environment without concern of it being a genetically modified organism. The biodegradation of *s*-trazines by TC1 is known in detail and mediated by the enzymes TrzN, AtrzB, and AtzC (Fig. 5.7). TrzN is a broad substrate range hydrolase that performs dechlorination of atrazine and can remove multiple functional groups so that it has potential to be applied to a wide variety of *s*-trazines[136]. AtzB and AtzC catalyse the elimination of *N*-alkyl substituents from the *s*-triazine ring to yield cyanuric acid[137, 138].

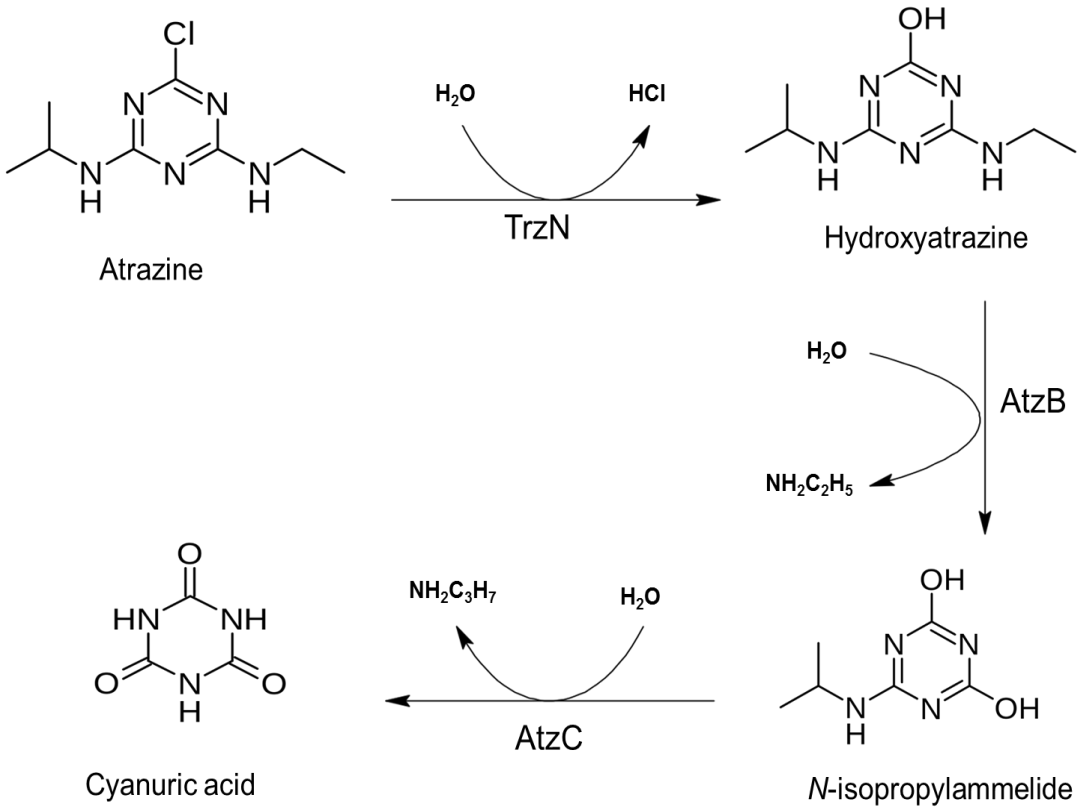

Figure 5. 7 Complete catabolic pathway for atrazine degradation in *A. aurescens* TC1.

The biodegradation of atrazine by the particles was monitored over time by measuring the products, hydroxyatrazine, *N*-isopropylammelide, and cyanuric acid, that are present in the supernatant (Fig. 5.8). Two different amounts of cells were tested. Interestingly as the biodegradation took place, mass balance was achieved at the end regardless of cell numbers. This results suggest that atrazine adsorbed to the particles are still available for bacteria to biodegrade and the complete biodegradation can be achieved with a small number of bacteria.

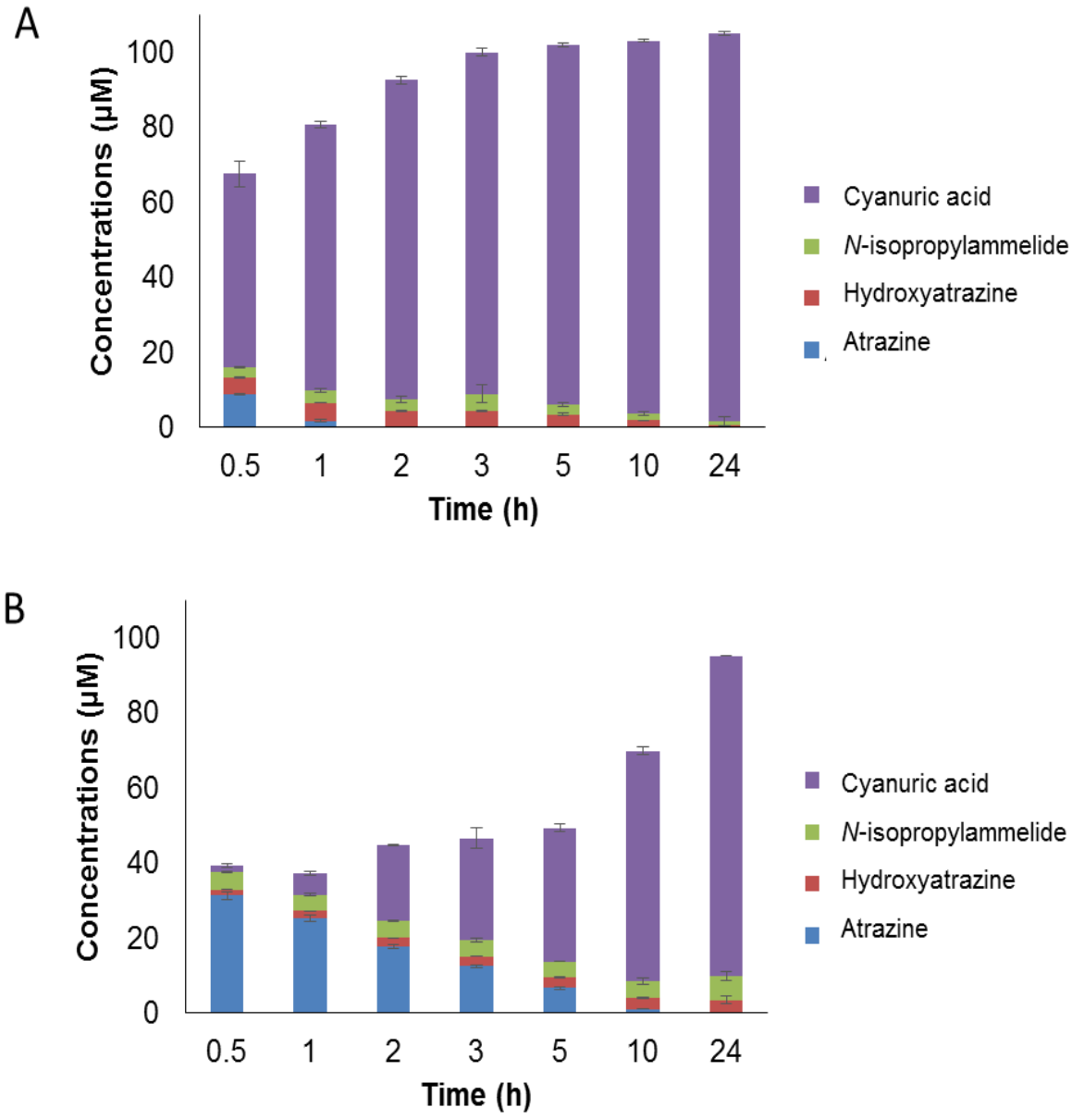

Figure 5. 8 Mass balance of atrazine and its metabolites measured during the degradation of atrazine by the hydrophobic particles over 24 hours. (A) 25% particles prepared in the presence of 0.01g of *A. aurescens* TC1 wet cells (B) 25% particles prepared in the presence of 0.001g of *A. aurescens* TC1 wet cells

Selective adsorption of the particles for atrazine suggests an advantage in using the hydrophobic particles in treating high concentration of atrazine. Selective binding allows atrazine to outcompete the products that are less hydrophobic, leading to regeneration of binding sites and additional biodegradation of atrazine. This research has generated a new strategy for *in sit* bioremediation of atrazine spills based on the selective adsorption by the hydrophobic particles and the renewal of adsorption sites by biodegradation via one-step preparation.

Contributions

I have been collaborating with Jonathan K. Sakkos, a Ph.D. candidate in Mechanical Engineering from Professor Aksan's laboratory. For this chapter, my contributions were: Literature searching and analysis, generating ideas, growing and maintaining bacterial cultures, designing and performing experiments, analyzing data, and writing the manuscript. Jonathan K. Sakkos has contributed in designing and performing experiments of SEM imaging and particle size analyzing.

CHAPTER 6 Conclusions

In this dissertation, studies were conducted to investigate the materials-biocatalysts hybrid to overcome the limitations of current technology in the field of bioremediation. The important results and conclusions drawn from these studies are summarized as follows:

In Chapter 2, atrazine, a widely-used herbicide, was chosen as a case study to develop a method that could potentially be applied to hundreds of different chemicals. *E. coli* expressing AtzA was encapsulated in novel silica components developed in the study. The atrazine chlorohydrolase enzyme displaces the chlorine atom, rendering it non-herbicidal and completely not toxic with respect to any health concerns. Since the Environmental Protection Agency regulates the atrazine level in drinking water at an upper limit of 3 parts per billion (ppb), a system for treating water containing levels of atrazine typically found in farm runoff water (3-15 ppb) was developed. The most desirable format for this purpose is filtering water through the biohybrid material. As such, a protocol was optimized step by step to make the material, and then to analyze the properties of hybrid materials. The ability of the enzyme to degrade atrazine was tested in a continuous-flow bioreactor filtration system. The atrazine concentration was maintained below the 3 ppb legal limit in the effluent of the flow-through system for 2 months.

In the next study, the method developed in chapter 2 was applied in a real-world treatment scenario. In order to utilize the hybrid material in a municipal water treatment

facility, specific parameters needed to be considered, such as: performance, operational costs and mechanical properties of the developed materials. The engineering parameters for bacterial loading density and material size to build a reaction/transport model were determined based on experimental results. A case study where the hybrid material could be used by a municipal water treatment facility to treat atrazine-contaminated water was investigated by modelling, and the method and findings were published in 2015[69].

After developing and optimizing hybrid material in chapter 2, the scope of the applications and materials was tested using different enzyme systems as well as different chemicals. Cyanuric acid was chosen to investigate in chapter 3. Cyanuric acid is a high volume industrial chemical. It is used at relatively high concentrations in a chlorinated form as a water disinfection agent in outdoor swimming pools, but cyanuric acid accumulates with repeated additions and must be removed to maintain the disinfection process. Three most well studied cyanuric acid hydrolase were compared for their efficiency in removing cyanuric acid. Cyanuric acid hydrolase originated from *M. thermoacetica* ATCC 39073 was selective for further investigation due to its high stability and activity. The selected hybrid materials were then tested in a flow-through system simulating a bioreactive pool filter. Two rounds of the simulated pool experiment were ran resulting in identical biodegradation kinetics for both tests. This indicates that the biocatalyst is robust enough for multiple uses. A pool water degradation experiment was also conducted by collecting municipal swimming pool water samples in the Twin Cities area. The results from actual swimming pool water showed the efficacy of the

process although hypochlorite present in pool samples affected the rate of cyanuric acid degradation negatively. Further studies to investigate the effects of hypochlorite and develop mitigation strategies were achieved and published in our research group[139].

One more interesting application tested is creating a structured environment that formed an ecosystem for synergistic biodegradation. The idea explored in chapter 4 is to produce a synthetic ecosystem consisting of more than one bacterial species in a structured silica matrix. Two distinct bacterial species were co-encapsulated in silica, a versatile soil bacterium, *Pseudomonas* sp. strain NCIB 9816-4 that has the ability to biodegrade more than 100 aromatic hydrocarbons and a photosynthetic bacterium, and *Synechococcus elongatus* PCC 7942 that can theoretically consume carbon dioxide from the breakdown of the aromatic compounds and more importantly, produce oxygen. The material was designed to be transparent to allow photons to penetrate to the photosynthetic bacterium. A mathematical model was derived to determine the critical cell density parameter to simultaneously optimize oxygen production by one bacterium and biodegradation by the other. Experimental results showed that the system was able to support the oxygen demand of the biodegradation reactions, and that it performed better than oxygenation by external supplementation.

In chapter 5 of my dissertation research, a hydrophobic silica material was synthesized in the presence of *Arthrobacter aurescens* TC1 that degrades atrazine faster than others. The bacterium has the enzyme, TrzN, that catalyzes the dechlorination of atrazine but has the

same reaction at a faster rate than AtzA. TrzN has a broad-specificity which allows the method can be applied to more than 20 *s*-trizine compounds. The hydrophobic silica material strongly and selectively adsorbs herbicides regenerating binding sites for herbicides. It was also observed that the bacterium physically associates with the hydrophobic material. The experiments that are in progress are to investigate the interaction between the bacterium and the hydrophobic particles. There have been no such studies elucidating the interaction mechanism between bacterial cells and silica. This research will provide not only a new bioremediation technology but also fundamental knowledge in the field of material science.

My concluding thesis studies have broad importance. Currently, society uses billions of pounds of activated carbon to adsorb chemical pollutants. The activated carbon must be land-filled or incinerated using very high heat. My research will hopefully lead to new materials that adsorb chemicals and then degrade them to safe end-products. This will save significant resources and energy and could be widely adopted by industry.

References

1. Smolin, E. M.; Rapoport, L., *The chemistry of heterocyclic compounds. A Series of Monographs. s-Triazines and Derivatives.* Interscience Publishers: New York, NY., 1959; Vol. 13, p 20-24.
2. Chemical structure of *s*-trizine. https://upload.wikimedia.org/wikipedia/commons/c/c1/135TriazineStructure.png.
3. USEPA *Decision Documents for Atrazine*; 2006.
4. USEPA *National Pesticide Survey: Summary Results of EPA's National Survey of Pesticides in Drinking Water Wells*; USEPA: 1990.
5. Gilliom, R. J.; Barbash, J. E.; Crawford, C. G.; Hamilton, P. A.; Martin, J. D.; Nakagaki, N.; Nowell, L. H.; Scott, J. C.; Stackelberg, P. E.; Thelin, G. P.; Wolock, D. M. *Pesticides in the nation's streams and ground water, 1992 – 2001: U.S. Geological Survey Circular 1291* USGS: 2006.
6. Jablonowski, N. D.; Schaffer, A.; Burauel, P., Still present after all these years: persistence plus potential toxicity raise questions about the use of atrazine. *Environmental Science and Pollution Research* **2011,** *18* (2), 328-331.
7. Albanito, L.; Lappano, R.; Madeo, A.; Chimento, A.; Prossnitz, E. R.; Cappello, A. R.; Dolce, V.; Abonante, S.; Pezzi, V.; Maggiolini, M., G-Protein-Coupled Receptor 30 and Estrogen Receptor-alpha Are Involved in the Proliferative Effects Induced by Atrazine in Ovarian Cancer Cells (Retracted article. See vol. 122, pg. A42, 2014). *Environmental Health Perspectives* **2008,** *116* (12), 1648-1655.
8. Hayes, T. B.; Collins, A.; Lee, M.; Mendoza, M.; Noriega, N.; Stuart, A. A.; Vonk, A., Hermaphroditic, demasculinized frogs after exposure to the herbicide atrazine at low ecologically relevant doses. *Proceedings of the National Academy of Sciences of the United States of America* **2002,** *99* (8), 5476-5480.
9. Biradar, D. P.; Rayburn, A. L., CHROMOSOMAL DAMAGE-INDUCED BY HERBICIDE CONTAMINATION AT CONCENTRATIONS OBSERVED IN PUBLIC WATER-SUPPLIES. *Journal of Environmental Quality* **1995,** *24* (6), 1222-1225.
10. Martinneto, L.; Vieira, E. M.; Sposito, G., MECHANISM OF ATRAZINE SORPTION BY HUMIC-ACID - A SPECTROSCOPIC STUDY. *Environmental Science & Technology* **1994,** *28* (11), 1867-1873.
11. Comber, S. D. W., Abiotic persistence of atrazine and simazine in water. *Pesticide Science* **1999,** *55* (7), 696-702.
12. Ellis, L. B. M.; Roe, D.; Wackett, L. P., The University of Minnesota Biocatalysis/Biodegradation Database: the first decade. *Nucleic Acids Research* **2006,** *34*, D517-D521.
13. Biocatalysis/Biodegaradation Database. http://eawag-bbd.ethz.ch/.
14. Atrazine Degradation Graphical Pathway. http://eawag-bbd.ethz.ch/atr/atr_image_map1.html.
15. Atrazine Degradation Graphical Pathway Map2. http://eawag-bbd.ethz.ch/atr/atr_image_map2.html.

16. WHO *Toxicological and Health Aspects of Melamine and Cyanuric Acid*; 2009.
17. Section of the extensive two-dimensional hydrogen bond network (dashed) between melamine (blue) and cyanuric acid (red). https://en.wikipedia.org/wiki/Melamine_cyanurate#/media/File:Melamine-cyanuric_acid_complex_color.png.
18. Schell, M. A., MOLECULAR-BIOLOGY OF THE LYSR FAMILY OF TRANSCRIPTIONAL REGULATORS. *Annual Review of Microbiology* **1993,** *47*, 597-626.
19. García-González, V.; Govantes, F.; Porrúa, O.; Santero, E., Regulation of the Pseudomonas sp. strain ADP cyanuric acid degradation operon. *J Bacteriol* **2005,** *187* (1), 155-67.
20. Cyanuric acid Graphical Pathway Map. http://eawag-bbd.ethz.ch/cya/cya_image_map.html.
21. USEPA, Basic information about atrazine in drinking water 2013.
22. Boopathy, R., Factors limiting bioremediation technologies. *Bioresource Technology* **2000,** *74* (1), 63-67.
23. Willaert , R. G. B., Gino V. Backer, Luc De., *Immobilised living cell systems : modelling and experimental methods.* J. Wiley & Sons.: New York, 1996.
24. Rowley, J. A.; Mooney, D. J., Alginate type and RGD density control myoblast phenotype. *Journal of Biomedical Materials Research* **2002,** *60* (2), 217-223.
25. Reategui, E.; Reynolds, E.; Kasinkas, L.; Aggarwal, A.; Sadowsky, M. J.; Aksan, A.; Wackett, L. P., Silica gel-encapsulated AtzA biocatalyst for atrazine biodegradation. *Applied Microbiology and Biotechnology* **2012,** *96* (1), 231-240.
26. Livage, J.; Coradin, T.; Roux, C., Encapsulation of biomolecules in silica gels. *Journal of Physics-Condensed Matter* **2001,** *13* (33), R673-R691.
27. Gill, I.; Ballesteros, A., Bioencapsulation within synthetic polymers (Part 1): sol-gel encapsulated biologicals. *Trends in Biotechnology* **2000,** *18* (7), 282-296.
28. Leonard, A.; Rooke, J. C.; Meunier, C. F.; Sarmento, H.; Descy, J.-P.; Su, B.-L., Cyanobacteria immobilised in porous silica gels: exploring biocompatible synthesis routes for the development of photobioreactors. *Energy & Environmental Science* **2010,** *3* (3), 370-377.
29. Ferrer, M. L.; Yuste, L.; Rojo, F.; del Monte, F., Biocompatible sol-gel route for encapsulation of living bacteria in organically modified silica matrixes. *Chemistry of Materials* **2003,** *15* (19), 3614-3618.
30. Nassif, N.; Roux, C.; Coradin, T.; Rager, M. N.; Bouvet, O. M. M.; Livage, J., A sol-gel matrix to preserve the viability of encapsulated bacteria. *Journal of Materials Chemistry* **2003,** *13* (2), 203-208.
31. Nassif, N.; Coiffier, A.; Coradin, T.; Roux, C.; Livage, J.; Bouvet, O., Viability of bacteria in hybrid aqueous silica gels. *Journal of Sol-Gel Science and Technology* **2003,** *26* (1-3), 1141-1144.

32. Fennouh, S.; Guyon, S.; Jourdat, C.; Livage, J.; Roux, C., Encapsulation of bacteria in silica gels. *Comptes Rendus De L Academie Des Sciences Serie Ii Fascicule C-Chimie* **1999,** *2* (11-13), 625-630.
33. Nassif, N.; Livage, J., From diatoms to silica-based biohybrids. *Chemical Society Reviews* **2011,** *40* (2), 849-859.
34. Oh, C. Y.; Park, J. K., The characteristics of encapsulated whole cell beta-galactosidase. *Bioprocess Engineering* **1998,** *19* (6), 419-425.
35. Coiffier, A.; Coradin, T.; Roux, C.; Bouvet, O. M. M.; Livage, J., Sol-gel encapsulation of bacteria: a comparison between alkoxide and aqueous routes. *Journal of Materials Chemistry* **2001,** *11* (8), 2039-2044.
36. Avnir, D.; Coradin, T.; Lev, O.; Livage, J., Recent bio-applications of sol-gel materials. *Journal of Materials Chemistry* **2006,** *16* (11), 1013-1030.
37. Finnie, K. S.; Bartlett, J. R.; Woolfrey, J. L., Encapsulation of sulfate-reducing bacteria in a silica host. *Journal of Materials Chemistry* **2000,** *10* (5), 1099-1101.
38. Perullini, M.; Amoura, M.; Roux, C.; Coradin, T.; Livage, J.; Laura Japas, M.; Jobbagy, M.; Bilmes, S. A., Improving silica matrices for encapsulation of Escherichia coli using osmoprotectors. *Journal of Materials Chemistry* **2011,** *21* (12), 4546-4552.
39. Organization, W. H. Atrazine and Its Metabolites in Drinking-water. http://www.who.int/water_sanitation_health/dwq/chemicals/dwq_background_20100701_en.pdf (accessed 6/3).
40. Agency, U. S. E. P. Interpreting the Atrazine Drinking Water Monitoring Data. http://www.epa.gov/oppsrrd1/reregistration/atrazine/atrazine_update.htm (accessed 6/3).
41. Zhu, L.; Ma, T.; Wang, J.; Xie, H.; Wang, J.; Xin, C.; Shao, B., Enhancement of Atrazine Removal by Free and Immobilized Arthrobacter Sp HB-5 in Soil and Wastewater. *Soil & Sediment Contamination* **2011,** *20* (1), 87-97.
42. Patricia Galindez-Najera, S.; Ramos-Monroy, O.; Ruiz-Ordaz, N.; Salmeron-Alcocer, A.; Juarez-Ramirez, C.; Ahuatzi-Chacon, D.; Curiel-Quesada, E.; Galindez-Mayer, J., Simultaneous degradation of atrazine and simazine by a binary culture of Stenotrophomonas maltophilia and Arthrobacter sp in a two-stage biofilm reactor. *Journal of Chemical Technology and Biotechnology* **2011,** *86* (4), 554-561.
43. Liu, C.; Huang, X.; Wang, H., Start-up of a membrane bioreactor bioaugmented with genetically engineered microorganism for enhanced treatment of atrazine containing wastewater. *Desalination* **2008,** *231* (1-3), 12-19.
44. Klein, S.; Avrahami, R.; Zussman, E.; Beliavski, M.; Tarre, S.; Green, M., Encapsulation of Pseudomonas sp ADP cells in electrospun microtubes for atrazine bioremediation. *Journal of Industrial Microbiology & Biotechnology* **2012,** *39* (11), 1605-1613.
45. Buttiglieri, G.; Migliorisi, L.; Malpei, F., Adsorption and removal at low atrazine concentration in an MBR pilot plant. *Water Science and Technology* **2011,** *63* (7), 1334-1340.
46. deSouza, M. L.; Sadowsky, M. J.; Wackett, L. P., Atrazine chlorohydrolase from Pseudomonas sp strain ADP: Gene sequence, enzyme purification, and protein characterization. *Journal of Bacteriology* **1996,** *178* (16).

47. Brinker, C. J., HYDROLYSIS AND CONDENSATION OF SILICATES - EFFECTS ON STRUCTURE. *Journal of Non-Crystalline Solids* **1988,** *100* (1-3), 31-50.
48. Siouffi, A. M., Silica gel-based monoliths prepared by the sol-gel method: facts and figures. *Journal of Chromatography A* **2003,** *1000* (1-2), 801-818.
49. Bird, R. B.; Stewart, W. E.; Lightfoot, E. N., *Transport Phenomena*. Wiley: 2007.
50. Brinker, C. J.; Scherer, G. W., *Sol-gel science: the physics and chemistry of sol-gel processing*. Academic Press: 1990.
51. Innocenzi, P.; Abdirashid, M. O.; Guglielmi, M., Structure and properties of sol-gel coatings from methyltriethoxysilane and tetraethoxysilane. *Journal of Sol-Gel Science and Technology* **1994,** *3* (1), 47-55.
52. Snyder, S. A.; Westerhoff, P.; Yoon, Y.; Sedlak, D. L., Pharmaceuticals, personal care products, and endocrine disruptors in water: Implications for the water industry. *Environmental Engineering Science* **2003,** *20* (5), 449-469.
53. Mutlu, B. R.; Yeom, S.; Tong, H. W.; Wackett, L. P.; Aksan, A., Silicon alkoxide cross-linked silica nanoparticle gels for encapsulation of bacterial biocatalysts. *Journal of Materials Chemistry A* **2013,** *1* (36), 11051-11060.
54. Huthmacher, K.; Most, D., *Cyanuric Acid and Cyanuric Chloride*. Ullmann's Encyclopedia of Industrial Chemistry: 2000.
55. Cook, A. M.; Beilstein, P.; Grossenbacher, H.; Hütter, R., Ring cleavage and degradative pathway of cyanuric acid in bacteria. *Biochem J* **1985,** *231* (1), 25-30.
56. Dobson, R. L.; Motlagh, S.; Quijano, M.; Cambron, R. T.; Baker, T. R.; Pullen, A. M.; Regg, B. T.; Bigalow-Kern, A. S.; Vennard, T.; Fix, A.; Reimschuessel, R.; Overmann, G.; Shan, Y.; Daston, G. P., Identification and characterization of toxicity of contaminants in pet food leading to an outbreak of renal toxicity in cats and dogs. *Toxicol Sci* **2008,** *106* (1), 251-62.
57. Puschner, B.; Poppenga, R. H.; Lowenstine, L. J.; Filigenzi, M. S.; Pesavento, P. A., Assessment of melamine and cyanuric acid toxicity in cats. *J Vet Diagn Invest* **2007,** *19* (6), 616-24.
58. Wackett, L. P.; Sadowsky, M. J.; Martinez, B.; Shapir, N., Biodegradation of atrazine and related s-triazine compounds: from enzymes to field studies. *Appl Microbiol Biotechnol* **2002,** *58* (1), 39-45.
59. Canelli, E., Chemical, bacteriological, and toxicological properties of cyanuric acid and chlorinated isocyanurates as applied to swimming pool disinfection: a review. *Am J Public Health* **1974,** *64* (2), 155-62.
60. Seffernick, J. L.; Erickson, J. S.; Cameron, S. M.; Cho, S.; Dodge, A. G.; Richman, J. E.; Sadowsky, M. J.; Wackett, L. P., Defining sequence space and reaction products within the cyanuric acid hydrolase (AtzD)/barbiturase protein family. *J Bacteriol* **2012,** *194* (17), 4579-88.
61. Martinez, B.; Tomkins, J.; Wackett, L. P.; Wing, R.; Sadowsky, M. J., Complete nucleotide sequence and organization of the atrazine catabolic plasmid pADP-1 from Pseudomonas sp. strain ADP. *J Bacteriol* **2001,** *183* (19), 5684-97.
62. Cho, S.; Shi, K.; Seffernick, J. L.; Dodge, A. G.; Wackett, L. P.; Aihara, H., Cyanuric acid hydrolase from Azorhizobium caulinodans ORS 571: crystal structure and insights into a new class of Ser-Lys dyad proteins. *PLoS One* **2014,** *9* (6), e99349.

63. Peat, T. S.; Balotra, S.; Wilding, M.; French, N. G.; Briggs, L. J.; Panjikar, S.; Cowieson, N.; Newman, J.; Scott, C., Cyanuric acid hydrolase: evolutionary innovation by structural concatenation. *Mol Microbiol* **2013,** *88* (6), 1149-63.
64. Dodge, A. G.; Preiner, C. S.; Wackett, L. P., Expanding the cyanuric acid hydrolase protein family to the fungal kingdom. *J Bacteriol* **2013,** *195* (23), 5233-41.
65. Karns, J. S., Gene sequence and properties of an s-triazine ring-cleavage enzyme from Pseudomonas sp. strain NRRLB-12227. *Appl Environ Microbiol* **1999,** *65* (8), 3512-7.
66. Li, Q.; Seffernick, J. L.; Sadowsky, M. J.; Wackett, L. P., Thermostable cyanuric acid hydrolase from Moorella thermoacetica ATCC 39073. *Appl Environ Microbiol* **2009,** *75* (22), 6986-91.
67. Schmidt-Dannert, C.; Umeno, D.; Arnold, F. H., Molecular breeding of carotenoid biosynthetic pathways. *Nat Biotechnol* **2000,** *18* (7), 750-3.
68. Cameron, S. M.; Durchschein, K.; Richman, J. E.; Sadowsky, M. J.; Wackett, L. P., A New Family of Biuret Hydrolases Involved in S-Triazine Ring Metabolism. *ACS Catal* **2011,** *2011* (1), 1075-1082.
69. Mutlu, B. R.; Yeom, S.; Wackett, L. P.; Aksan, A., Modelling and optimization of a bioremediation system utilizing silica gel encapsulated whole-cell biocatalyst. *Chemical Engineering Journal* **2015,** *259*, 574-580.
70. Jepras, R. I.; Carter, J.; Pearson, S. C.; Paul, F. E.; Wilkinson, M. J., Development of a robust flow cytometric assay for determining numbers of viable bacteria. *Appl Environ Microbiol* **1995,** *61* (7), 2696-701.
71. López-Amorós, R.; Comas, J.; Vives-Rego, J., Flow cytometric assessment of Escherichia coli and Salmonella typhimurium starvation-survival in seawater using rhodamine 123, propidium iodide, and oxonol. *Appl Environ Microbiol* **1995,** *61* (7), 2521-6.
72. Nocker, A.; Cheung, C. Y.; Camper, A. K., Comparison of propidium monoazide with ethidium monoazide for differentiation of live vs. dead bacteria by selective removal of DNA from dead cells. *J Microbiol Methods* **2006,** *67* (2), 310-20.
73. Mackey, B. M.; Miles, C. A.; Seymour, D. A.; Parsons, S. E., THERMAL-DENATURATION AND LOSS OF VIABILITY IN ESCHERICHIA-COLI AND BACILLUS-STEAROTHERMOPHILUS. *Letters in Applied Microbiology* **1993,** *16* (2), 56-58.
74. Singh, A. V.; Vyas, V.; Patil, R.; Sharma, V.; Scopelliti, P. E.; Bongiorno, G.; Podestà, A.; Lenardi, C.; Gade, W. N.; Milani, P., Quantitative characterization of the influence of the nanoscale morphology of nanostructured surfaces on bacterial adhesion and biofilm formation. *PLoS One* **2011,** *6* (9), e25029.
75. Banning, N.; Toze, S.; Mee, B. J., Escherichia coli survival in groundwater and effluent measured using a combination of propidium iodide and the green fluorescent protein. *J Appl Microbiol* **2002,** *93* (1), 69-76.
76. Katsui, N.; Tsuchido, T.; Hiramatsu, R.; Fujikawa, S.; Takano, M.; Shibasaki, I., Heat-induced blebbing and vesiculation of the outer membrane of Escherichia coli. *J Bacteriol* **1982,** *151* (3), 1523-31.

77. Katsui, N.; Tsuchido, T.; Takano, M.; Shibasaki, I., Effect of preincubation temperature on the heat resistance of Escherichia coli having different fatty acid compositions. *J Gen Microbiol* **1981,** *122* (2), 357-61.
78. Tsuchido, T.; Katsui, N.; Takeuchi, A.; Takano, M.; Shibasaki, I., Destruction of the outer membrane permeability barrier of Escherichia coli by heat treatment. *Appl Environ Microbiol* **1985,** *50* (2), 298-303.
79. Lee, Y. J.; Kim, C. S.; Oh, D. K., Lactulose production by beta-galactosidase in permeabilized cells of Kluyveromyces lactis. *Appl Microbiol Biotechnol* **2004,** *64* (6), 787-93.
80. Silveira, M. M.; Jonas, R., The biotechnological production of sorbitol. *Appl Microbiol Biotechnol* **2002,** *59* (4-5), 400-8.
81. Fontanille, P.; Larroche, C., Optimization of isonovalal production from alpha-pinene oxide using permeabilized cells of Pseudomonas rhodesiae CIP 107491. *Appl Microbiol Biotechnol* **2003,** *60* (5), 534-40.
82. Yeom, S.; Mutlu, B. R.; Aksan, A.; Wackett, L. P., Bacterial Cyanuric Acid Hydrolase for Water Treatment. *Applied and Environmental Microbiology* **2015,** *81* (19), 6660-6668.
83. Martens, J. H.; Barg, H.; Warren, M. J.; Jahn, D., Microbial production of vitamin B-12. *Applied Microbiology and Biotechnology* **2002,** *58* (3), 275-285.
84. Desai, J. D.; Banat, I. M., Microbial production of surfactants and their commercial potential. *Microbiology and Molecular Biology Reviews* **1997,** *61* (1), 47-&.
85. Biebl, H.; Menzel, K.; Zeng, A. P.; Deckwer, W. D., Microbial production of 1,3-propanediol. *Applied Microbiology and Biotechnology* **1999,** *52* (3), 289-297.
86. Du, J.; Shao, Z.; Zhao, H., Engineering microbial factories for synthesis of value-added products. *Journal of Industrial Microbiology & Biotechnology* **2011,** *38* (8), 873-890.
87. Ferrer-Miralles, N.; Domingo-Espin, J.; Corchero, J. L.; Vazquez, E.; Villaverde, A., Microbial factories for recombinant pharmaceuticals. *Microbial Cell Factories* **2009,** *8*.
88. Chance, R. E.; Frank, B. H., RESEARCH, DEVELOPMENT, PRODUCTION, AND SAFETY OF BIOSYNTHETIC HUMAN INSULIN. *Diabetes Care* **1993,** *16*, 133-142.
89. Amarger, N., Genetically modified bacteria in agriculture. *Biochimie* **2002,** *84* (11), 1061-1072.
90. Pieper, D. H.; Reineke, W., Engineering bacteria for bioremediation. *Current Opinion in Biotechnology* **2000,** *11* (3), 262-270.
91. Brenner, K.; You, L.; Arnold, F. H., Engineering microbial consortia: a new frontier in synthetic biology. *Trends in Biotechnology* **2008,** *26* (9), 483-489.
92. Minty, J. J.; Singer, M. E.; Scholz, S. A.; Bae, C.-H.; Ahn, J.-H.; Foster, C. E.; Liao, J. C.; Lin, X. N., Design and characterization of synthetic fungal-bacterial consortia for direct production of isobutanol from cellulosic biomass. *Proceedings of the National Academy of Sciences of the United States of America* **2013,** *110* (36), 14592-14597.
93. Shong, J.; Diaz, M. R. J.; Collins, C. H., Towards synthetic microbial consortia for bioprocessing. *Current Opinion in Biotechnology* **2012,** *23* (5), 798-802.

94. Pashin, Y. V.; Bakhitova, L. M., MUTAGENIC AND CARCINOGENIC PROPERTIES OF POLYCYCLIC AROMATIC-HYDROCARBONS. *Environmental Health Perspectives* **1979,** *30* (JUN), 185-189.
95. Aukema, K. G.; Kasinkas, L.; Aksan, A.; Wackett, L. P., Use of Silica-Encapsulated Pseudomonas sp Strain NCIB 9816-4 in Biodegradation of Novel Hydrocarbon Ring Structures Found in Hydraulic Fracturing Waters. *Applied and Environmental Microbiology* **2014,** *80* (16), 4968-4976.
96. Tchobanoglous, G.; Burton, F. L.; Stensel, H. D.; Metcalf; Eddy, *Wastewater Engineering: Treatment and Reuse*. McGraw-Hill Education: 2003.
97. Meunier, C. F.; Dandoy, P.; Su, B.-L., Encapsulation of cells within silica matrixes: Towards a new advance in the conception of living hybrid materials. *Journal of Colloid and Interface Science* **2010,** *342* (2), 211-224.
98. Resnick, S. M.; Lee, K.; Gibson, D. T., Diverse reactions catalyzed by naphthalene dioxygenase from Pseudomonas sp strain NCIB 9816. *Journal of Industrial Microbiology & Biotechnology* **1996,** *17* (5-6), 438-457.
99. Rippka, R.; Deruelles, J.; Waterbury, J. B.; Herdman, M.; Stanier, R. Y., GENERIC ASSIGNMENTS, STRAIN HISTORIES AND PROPERTIES OF PURE CULTURES OF CYANOBACTERIA. *Journal of General Microbiology* **1979,** *111* (MAR), 1-61.
100. Turner, K.; Xu, S.; Pasini, P.; Deo, S.; Bachas, L.; Daunert, S., Hydroxylated polychlorinated biphenyl detection based on a genetically engineered bioluminescent whole-cell sensing system. *Analytical Chemistry* **2007,** *79* (15), 5740-5745.
101. Barber, J.; Archer, M. D., P680, the primary electron donor of photosystem II. *Journal of Photochemistry and Photobiology a-Chemistry* **2001,** *142* (2-3), 97-106.
102. Bechet, Q.; Shilton, A.; Guieysse, B., Modeling the effects of light and temperature on algae growth: State of the art and critical assessment for productivity prediction during outdoor cultivation. *Biotechnology Advances* **2013,** *31* (8), 1648-1663.
103. Sakkos, J. K.; Kieffer, D. P.; Mutlu, B. R.; Wackett, L. P.; Aksan, A., Engineering of a silica encapsulation platform for hydrocarbon degradation using Pseudomonas sp. NCIB 9816-4. *Biotechnology and bioengineering* **2015**.
104. Pottier, L.; Pruvost, J.; Derernetz, J.; Cornet, J. F.; Legrand, J.; Dussap, C. G., A fully predictive model for one-dimensional light attenuation by Chlamydomonas reinhardtii in a torus photobioreactor. *Biotechnology and Bioengineering* **2005,** *91* (5), 569-582.
105. Borde, X.; Guieysse, B.; Delgado, O.; Munoz, R.; Hatti-Kaul, R.; Nugier-Chauvin, C.; Patin, H.; Mattiasson, B., Synergistic relationships in algal-bacterial microcosms for the treatment of aromatic pollutants. *Bioresource Technology* **2003,** *86* (3), 293-300.
106. Munoz, R.; Guieysse, B.; Mattiasson, B., Phenanthrene biodegradation by an algal-bacterial consortium in two-phase partitioning bioreactors. *Applied Microbiology and Biotechnology* **2003,** *61* (3), 261-267.

107. Praveen, P.; Loh, K.-C., Photosynthetic aeration in biological wastewater treatment using immobilized microalgae-bacteria symbiosis. *Applied Microbiology and Biotechnology* **2015**, 1-10.
108. Nassif, N.; Bouvet, O.; Rager, M. N.; Roux, C.; Coradin, T.; Livage, J., Living bacteria in silica gels. *Nature Materials* **2002,** *1* (1), 42-44.
109. Premkumar, J. R.; Rosen, R.; Belkin, S.; Lev, O., Sol-gel luminescence biosensors: Encapsulation of recombinant E-coli reporters in thick silicate films. *Analytica Chimica Acta* **2002,** *462* (1), 11-23.
110. Depagne, C.; Roux, C.; Coradin, T., How to design cell-based biosensors using the sol-gel process. *Analytical and Bioanalytical Chemistry* **2011,** *400* (4), 965-976.
111. Federle, M. J.; Bassler, B. L., Interspecies communication in bacteria. *Journal of Clinical Investigation* **2003,** *112* (9), 1291-1299.
112. Mutlu, B. R.; Sakkos, J. K.; Yeom, S.; Wackett, L. P.; Aksan, A., Silica ecosystem for synergistic biotransformation. *Scientific Reports* **2016,** *6*.
113. Reichenberger, S.; Bach, M.; Skitschak, A.; Frede, H. G., Mitigation strategies to reduce pesticide inputs into ground- and surface water and their effectiveness; A review. *Science of the Total Environment* **2007,** *384* (1-3), 1-35.
114. Carter, A., How pesticides get into water — and proposed reduction measures. *Pesticide Outlook* **2000,** *11*, 149-156.
115. Benotti, M. J.; Trenholm, R. A.; Vanderford, B. J.; Holady, J. C.; Stanford, B. D.; Snyder, S. A., Pharmaceuticals and Endocrine Disrupting Compounds in US Drinking Water. *Environmental Science & Technology* **2009,** *43* (3), 597-603.
116. Lima, D.; Viana, P.; Andre, S.; Chelinho, S.; Costa, C.; Ribeiro, R.; Sousa, J. P.; Fialho, A. M.; Viegas, C. A., Evaluating a bioremediation tool for atrazine contaminated soils in open soil microcosms: The effectiveness of bioaugmentation and biostimulation approaches. *Chemosphere* **2009,** *74* (2), 187-192.
117. Chelinho, S.; Moreira-Santos, M.; Lima, D.; Silva, C.; Viana, P.; Andre, S.; Lopes, I.; Ribeiro, R.; Fialho, A. M.; Viegas, C. A.; Sousa, J. P., Cleanup of atrazine-contaminated soils: ecotoxicological study on the efficacy of a bioremediation tool with Pseudomonas sp ADP. *Journal of Soils and Sediments* **2010,** *10* (3), 568-578.
118. Wang, Q. F.; Xie, S. G.; Hu, R., Bioaugmentation with Arthrobacter sp strain DAT1 for remediation of heavily atrazine-contaminated soil. *International Biodeterioration & Biodegradation* **2013,** *77*, 63-67.
119. Strong, L. C.; McTavish, H.; Sadowsky, M. J.; Wackett, L. P., Field-scale remediation of atrazine-contaminated soil using recombinant Escherichia coli expressing atrazine chlorohydrolase. *Environmental Microbiology* **2000,** *2* (1), 91-98.
120. Li, Q. Y.; Li, Y.; Zhu, X. K.; Cai, B. L., Isolation and characterization of atrazine-degrading Arthrobacter sp AD26 and use of this strain in bioremediation of contaminated soil. *Journal of Environmental Sciences* **2008,** *20* (10), 1226-1230.
121. Newcombe, D. A.; Crowley, D. E., Bioremediation of atrazine-contaminated soil by repeated applications of atrazine-degrading bacteria. *Applied Microbiology and Biotechnology* **1999,** *51* (6), 877-882.

122. Brown, D. S.; Flagg, E. W., EMPIRICAL PREDICTION OF ORGANIC POLLUTANT SORPTION IN NATURAL SEDIMENTS. *Journal of Environmental Quality* **1981,** *10* (3), 382-386.
123. Wu, Z. J.; Ahn, I. S.; Lee, C. H.; Kim, J. H.; Shul, Y. G.; Lee, K. T., Enhancing the organic dye adsorption on porous xerogels. *Colloids and Surfaces a-Physicochemical and Engineering Aspects* **2004,** *240* (1-3), 157-164.
124. Liu, C. Q.; Naismith, N.; Fu, L.; Economy, J., Ordered mesoporous organic-inorganic hybrid materials containing microporous functional calix 8 arene amides. *Chemical Communications* **2003,** (19), 2472-2473.
125. Jayasundera, S.; Burleigh, M. C.; Zeinali, M.; Spector, M. S.; Miller, J. B.; Yan, W. F.; Dai, S.; Markowitz, M. A., Organosilica copolymers for the adsorption and separation of multiple pollutants. *Journal of Physical Chemistry B* **2005,** *109* (19), 9198-9201.
126. Hoffmann, F.; Cornelius, M.; Morell, J.; Froba, M., Silica-based mesoporous organic-inorganic hybrid materials. *Angewandte Chemie-International Edition* **2006,** *45* (20), 3216-3251.
127. Strong, L. C.; Rosendahl, C.; Johnson, G.; Sadowsky, M. J.; Wackett, L. P., Arthrobacter aurescens TC1 metabolizes diverse s-triazine ring compounds. *Applied and Environmental Microbiology* **2002,** *68* (12), 5973-5980.
128. Eaton, R. W.; Ribbons, D. W., METABOLISM OF DIBUTYLPHTHALATE AND PHTHALATE BY MICROCOCCUS SP STRAIN-12B. *Journal of Bacteriology* **1982,** *151* (1), 48-57.
129. Sandu, C.; Chiribau, C. B.; Sachelaru, P.; Brandsch, R., Plasmids for nicotine-dependent and -independent gene expression in Arthrobacter nicotinovorans and other Arthrobacter species. *Applied and Environmental Microbiology* **2005,** *71* (12), 8920-8924.
130. Desouza, M. L.; Wackett, L. P.; Boundymills, K. L.; Mandelbaum, R. T.; Sadowsky, M. J., CLONING, CHARACTERIZATION, AND EXPRESSION OF A GENE REGION FROM PSEUDOMONAS SP STRAIN ADP INVOLVED IN THE DECHLORINATION OF ATRAZINE. *Applied and Environmental Microbiology* **1995,** *61* (9), 3373-3378.
131. Yan, L. J.; Zhang, Q. H.; Zhang, W. B.; Feng, Y. Q.; Zhang, L. H.; Li, T.; Zhang, Y. K., Hybrid organic-inorganic phenyl monolithic column for capillary electrochromatography. *Electrophoresis* **2005,** *26* (15), 2935-2941.
132. Nakanishi, K.; Soga, N., PHASE-SEPARATION IN SILICA SOL-GEL SYSTEM CONTAINING POLYACRYLIC-ACID .2. EFFECTS OF MOLECULAR-WEIGHT AND TEMPERATURE. *Journal of Non-Crystalline Solids* **1992,** *139* (1), 14-24.
133. Rao, A. V.; Kalesh, R. R.; Pajonk, G. M., Hydrophobicity and physical properties of TEOS based silica aerogels using phenyltriethoxysilane as a synthesis component. *Journal of Materials Science* **2003,** *38* (21), 4407-4413.
134. Fowler, S. D.; Greenspan, P., APPLICATION OF NILE RED, A FLUORESCENT HYDROPHOBIC PROBE, FOR THE DETECTION OF NEUTRAL LIPID DEPOSITS IN TISSUE-SECTIONS - COMPARISON WITH OIL RED O. *Journal of Histochemistry & Cytochemistry* **1985,** *33* (8), 833-836.

135. Sackett, D. L.; Wolff, J., NILE RED AS A POLARITY-SENSITIVE FLUORESCENT-PROBE OF HYDROPHOBIC PROTEIN SURFACES. *Analytical Biochemistry* **1987,** *167* (2), 228-234.
136. Shapir, N.; Rosendahl, C.; Johnson, G.; Andreina, M.; Sadowsky, M. J.; Wackett, L. P., Substrate specificity and colorimetric assay for recombinant TrzN derived from Arthrobacter aurescens TC1. *Applied and Environmental Microbiology* **2005,** *71* (5), 2214-2220.
137. BoundyMills, K. L.; deSouza, M. L.; Mandelbaum, R. T.; Wackett, L. P.; Sadowsky, M. J., The atzB gene of Pseudomonas sp strain ADP encodes the second enzyme of a novel atrazine degradation pathway. *Applied and Environmental Microbiology* **1997,** *63* (3), 916-923.
138. Sadowsky, M. J.; Tong, Z. K.; de Souza, M.; Wackett, L. P., AtzC is a new member of the amidohydrolase protein superfamily and is homologous to other atrazine-metabolizing enzymes. *Journal of Bacteriology* **1998,** *180* (1), 152-158.
139. Radian, A.; Aukema, K. G.; Aksan, A.; Wackett, L. P., Silica Gel for Enhanced Activity and Hypochlorite Protection of Cyanuric Acid Hydrolase in Recombinant Escherichia coli. *Mbio* **2015,** *6* (6).

Appendix Permissions to use publications in dissertation

Author reusing their own work published by the Royal Society of Chemistry

You do not need to request permission to reuse your own figures, diagrams, etc, that were originally published in a Royal Society of Chemistry publication. However, permission should be requested for use of the whole article or chapter except if reusing it in a thesis. If you are including an article or book chapter published by us in your thesis please ensure that your co-authors are aware of this.

Reuse of material that was published originally by the Royal Society of Chemistry must be accompanied by the appropriate acknowledgement of the publication. The form of the acknowledgement is dependent on the journal in which it was published originally, as detailed in 'Acknowledgements'.

http://www.rsc.org/journals-books-databases/journal-authors-reviewers/licences-copyright-permissions/